Equilibrium Phase Behaviour of Liquid Crystalline Polymer Brushes

by

Steven Blaber

A thesis
presented to the University of Waterloo
in fulfillment of the
thesis requirement for the degree of
Master of Science
in
Physics

Waterloo, Ontario, Canada, 2019

I hereby declare that I am the sole author of this thesis. This is a true copy of the thesis, including any required final revisions, as accepted by my examiners.

I understand that my thesis may be made electronically available to the public.

Abstract

Using self-consistent field theory of worm-like chains with Maier-Saupe interactions we study the equilibrium phase behaviour of liquid crystalline (LC) polymer brushes. In a good solvent the brush extends out normal to the grafting plane in order to maximize the contact between polymer and solvent molecules which results in a continuous transition to an extended nematic state with increasing LC interaction strength. As LC interactions are further increased the brush collapses into a high density nematic state. In contrast to previous calculations, that assumed azimuthal symmetry and predict a collapse through folding into a high density nematic state we find that for semi-flexible polymers the folded state becomes unstable and the brush instead collapses through a continuous symmetry breaking transition into a tilted state.

Acknowledgements

I would like to thank my supervisors Prof. Mark Matsen and Prof. Nasser Mohieddin Abukhdeir for their mentorship and guidance, without them this project would not have been possible. Thanks to the additional members of my graduate committee, Prof. Jeff Chen and Prof. Robert Wickham for insightful discussion and feedback. Special thanks to Dr. Pendar Mahmoudi for helping develop some of the numerical method and Dr. Russell Spencer for helping code some of the SCFT. Computer resources were provided by Compute Canada.

Table of Contents

List of Figures

Abbreviations

LC	Liquid Crystal
SCFT	Self-Consistent Field Theory
MS	Maier-Saupe
CB	Conventional Brush
LCB	Liquid Crystal Brush
MSB	Microphase-Segregated Brush
SST	Strong-Stretching theory

List of Symbols

$\mathbf{n}$	The director
$\mathcal{Q}$	Tensor order parameter
$\mathcal{S}$	Uniaxial scalar nematic order parameter
$\mathcal{P}$	Biaxial scalar nematic order parameter
n_{p}	Number of polymers
n_{s}	Number of solvent molecules
N	Degree of polymerization
V	Total system volume
T	Temperature
k_{B}	Boltzmann's constant
$\mathcal{A}$	Grafting Area
σ	Grafting Density
Σ	Scaled grafting density
ρ_0	Polymer segment density
v_{s}	Solvent size
α	Ratio of solvent to polymer size
κ	Dimensionless bending modulus
b	Fixed bond length
ℓ_p	Persistence length
ℓ_c	Contour length
s	Backbone parameter
z	Distance from the grafting plane
$\mathbf{u}$	Unit tangent vector to the polymer chain
ν_0	Isotropic interaction parameter
ν_2	Liquid crystalline interaction parameter
Λ_0	Scaled isotropic interaction parameter
Λ_2	Scaled liquid crystalline interaction parameter
χ	Flory-Huggins polymer-solvent interaction parameter

F	Canonical free energy
S_{s}	Solvent entropy
Z	Canonical partition function
H	Effective Hamiltonian
Q	Single chain partition function
q	Partial partition function
$q^{\dagger}$	Reverse partial partition function
ϕ	Polymer concentration
ϕ_{s}	Solvent concentration
R_0	Mean square end-end distance
L	Classical brush height from strong-stretching theory
w	Mean field
U_{B}	Bending energy
U_0	Isotropic interaction energy
U_2	Liquid crystalline interaction energy
U_{ps}	Polymer-solvent interaction energy

Chapter 1

Introduction

1.1 Motivation

Polymer brushes offer a convenient method to modify the surface properties of materials,[1,2,3] for this reason they are pervasive throughout biology and widely used in industrial applications. By altering the surface chemistry polymer brushes enhance properties such as wetting, lubrication, adhesion, and anti-fouling. Naturally occurring brushes control surface wetting of the cartilage in joints, lubrication in lung tissue and limit deposition of macromolecules onto surfaces (anti-fouling).[3,4,5] These properties depend critically on the equilibrium phase behaviour of the brush. The majority of studies focus on flexible brushes, but the often ignored stiffness of the polymer will effect the height of the brush and can result in liquid crystal (LC) phases. Most notably, many biopolymers have persistence lengths comparable to their contour length, so their stiffness can result in anisotropic interaction and have a significant impact on their equilibrium phase behaviour. For example, anisotropic excluded volume or van der Waals interactions between polymer segments can give rise to LC phases,[6,7,8,9,10] which can be exploited for their chemical, mechanical and optical properties.

One notable application of LC polymer brushes is to tailor the surface properties of an LC material.[8,11] LC displays use the surface alignment of LCs to polarize light and produce the high quality visuals present in most modern displays. Currently the only large scale industrially applicable method for inducing surface anchoring consists of mechanically rubbing spin-coated polymers with a piece of velvet cloth. Debris and static discharge cause defects and can interfere or break electronic circuits reducing the overall quality and increasing the cost associated with producing high definition displays.[12] Liquid crystalline

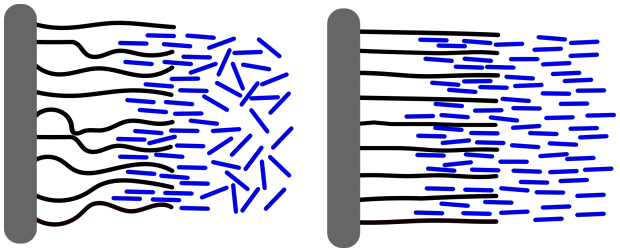

Fig 1.1. Diagram depicting the possible surface anchoring effects of a polymer brush (black) on liquid crystals (blue). The left image represents the bulk isotropic phase and the right the bulk nematic.

polymer brushes are easy to produce, scalable and can be manufactured with a high degree of homogeneity.[1] Additionally, brushes with different chemical properties or grafting densities will allow for increased control over local LC alignment. Therefore, LC polymer brushes are a promising candidate for surface anchoring conventional LC materials.

A polymer brush consists of a series of polymers grafted to a substrate with sufficient density that they stretch out normal to the surface. Interactions between the polymers and LCs give rise to surface anchoring effects that can be used to tailor the local LC alignment. Although the bulk LC phase might be isotropic, close to the surface intermolecular interactions between the brush and the LCs could induce locally preferential alignments. A schematic diagram is presented in Fig. 1.1. The direction and strength of alignment will depend on the chemical structure and grafting density of the brush; therefore, adjusting these properties allows for specific surface tailoring of LC order.

The theoretical framework we will be using is self-consistent field theory (SCFT) of worm-like chains with Maier-Saupe (MS) interactions. SCFT is a mean field description which has seen much success in providing a rigorous theoretical description of polymers.[13] Much of the success of SCFT is in the precise universal description of the phase behaviour of polymer systems[13,14] and the standard Gaussian chain model accurately describes the equilibrium phase behaviour of a flexible polymer brush.[15,16,1,17] A key property of LCs is orientational order; however, mesoscopic models of polymers accounting for orientation (worm-like chain) are significantly more complex than those with no definite orientation (Gaussian chain) or a fixed orientation (rigid rod). Additional complexity is added from anisotropic intermolecular interactions such as Onsager and MS which are key to the description of LCs. Much of the difficulty in describing LC polymers comes from the complexity and dimensionality of the problem.[18] It is important to account for both orientation and non-trivial intermolecular interactions; therefore, we will rely on numerical SCFT. Despite these issues, spectral and pseudo spectral methods can provide efficient solutions to

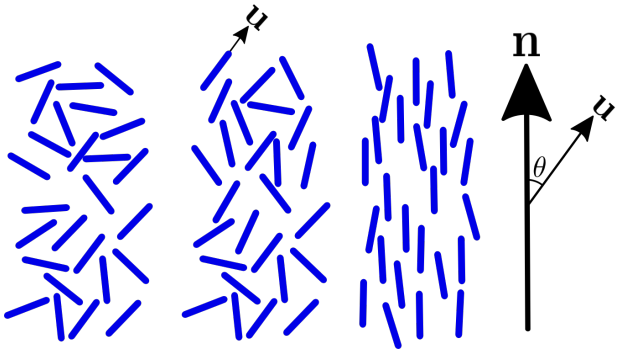

Fig 1.2. From left to right increasing LC alignment of rigid molecules with orientation **u**. The director, **n**, is the average local orientation of the molecules and the angle, θ, is the angle that an individual molecular axis makes with the director.

SCFT problems.[19,20] Since SCFT has seen tremendous success in both qualitatively and quantitatively describing the phase behaviour of many polymeric systems it is well suited to the task of describing liquid crystalline polymer brushes.

Recently, worm-like chain SCFT models have been used to describe a number of related systems: liquid crystalline polymer brushes,[21] worm-like chains in confinement,[22] Maier Saupe models of polymer nematics[23] and compressible Maier Saupe models.[24] However, when it comes to LC polymeric brushes, previous models have either used the Alexander-de Gennes model,[25,9,8] freely jointed chain model[26] or Onsager interactions.[21] It is known that the Alexander-de Gennes model does not generally give an accurate description of polymer brushes,[27,28] the freely-jointed chain model yields hairpin defects which it cannot accurately describe[29] and the Onsager model limits the types of allowed interactions. By using the worm-like chain model with MS interactions we can achieve a complete theoretical description of the equilibrium phase behaviour of an LC polymer brush. LC polymers are a diverse class of materials with novel physical properties that have relevant industrial applications. A complete theoretical description is critical to understanding these material properties.

1.2 Liquid Crystals

Liquid crystals are often exploited for their optical properties, most notably in LC displays. The optical properties of an LC material depends critically on the orientational order of the molecules. Due to the elongated, anisotropic shape of the molecules LCs transition into an ordered phase with a shared orientation between molecules that persists over a macroscopic

scale. In the simplest case the molecules align into what is known as a *nematic* phase, with orientational but no translational order, as depicted in Fig. 1.2. For *thermotropic* LC materials this transition takes place at a critical temperature while for *lyotropic* it occurs at a critical concentration in a mixture. The isotropic (disordered) phase is found at high temperature or low concentration with the nematic phase correspondingly at low temperature or high concentration. In either case a strong electric field can induce directed ordering. The anisotropic dielectric tensor caused by the orientational ordering of the molecules is used to alter the polarization of incident light. Through this, electrically induced transitions and surface anchoring allow for fine tuned optical displays.[30]

The ordering of an LC arises from the anisotropic shape of the molecule. Many LCs are rod-like molecules (or contain a rod-like core), which are longer in one direction resulting in preferential alignment. The nature and strength of the alignment will depend on the intermolecular interactions and the two most common models are Onsager[6] and MS.[7] Onsagers model of elongated hard rods emphasizes repulsive interactions and the associated effects of the orientational dependent excluded volume. The model of Maier and Saupe is more general and allows for anisotropic van der Waals forces of attraction in addition to excluded volume and repulsive interactions. Both give rise LC phase transitions.[30]

Currently the most popular model of LC materials is based on Landau's theory of phase transitions,[30] which offers a simple and intuitive description. By representing the free energy as a Taylor series expansion of an order parameter and accounting for the symmetries of the underlying system we can discern key properties of phase transitions. The difficulty arises from trying to find a good order parameter, one that captures the phase behaviour of the system. Since we are interested in the orientational ordering we define the *director*, $\mathbf{n}$, which is a local average of the LCs orientation depicted in Fig. 1.2. The director is obtained by averaging over several molecules but on a scale much smaller than the size of the system. The director can represent the alignment of the molecules but not the strength of alignment; therefore, we also introduce the uniaxial scalar nematic order parameter,

$$\mathcal{S} = \frac{1}{2}\langle 3\cos^2(\theta) - 1\rangle \tag{1.1}$$

the spatial average of the second Legendre Polynomial of $\cos(\theta)$, the component of the individual molecular axis, $\mathbf{u}$, along the direction of the director, $\mathbf{n}$. $\mathcal{S}$ is 0 in the isotropic phase and 1 when the LC is perfectly aligned. For LCs the standard approach is called the Landau-de Gennes model of phase transitions for which modern approaches use a more general tensor order parameter, $\mathcal{Q}$, which accounts for biaxiality. The $\mathcal{Q}$-tensor is defined

to be symmetric and traceless and takes the form:

$$\mathcal{Q}_{ij} = \lambda_1 \mathbf{nn} + \lambda_2 \mathbf{mm} + \lambda_3 \mathbf{ll} = \frac{3\mathcal{S}}{2}(\mathbf{nn} - \frac{1}{3}\mathbf{I}) + \frac{\mathcal{P}}{2}(\mathbf{mm} - \mathbf{ll}) \tag{1.2}$$

$\mathbf{n}$, $\mathbf{m}$ and $\mathbf{l}$ are eigenvectors of $\mathcal{Q}$ corresponding to axes of molecular orientation and λ_i are their corresponding eigenvalues. $\mathcal{S} = \lambda_1$ is the uniaxial scalar nematic order parameter and $\mathcal{P} = (\lambda_2 - \lambda_3)$ the biaxial scalar nematic order parameter.

A common application of LCs are liquid crystal displays (LCDs), which are the most common modern display. LCDs rely on two key properties: orientational alignment with an electric field and surface anchoring. In the presence of an applied electric field LCs tend to preferential align in the direction of the field, and different surface geometries can result in preferential local alignment at the boundary. By inducing an alignment at the boundaries and applying an electric field a tunable alignment gradient is achieved which will polarize incident light.

1.3 Polymer Brushes

A polymer brush is formed by binding a series of polymers to a substrate with sufficient density that they stretch out normal to the surface. In a good solvent, and moderately high grafting densities, interactions between the polymers and polymer-solvent mixing entropy force them to extend outwards creating a brush-like appearance. There are two main methods for producing polymer brushes: *grafting to* and *grafting from.*[31,3] When grafting from, polymerization initiators are bonded to the substrate at the desired density. Monomers are then diffused onto the substrate and begin to polymerize at the initiator sites. This procedure is carried out until polymers of the desired length have formed. Grafting from has the ability to form complex architectures by coupling the appropriate surface initiator to controlled radical polymerization methods. For example, atom transfer radical polymerization (ATRP), nitroxide-mediated polymerization (NMP), and reversible additionfragmentation chain transfer (RAFT) enable the precise control of grafting density.[32,33,34]

At the cost of control over grafting density, grafting to allows for a high degree of homogeneity between polymers. This is done by immersing prepared polymers with end functionalized groups into a solvent with the substrate. A chemical is added which reacts with the substrate causing the polymers to bond with the activated site. Once a sufficient polymer density is achieved another chemical is added to bond and close off the free end of the polymer. Since the polymers are prefabricated their physical properties, such as degree of polymerization, or chain architecture can be precisely controlled. However,

due to the diffusive nature of the bonding it can be difficult to achieve high densities and homogeneous distributions. In either case, grafting from or to, the method is stable, easy to produce and scalable; however, there are trade offs between control of grafting density and polymer structure. Nevertheless, both grafting from and to present promising techniques for producing large scale polymer brushes with minimal imperfections.

Depending on the density and solvent conditions, grafted polymers can exhibit several phases. At very low grafting densities the polymers do not strongly interact and are in what is know as the mushroom regime, for moderate grafting densities, when the pervaded volumes of the polymers significantly overlap, they form a brush. In a *poor solvent* the intermolecular interactions overcome the mixing entropy and the brush and solvent phase separate, forming a collapsed brush. In a *good solvent* the mixing entropy dominates and the brush adopts an extended conformation. Generally, good solvent conditions are achieved at high temperature and poor solvents at low temperatures. For an LC polymer, the extended conformation causes the brush to align along the axis normal to the grafting plane and LC interactions induce a continuous transition into the nematic phase. For increasing LC interaction strength a number of theoretical studies have predicted that the brush will collapse into a high density nematic state,[35] which has since been observed in simulations.[36]

1.4 Previous Work

One of the earliest theoretical descriptions of a polymer brush is the Alexander-de Gennes model, which yields a step profile with all the free ends at the outer edge of the brush.[25,37] Although this model results in the correct linear scaling of the brush height with the degree of polymerization, N, a more sophisticated model, using the classical trajectory theory limit of SCFT, originally explored by Semenov[38] in the case of diblock copolymers, Milner, Witten and Cates[15] elegantly showed that the concentration of a flexible polymer brush has a parabolic profile. In general the step profile of the Alexander-de Gennes model is unrealistic[28,27] while the parabolic profile has shown very good agreement with both experiment[28,27,39,40,41,42,43] and simulation,[44,45,46] and the deviations, such as the depletion layer near the grafting surface and exponential tail at the solvent boundary are well understood and described through numerical SCFT.[43,47,16,17] However, this model is not without its limitations.

The Gaussian chain model that is the basis for the parabolic profile has no orientational dependence and therefore cannot describe the brush's possible LC phases, additionally the Gaussian chain is infinitely extensible so when the brush height approaches the contour

length of the polymer, the model is no longer accurate.[48,49,21] As an alternative, the worm-like chain model has finite extensibility and continuously interpolates between the flexible Gaussian and rigid rod models, producing parabolic and step-like profiles in each limit respectively.[21] As previously mentioned, the parabolic profile has been shown to be quantitatively accurate in comparison with experiment, while the semi-flexible to rigid cases are in agreement with simulations. A study by Deng *et al.*[21] explored the properties of a semi-flexible polymer brush for degrees of flexibility ranging from Gaussian to rigid rods and examined in detail the scaling behaviour of various physical quantities such as the free energy and scalar nematic order parameter.

Brush calculations typically ignore the orientational interactions between polymer chains, which generally favour parallel alignment. Even though they are relatively weak for flexible polymers, they still enhance the degree of stretching.[50] More interesting, however, are the stiffer LC polymers that tend to align into a nematic phase. Using an Alexander-de Gennes type calculation, Halperin and Williams[8,11] demonstrated how LC brushes could be used to control the alignment of a liquid-crystalline solvent, an important issue for LC display technology. This potential application, along with others such as organic electronics, switches, and sensor, has spurred numerous experimental studies.[51,52,53,54,55,56,57,58,59,60,61]

Subsequent theoretical calculations have, so far, concentrated on the simpler system of LC brushes in isotropic solvent. In particular, Birshtein *et al.*,[9] examined freely-jointed chains interacting by MS LC interactions.[7] They initially solved the statistical mechanics assuming uniform stretching (i.e., the Alexander-de Gennes approximation) with the rigid segments constrained to the bonds of a simple-cubic lattice. Provided the solvent quality was sufficiently good, increasing the LC interactions produced a first-order transition from a conventional brush (CB) to a collapsed liquid crystal brush (LCB). Kuznetsov and Chen[10] performed a similar off-lattice calculation, which likewise predicted an analogous transition for good solvents.

Birshtein and coworkers later dropped the Alexander-de Gennes approximation and instead solved the statistical mechanics using lattice SCFT of a brush of freely jointed chains, incorporating MS type LC interactions. In a series of papers[26,62,63,35] they find that the brush evolved continuously from CB to LCB via the formation of a microphase-segregated brush (MSB) in which an extended state coexists with a high density collapsed nematic state. A characteristic concentration profile from Ref. [26] as well as a diagram illustrating the behaviour is given in Fig. 1.3. In the collapsed region, the brush backfolds several times forming multiple hairpin defects. Computer simulations of freely-jointed polymers have since observed this phase.[36] However, since the freely jointed chain model has no bending energy penalty there is no cost to forming hairpin defects.[8,11,64] Since the folds take place over very short length scales one would expect that for real polymers, even

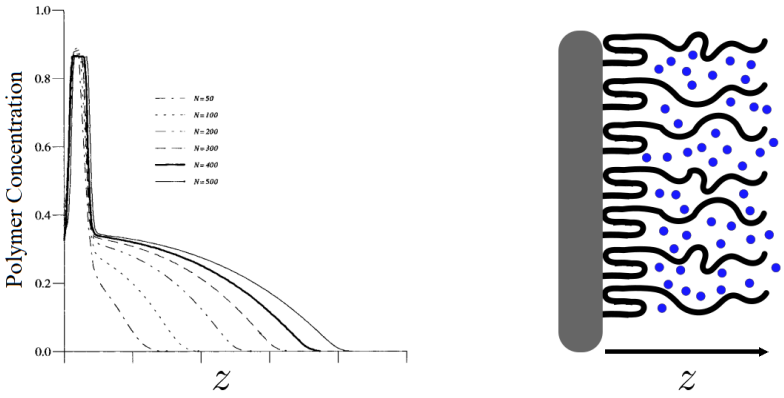

Fig 1.3. Left: characteristic brush profile of a microphase-segregated brush, as observed in Ref. [26]. Right: cartoon depicting the possible configurations of the polymers in this state. The high density region near the grafting plane $z = 0$ is a highly nematically ordered state with backfolds while the low density region is a coexisting conventional brush.

when they are relatively flexible, the cost would be non negligible (recent work by Odjik[65] and Chen[66] discuss the energy cost of hairpin folds). Additionally, polymers exhibiting LC phases tend to be relatively rigid so if the penalty was included the brush may opt for other ways of increasing its concentration.

Indeed, simulations of short-chains LC molecules with an energy penalty for folding observe tilting.[67,68,69,70] Birshtein and coworkers[26] did in fact perform some calculations, where the bending between consecutive chain segments was restricted, but nevertheless their lattice precluded the possibility of tilting. Deng *et al.*[21] did perform off-lattice SCFT for worm-like chains[71,72] with Onsager LC interactions.[6] In their work they did not observe the nematic collapse of the polymer brush; however, this can be attributed to the LC interactions being of Onsager type rather than the MS form used by Birshtein. Since Onsager interactions are purely excluded volume it will always favour the extended state. In general, interactions will not be purely excluded volume and attractive potentials can arise from, for example, van der Waals forces. The MS form allows for this type of interaction and is more general than the Onsager form.

Some studies have accounted for the possibility of tilting when considering LC polymeric brushes subjected to external forces, either shear[73] or compression.[74,75,76] However, it seems that the possibility of spontaneous tilting due to strong LC interactions has so far been overlooked. Therefore, we reconsider the SCFT for worm-like chains by Deng *et al.*,[21] allowing for breaking of the azimuthal symmetry. We also switch to the more general MS

interactions, rather than the Onsager interactions specific to hard-core cylindrical segments.

1.5 Organization

This thesis is organized as follows. We begin by outlining the model of LC polymer brushes in Chapter 2 and discuss popular alternatives. In order to study the equilibrium properties of the brush, we evaluate the statistical mechanics in the mean field approximation using SCFT, which we outline in Chapter 3.

With the model and theory well established, we begin by studying the phase behaviour of an LC polymer brush. In general we study three separate phases and their transitions: extended, folded and tilted. In Chapter 4 we begin by studying the effects of finite extensibility on the predictions from strong-stretching theory (SST) for flexible polymers before turning our attention to the extended nematic state of semi-flexible to rigid polymers. In the extended state the polymers align normal to the grafting plane, which allows us to assume azimuthal symmetry. Continuing to assume azimuthal symmetry, we study the nematic collapse of a brush into a folded state in Chapter 5. Finally, in Chapter 6 we arrive at the main result of this thesis by breaking azimuthal symmetry and demonstrating that the folded state becomes unstable and is pre-empted by a tilting transition. We then conclude by summarizing our findings and present the outlook for future work in Chapter 7.

Chapter 2

Model

In this chapter, we describe the model of LC polymer brushes immersed in solvent as well as some comparisons to other popular model choices. We will be using the worm-like chain model with MS LC interactions and implicit solvent in the canonical ensemble with fixed number of polymers, n_p, and solvent molecules, n_s, in a volume V at temperature T.

In general, for a given model system there are many methods for evaluating the statistical mechanical properties and determining the equilibrium phase behaviour. Discussion of this will be reserved to Chapter 3. In this chapter, our aim is simply to describe the model which can then be evaluated using statistical mechanics; however, we use notation and expressions that translate easily onto field theoretic methods and express the model in terms of its energetics.

2.1 Worm-like Chain

Some of the most popular polymer models are the Gaussian chain, freely jointed chain, rigid rod and worm-like chain, shown in Fig. 2.1.[77,13] Due to its simplicity and universality, the most popular among these is the Gaussian chain model which represents the flexible limit. In this model there is no cost associated with bending. The Gaussian chain has a fractal structure (Fig. 2.1) meaning that the orientation is completely isotropic on any scale which ignores the orientation of the chain reducing the dimensionality and significantly simplifying the system. For a real polymer this is achieved in the high molecular weight limit.[13] Although the Gaussian chain has seen success in describing the phase behaviour of many polymer systems,[77,13] it has significant limitations. The Gaussian chain model is

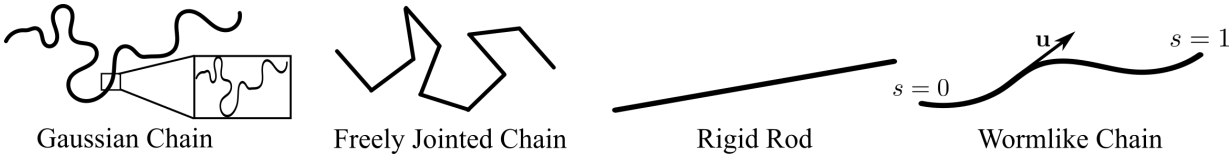

Fig 2.1. Schematic diagrams depicting from left to right: Gaussian chain model demonstrating isotropic fractal nature, freely jointed chain model with rigid segments isotropically and independently connected, rigid rod model with fixed orientation and finally the worm-like chain model with orientation $\mathbf{u}$ at contour position s.

only valid in the limit of high molecular weight, is infinitely extensible, and ignores possible LC phases.

In the opposite limit we have the rigid rod. As the name implies, this model describes polymers with a fixed orientation (infinite rigidity). LCs are often modelled as rigid rods, most famously by Onsager,[6] Maier and Saupe.[7] Similarly, SCFT can be applied to rigid rod polymers.[77] Since rigid rods can have a locally preferential alignment, these models can give rise to orientational order which is a key property of LCs. Although the rigid rod model is often sufficient for describing conventional LCs, due to the high degree of polymerization, most polymers have some ability to bend; therefore, it is important to account for the polymers flexibility but not so much that we lose all orientation dependence.

The freely jointed chain model is similar to a combination of the Gaussian chain and rigid rod models. In this model, the polymers are made up of a series of rigid segments connected by isotropic and independent bonds. Since the rigid segments have a definite orientation this model can be used to describe a polymers possible LC phases and has been used to model LC polymer brushes in the past.[35] However, most LC polymers are relatively rigid and therefore the freely jointed segments can be unrealistic. Additionally, previous models of LC polymer brushes found many hairpin folds (rapid reversals in direction) which will have a large energetic cost for a semi-flexible polymer brush[65,66] but are not penalised within the freely jointed chain model. It will be important to use a semi-flexible model to verify whether these hairpin folds persist once this energetic cost is accounted for.

The most popular and successful model of semi-flexible polymers, which accounts for the energy cost associated with chain bending, is the worm-like chain. This is the model we will be using to describe the polymer brush. The worm-like chain model is not as commonly used as the Gaussian or freely jointed chain models due to the added complexity arising from the increased dimensionality of the problem; however, it is often used for the description of biopolymers, which have persistence lengths comparable to their contour length. The complexity arises from accounting for the orientation at every point along

the chain; however, this represents a more realistic model which reveals the orientational properties of the system and reduces to both the Gaussian and rigid rod models in the appropriate limits. Additionally, spectral and pseudo spectral methods can be employed to efficiently solve the worm-like chain model.[78,79]

In the worm-like chain model a polymer with degree of polymerization N has segments with a fixed bond length b such that the total contour length $\ell_c = bN$ is fixed. The conformation of a worm-like chain is determined by a harmonic bending energy penalty

$$\frac{U_{\mathrm{B}}}{k_{\mathrm{B}}T} = \frac{\kappa}{2N}\int_0^1 ds \left|\frac{d\mathbf{u}(s)}{ds}\right|^2 . \tag{2.1}$$

The dimensionless bending modulus κ controls the persistence length $\ell_p = b\kappa$, $\mathbf{u}$ is the unit tangent vector to the chain and s is the backbone parameter which runs from 0 to 1, depicted in Fig. 2.1. It should be noted that this is a coarse grained model and the bond length will not in general directly correspond to the microscopic bond length between monomers.

We are interested in the equilibrium phase behaviour of a brush of worm-like chains. This amounts to evaluating the statistical mechanics of a series of polymers grafted to a rigid substrate and determining the stable phases from free energies. To create a brush one simply needs to graft one end of each chain, say $s = 0$, to a rigid substrate. Eq. (2.1) is for an individual polymer; however, in a brush, due to the relatively high density, the polymers will be strongly interacting with themselves and each other. Additionally, the brush will be in contact with solvent molecules so we must specify the polymer-polymer and polymer-solvent interactions. In general we can group the interactions into two categories: isotropic and anisotropic. The interactions between the polymers will consist of repulsive excluded volume and attractive van der Waals forces which will have both isotropic and anisotropic contributions. For a simple solvent, polymer-solvent interactions will also result from excluded volume and van der Waals forces but will be purely isotropic. We will refer to all anisotropic interactions as LC interactions.

2.2 Liquid Crystalline Interactions

Their are two popular models of LC polymers: one based on Onsagers model of rigid rods[6] and another based on the MS[7] theory.[18] Previously, most studies used the Onsager form; however, recently the MS model has become increasingly popular. This is in large part due to the generality of the MS model as compared to Onsagers. The Onsager model is specific

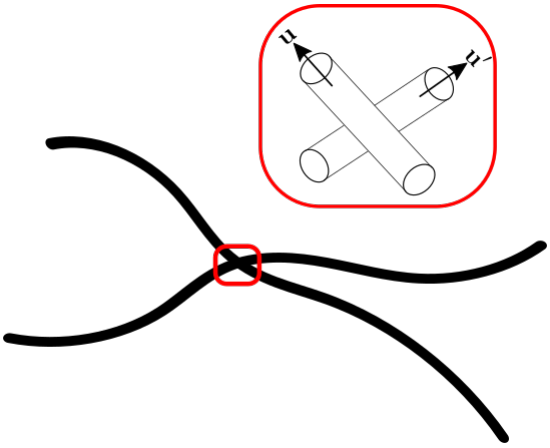

Fig 2.2. Cartoon depicting Onsager interactions between two polymers with orientation $\mathbf{u}$ and $\mathbf{u}'$ respectively. The overlapping segments are approximated as cylinders.

to rigid rods interacting purely through excluded volume, while the MS is a truncated series expansion which combines all the interactions (excluded volume, van der Waals, etc.) into one anisotropic parameter, analogous to the Flory-Huggins χ parameter for isotropic interactions. Both the Onsager and MS interactions will be discussed and compared in detail here and in subsequent sections. In general we will express the interactions between polymers indexed by α and α' as a general pair potential

$$\frac{U(\{\mathbf{r}_\alpha\})}{k_\mathrm{B}T} = \frac{1}{2}\sum_{\alpha=1}^{n_\mathrm{p}}\sum_{\alpha'=1,\alpha'\neq\alpha}^{n_\mathrm{p}}\int dsds' u(\mathbf{r}_\alpha(s),\mathbf{r}_{\alpha'}(s'),\mathbf{u}_\alpha(s),\mathbf{u}_{\alpha'}(s'))\ . \tag{2.2}$$

2.2.1 Onsager

One of the earliest models of LC interactions is the Onsager model. Consider two polymers with excluded volume interactions as depicted in Fig. 2.2. The interaction is regarded as excluded volume from cylindrical filaments characterised by a cross-sectional diameter d so the interaction between the two polymer segments is

$$u(\mathbf{r},\mathbf{r}',\mathbf{u},\mathbf{u}') = \epsilon\delta(\mathbf{r}-\mathbf{r}')|\mathbf{u}\times\mathbf{u}'| \tag{2.3}$$

where $\epsilon = 2db^2\kappa^2$ and $\delta(\mathbf{r}-\mathbf{r}')$ the Dirac delta function. Since our model is coarse-grained, d is not generally known and so ϵ is treated as an independent parameter.

This model gives rise to many of the LC phases observed in nature and provides a relatively simple qualitative description of LC polymers. The main shortcoming of this

model is that it assumes the interactions are purely excluded volume, which is in general not the case. Additionally, this model fails in the presence of solvent, where the polymer interactions are mediated by solvent molecules. This model might be reasonably accurate for a pure melt of chemically identical polymers, but in most other cases we expect it to be inaccurate, not just quantitatively but qualitatively as well.

2.2.2 Maier-Saupe

In general the interactions between two polymers will not be purely excluded volume and attractive potentials can arise from van der Waals forces, schematically depicted in Fig. 2.3. Instead of assuming a particular type of interaction, as is the case with Onsager, we instead expand the interactions in a general orientation dependent series. Convenient basis functions are the Legendre polynomials

$$u(\mathbf{r},\mathbf{r}',\mathbf{u},\mathbf{u}') = \delta(\mathbf{r}-\mathbf{r}')\sum_l \nu_l P_l(\mathbf{u}\cdot\mathbf{u}') \ , \tag{2.4}$$

defined as

$$P_l(x) \equiv \frac{1}{2^l l!}\frac{d^l}{dx^l}(x^2-1)^l \ . \tag{2.5}$$

Since the orientation of an LC is symmetric in $\mathbf{u}\to-\mathbf{u}$ all the odd terms are zero. Keeping only the first anisotropic interaction we have,

$$u(\mathbf{r},\mathbf{r}',\mathbf{u},\mathbf{u}') = \nu_0\delta(\mathbf{r}-\mathbf{r}') - \nu_2\delta(\mathbf{r}-\mathbf{r}')P_2(\mathbf{u}\cdot\mathbf{u}') \ . \tag{2.6}$$

This is what we refer to as MS interactions.

It should be noted that if we did not truncate the series, MS interactions could exactly reproduce Onsager. Consider their spherical harmonic expansion: from the addition theorem it follows that

$$|\mathbf{u}\times\mathbf{u}'| = \sum_{lm}\frac{4\pi}{4l+1}d_{2l}Y_{2l,m}(\mathbf{u})Y^*_{2l,m}(\mathbf{u}') \ , \tag{2.7}$$

where

$$d_0 = \frac{\pi}{4} \ , \ d_{2l} = \frac{-\pi(4l+1)(2l)!(2l-2)!}{2^{4l+1}(l-1)!l!(l+1)!} \ , \tag{2.8}$$

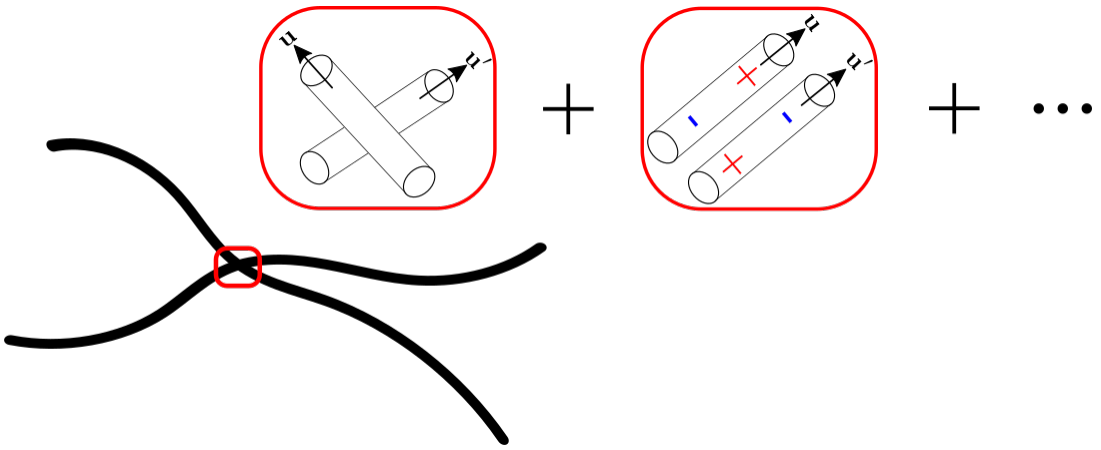

Fig 2.3. Cartoon depicting MS interactions between two polymers with orientation $\mathbf{u}$ and $\mathbf{u}'$ respectively. In contrast to the Onsager interactions which treat the polymers as rigid cylinder the MS form allows for any type. Cartoons of excluded volume of rigid rods and van der Waals forces are shown to illustrate possible repulsive and attractive potentials.

and $Y_{l,m}(\mathbf{u})$ are the spherical harmonics, defined in more detail in Appendix A. Similarly

$$\sum_l P_l(\mathbf{u}\cdot\mathbf{u}') = \sum_{lm} \frac{4\pi}{2l+1} Y_{l,m}(\mathbf{u}) Y^*_{l,m}(\mathbf{u}') \ , \tag{2.9}$$

so setting

$$\nu_0 = \epsilon\frac{\pi}{4} \ , \ \nu_{2l} = \epsilon\frac{-\pi(4l+1)(2l)!(2l-2)!}{2^{4l+1}(l-1)!l!(l+1)!} \ , \tag{2.10}$$

and $\nu_l = 0$ if l is odd reproduces the Onsager interactions.

As we show in Appendix B for a melt of polymers, the MS interactions can reproduce not only the same qualitative behaviour but quantitatively similar values for the bulk isotropic-nematic phase transition even when truncated at leading order, ν_2. Therefore, the MS interactions are more general than Onsager interactions.

2.3 Solvent Models

Solvent molecules are generally much smaller than polymers. Due to the size discrepancy and the large pervaded volume of polymers, the solvent molecules tend to be at a relatively

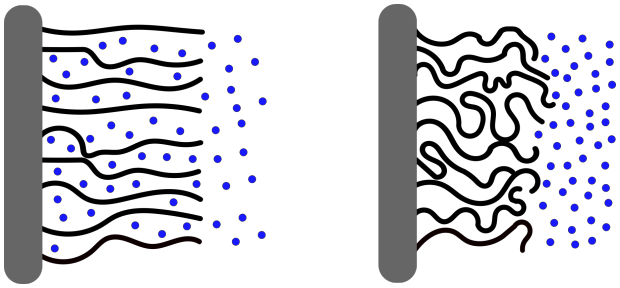

Fig 2.4. Left: Polymer brush (black) in contact with a good solvent (blue circles), since the solvent is good the brush and solvent mix. Right: Polymer brush in contact with a poor solvent, since the solvent is poor the brush and solvent phase separate.

high concentration (compared to polymers in the brush). In this work we will be considering only simple solvents, which are treated as isotropic spheres, rather than LC solvents which would be treated as rigid rods. A brush in contact with a simple solvent is schematically depicted in Fig. 2.4. Depending on the chemistry and temperature the solvent can be a *good*, *poor*, or *theta* solvent. In a good solvent the mixing entropy dominates, which causes the brush to stretch out away from the grafting plane and into the solvent. In a poor solvent intermolecular interactions dominate causing the polymers and solvents to phase separate, resulting in a collapsed brush. In a theta solvent these two contributions exactly balance and the solvent is perfectly neutral. In general, varying the temperature from high to low will always cause the solvent to go from good to theta and finally to poor; however, some solvent-polymer mixtures evaporate (crystallise) before reaching the good (poor) regime so it is not always possible to explore all three with a single combination.

Consider a mixture of n_s solvent and n_p polymer molecules in a system of volume V and temperature T. We assume each chain occupies a fixed volume $N\rho_0^{-1}$, with ρ_0 the segment density of the polymer in a pure melt. Each solvent molecule occupies a volume v_s, with the segment density chosen such that $v_\mathrm{s} = \rho_0^{-1}$. Analogously to the LC interactions, we represent the polymer solvent interactions with a pairwise potential

$$\frac{U(\{\mathbf{r}_\alpha, \mathbf{r}_k\})}{k_\mathrm{B}T} = \frac{1}{2}\sum_{\alpha=1}^{n_\mathrm{p}} \int ds \sum_{\alpha'=1}^{n_\mathrm{s}} u(\mathbf{r}_\alpha(s), \mathbf{r}_{\mathrm{s},\alpha'}) \ , \tag{2.11}$$

with the key differences being that since the solvent is isotropic we have integrated out the orientations and now we have the polymer at position $\mathbf{r}(s)$, interacting with a solvent at position $\mathbf{r}_\mathrm{s}$.

If the polymer concentration is relatively high the solvent molecules need to be modelled explicitly, but in the semi-dilute regime the solvent molecules can be modelled fully

implicitly. Generally the implicit model will be accurate provided it is a good solvent with the polymers grafted at a relatively low grafting density, while the explicit solvent model is always required for a poor solvent since the phase separation increases the polymer density and the semi-dilute approximation will break down.

2.3.1 Explicit

The most general solvent model involves explicitly solving the statistical mechanics of the solvent and polymer simultaneously. We assume that the system is locally incompressible, such that the total concentration at any point $\mathbf{r}$ is 1 in dimensionless units. The polymer-solvent interactions are described by a local pairwise interaction of the form

$$u(\mathbf{r}, \mathbf{r}') = \chi\delta(\mathbf{r} - \mathbf{r}') \ , \tag{2.12}$$

with χ the Flory-Huggins polymer-solvent interaction parameter. In general we additionally require separate polymer-polymer and solvent-solvent Flory-Huggins χ parameters; however, these terms will simply rescale the polymer-solvent interaction parameter or add a constant to the free energy and can be safely ignored.

This interaction potential, along with the LC interactions and bending energy of the worm-like chain are sufficient to specify the statistical mechanics of LC polymer brushes; however, there are further simplifications that can be made provided there are good solvent conditions. In the semi-dilute approximation, the solvent degrees of freedom can be integrated out and treated implicitly.

2.3.2 Implicit

The implicit solvent model is a mean field approximation. We combine the polymer-solvent interactions and solvent entropy into a polymer-polymer interaction representing the mean enthalpic and entropic forces acting on the polymers from the solvent assuming a semi-dilute mixture. In this way the solvent degrees of freedom can be integrated out significantly simplifying the model and reducing the parameter space. To arrive at the implicit solvent model, we assume a form of the free energy common to mean field theory.

Consider the free energy contributions from the solvent molecules within the polymer solvent mixture: there is an enthalpic contribution through the Flory-Huggins χ parameter as well as an entropic contribution through mixing. Denoting the polymer concentration

by $\phi(\mathbf{r})$ and the solvent concentration by $\phi_{\rm s}(\mathbf{r})$, we can write these contributions as

$$\frac{F}{n_{\rm p}k_{\rm B}T} = \frac{\chi\rho_0}{2}\int d\mathbf{r}\phi(\mathbf{r})\phi_{\rm s}(\mathbf{r}) - \frac{1}{v_{\rm s}}\int d\mathbf{r}\phi_{\rm s}(\mathbf{r})\ln(\phi_{\rm s}(\mathbf{r}))\ . \tag{2.13}$$

Since we have assumed incompressibility, we can express the solvent concentration as $\phi_{\rm s}(\mathbf{r}) = 1 - \phi(\mathbf{r})$, so that the free energy becomes

$$\frac{F}{n_{\rm p}k_{\rm B}T} = \frac{\chi\rho_0}{2}\int d\mathbf{r}\phi(\mathbf{r})(1-\phi(\mathbf{r})) - \frac{1}{v_{\rm s}}\int d\mathbf{r}(1-\phi(\mathbf{r}))\ln(1-\phi(\mathbf{r}))\ . \tag{2.14}$$

We now arrive at the first major approximation of the implicit solvent model, the *semi-dilute* approximation, assuming the polymer concentration is relatively low, the entropy term can be expanded in Taylor series so that the free energy becomes

$$\frac{F}{n_{\rm p}k_{\rm B}T} = \frac{\chi\rho_0}{2}\int d\mathbf{r}\phi(\mathbf{r})(1-\phi(\mathbf{r})) + \frac{1}{v_{\rm s}}\int d\mathbf{r}\left[\phi(\mathbf{r}) - \frac{\phi^2(\mathbf{r})}{2} - \mathcal{O}(\phi^3(\mathbf{r}))\right]\ . \tag{2.15}$$

Integrals over $\phi(\mathbf{r})$ give the total amount of material and just add a constant to the free energy and therefore can be ignored. Combining and dropping constant terms we arrive at

$$\frac{F}{n_{\rm p}k_{\rm B}T} = \frac{\rho_0}{2}\left(\frac{1}{v_{\rm s}\rho_0} - 2\chi\right)\int d\mathbf{r}\phi^2(\mathbf{r})\ . \tag{2.16}$$

The second simplification is to replace the polymer solvent interaction energy, Eq. (2.12), that describes the polymer-solvent interactions into a new effective potential between polymer segments (no solvent) that incorporates the solvent contributions as an average effect. This new potential takes the form

$$u(\mathbf{r},\mathbf{r}') = \nu_0\delta(\mathbf{r}-\mathbf{r}')\ , \tag{2.17}$$

where ν_0 is called the excluded volume parameter, and now it is an interaction between polymer segments,

$$\frac{U(\{\mathbf{r}_\alpha\})}{k_{\rm B}T} = \frac{1}{2}\sum_{\alpha=1}^{n_{\rm p}}\sum_{\alpha'=1,\alpha'\neq\alpha}^{n_{\rm p}}\int dsds' u(\mathbf{r}_\alpha(s),\mathbf{r}_{\alpha'}(s'))\ , \tag{2.18}$$

rather than polymer-solvent as in Eq. (2.12). By setting $\nu_0 = (v_{\rm s}\rho_0)^{-1} - 2\chi$ we arrive at an identical form for the free energy as in Eq. (2.16). We have now replaced the entropy of mixing with a mean entropic force which will stretch the polymer brush.

It is important to note some key properties of the excluded volume parameter, ν_0. If $\nu_0 > 0$ then the entropic contribution $(v_s\rho_0)^{-1}$ is dominant and the polymer will mix with the solvent resulting in good solvent conditions. When $\nu_0 = 0$, then the enthalpic contribution exactly balances the entropy of mixing and it is a theta solvent. Finally, if $\nu_0 < 0$ than the enthalpic contribution dominates causing the polymer and solvents to phase separate meaning it is a poor solvent. Since the implicit solvent model relies on the semi-dilute approximation, it is only valid for good (or theta) solvent conditions, so we are restricted to the case $\nu_0 \geq 0$ in this model.

Chapter 3

Self-Consistent Field Theory

The theoretical framework we use is self-consistent field theory (SCFT). SCFT is a mean field theory, which is an approach commonly used in statistical mechanics to describe a many body interacting system and is especially useful for describing emergent properties. By replacing the system with a single body in an external field, we can gain insight into the properties of the system while significantly reducing complexity. Since the external field represents the many body interactions, it will itself depend on the single body solution and therefore must be solved self-consistently. The particle to field transformation is schematically depicted in Fig. 3.1. In polymer physics, SCFT has been widely used to accurately describe the properties of polymeric systems, with its most notable success from attaining both qualitative and quantitative agreement with experimental results for the stable phases of block-copolymer melts.[13]

The focus of this chapter is to derive the statistical field theory and mean field approximation for the worm-like chain model with LC interactions, closely following analogous arguments as presented by Fredrickson.[77] For the purposes of calculation and the results of the following chapters only the main results are required, and could be directly cited from Fredrickson.[77] In the interest of clarity we will first summarise the main results here which constitute the full 6-dimensional (3 Cartesian, 2 polar and 1 contour) form of the equation we will be solving in subsequent chapters.

We assume each polymer occupies a fixed volume N/ρ_0 and has a fixed contour length $\ell_c = bN$, where N is the degree of polymerization, ρ_0 represents the segment density in a pure melt and b is the fixed bond length. The configuration of the α'th molecule is specified by the space curve $\mathbf{r}_\alpha(s)$, with unit tangent vector $\mathbf{u}_\alpha(s) \equiv \ell_c^{-1}\frac{d}{ds}\mathbf{r}_\alpha(s)$, where the backbone parameter runs from $s = 0$ to 1. The energetics and interactions are assumed to

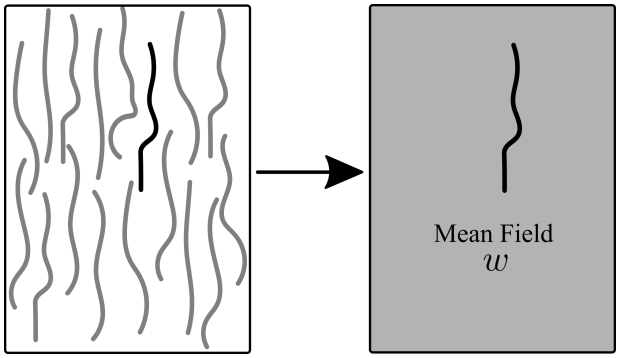

Fig 3.1. Image illustrating the particle to field transformation in SCFT. The many body interacting system of polymers on the left is averaged over and replaced by a single polymer interacting with a mean field w.

be of the form described in Chapter 2.

The partial partition function $q(\mathbf{r}, \mathbf{u}, s)$ satisfies the diffusion equation for a continuous worm-like chain in an external field $w(\mathbf{r}, \mathbf{u})$

$$\frac{\partial q(\mathbf{r}, \mathbf{u}, s)}{\partial s} + \ell_c \mathbf{u} \cdot \nabla_{\mathbf{r}} q(\mathbf{r}, \mathbf{u}, s) = \frac{\ell_c}{2\ell_p} \nabla^2_{\mathbf{u}} q(\mathbf{r}, \mathbf{u}, s) - w(\mathbf{r}, \mathbf{u}) q(\mathbf{r}, \mathbf{u}, s) \ , \tag{3.1}$$

and the reverse partial partition function $q^\dagger(\mathbf{r}, \mathbf{u}, s)$ satisfies the same equation with the left hand side multiplied by -1. Throughout, $\nabla_{\mathbf{r}}$ denotes the gradient with respect to $\mathbf{r}$ and $\nabla^2_{\mathbf{u}}$ the spherical Laplacian. In the mean field approximation the interactions from Chapter 2 are replaced by a self-consistent field, $w(\mathbf{r}, \mathbf{u})$, which satisfies

$$w(\mathbf{r}, \mathbf{u}) = N \int d\mathbf{r}' d\mathbf{u}' f(\mathbf{r}, \mathbf{r}', \mathbf{u}, \mathbf{u}') \phi(\mathbf{r}', \mathbf{u}') \ , \tag{3.2}$$

with MS interactions

$$f(\mathbf{r}, \mathbf{r}', \mathbf{u}, \mathbf{u}') = \nu_0 \delta(\mathbf{r} - \mathbf{r}') - \nu_2 \delta(\mathbf{r} - \mathbf{r}') P_2(\mathbf{u} \cdot \mathbf{u}') \ . \tag{3.3}$$

The concentration is

$$\phi(\mathbf{r}, \mathbf{u}) = \frac{1}{Q} \int ds q(\mathbf{r}, \mathbf{u}, s) q^\dagger(\mathbf{r}, \mathbf{u}, s) \ , \tag{3.4}$$

where Q is the single chain partition function, which satisfies

$$Q = \int d\mathbf{r} d\mathbf{u} \, q(\mathbf{r}, \mathbf{u}, s) q^\dagger(\mathbf{r}, \mathbf{u}, s) \ . \tag{3.5}$$

Finally, the free energy per polymer is

$$\frac{F}{n_{\mathrm{p}} k_{\mathrm{B}} T} = -\ln Q - \frac{\rho_0}{2V} \int d\mathbf{r} d\mathbf{u} w(\mathbf{r}, \mathbf{u}) \phi(\mathbf{r}, \mathbf{u}) \ . \tag{3.6}$$

It is at this point that we would like to introduce some notation for the following sections: throughout, square brackets, $g[\Phi]$, will denote a functional, a hat, $\hat{\Phi}$, an operator, $\mathcal{D}g[\Phi]/\mathcal{D}\Phi$ a functional derivative, $\int \mathcal{D}\Phi$ a functional integral and a semi colon $(a; b)$ the conditional probability of a given b.

3.1 Statistical field theory of a worm-like chain

All of the statistical mechanics of a system can be calculated provided one has knowledge of the partition function. In the canonical ensemble, the partition function can be expressed as an integral over all coordinates with probabilities taking the usual Boltzmann weighting

$$Z \propto \int \mathcal{D}\mathbf{r}_\alpha e^{-\frac{U(\{\mathbf{r}_\alpha\})}{k_{\mathrm{B}} T}} \ , \tag{3.7}$$

where Z is the canonical partition function, and U the internal energy of the system. Throughout we will be dropping any constant pre-factors multiplying Z as they will not affect any observable quantities. We will only be concerned with pairwise potentials, in which case the internal energy can be expressed as

$$U(\{\mathbf{r}_\alpha\}) = \frac{\kappa}{2N} \sum_{\alpha=1}^{n_{\mathrm{p}}} \int_0^1 ds \left| \frac{d\mathbf{u}_\alpha(s)}{ds} \right|^2 + \frac{1}{2} \sum_{\alpha=1}^{n_{\mathrm{p}}} \sum_{\alpha=1, \alpha' \neq \alpha}^{n_{\mathrm{p}}} u(\mathbf{r}_\alpha, \mathbf{r}_{\alpha'}, \mathbf{u}_\alpha, \mathbf{u}_{\alpha'}) \ , \tag{3.8}$$

as defined in Chapter 2. Introducing the microscopic density operator, $\hat{\Phi}(\mathbf{r}, \mathbf{u})$, defined as

$$\hat{\Phi}(\mathbf{r}, \mathbf{u}) \equiv \frac{N}{\rho_0} \sum_{\alpha=1}^{n_{\mathrm{p}}} \int_0^1 ds \delta(\mathbf{r} - \mathbf{r}_\alpha(s)) \delta(\mathbf{u} - \mathbf{u}_\alpha(s)) \tag{3.9}$$

and the bending energy

$$U_{\mathrm{B}}(\{\mathbf{r}_\alpha\}) = \frac{\kappa}{2N} \sum_{\alpha=1}^{n_{\mathrm{p}}} \int_0^1 ds \left| \frac{d\mathbf{u}_\alpha(s)}{ds} \right|^2 \ , \tag{3.10}$$

we can write the energy

$$\frac{U(\{\mathbf{r}_\alpha\})}{k_{\rm B}T} = U_{\rm B}(\{\mathbf{r}_\alpha\}) + \frac{\rho_0}{2V}\int d\mathbf{r}d\mathbf{r}'\hat{\Phi}(\mathbf{r})f(\mathbf{r},\mathbf{r}')\hat{\Phi}(\mathbf{r}') - \frac{1}{2}n_{\rm p}u(0)\ . \tag{3.11}$$

Here, and for the remainder of this section we suppress the explicit dependence on $\mathbf{u}$ where it is understood that dependence on, or integration over, $\mathbf{r}$ includes $\mathbf{u}$. The first two terms are the familiar form presented in Chapter 2, while the third subtracts off the self interactions and simply affects the reference chemical potential and will have no thermodynamic consequence. The partition function, Eq. (3.7), can now be expressed as

$$Z \propto \int \mathcal{D}\mathbf{r}_\alpha \exp\left[-\frac{1}{k_{\rm B}T}\left(U_{\rm B}(\{\mathbf{r}_\alpha\}) + \frac{\rho_0}{2V}\int d\mathbf{r}d\mathbf{r}'\hat{\Phi}(\mathbf{r})f(\mathbf{r},\mathbf{r}')\hat{\Phi}(\mathbf{r}')\right)\right]\ . \tag{3.12}$$

We now introduce the delta functional, $\delta[\Phi - \hat{\Phi}]$, defined by the sifting property

$$\int \mathcal{D}\Phi\delta[\Phi - \hat{\Phi}]g[\Phi] = g[\hat{\Phi}] \tag{3.13}$$

for any functional $g[\Phi]$, and express it in exponential form

$$\delta[\Phi - \hat{\Phi}] \propto \int \mathcal{D}W \exp\left(\int d\mathbf{r}W(\mathbf{r})[\Phi(\mathbf{r}) - \hat{\Phi}(\mathbf{r})]\right)\ . \tag{3.14}$$

Inserting this definition into Eq. (3.12) we have

$$\begin{aligned} Z &\propto \int \mathcal{D}\Phi\mathcal{D}\mathbf{r}_\alpha\delta[\Phi - \hat{\Phi}]\exp\left[-\frac{1}{k_{\rm B}T}\left(U_{\rm B}(\{\mathbf{r}_\alpha\}) + \frac{\rho_0}{2V}\int d\mathbf{r}d\mathbf{r}'\Phi(\mathbf{r})f(\mathbf{r},\mathbf{r}')\Phi(\mathbf{r}')\right)\right] \\ &\propto \int \mathcal{D}\Phi\mathcal{D}W\mathcal{D}\mathbf{r}_\alpha \exp\left[\int d\mathbf{r}W(\mathbf{r})[\Phi(\mathbf{r}) - \hat{\Phi}(\mathbf{r})] - \frac{1}{k_{\rm B}T}\left(U_{\rm B}(\{\mathbf{r}_\alpha\}) + \frac{\rho_0}{2V}\int d\mathbf{r}d\mathbf{r}'\Phi(\mathbf{r})f(\mathbf{r},\mathbf{r}')\Phi(\mathbf{r}')\right)\right]\ . \end{aligned} \tag{3.15}$$

Finally, integrating over the coordinates $\{\mathbf{r}_\alpha\}$ our partition function becomes

$$Z \propto \int \mathcal{D}\Phi\mathcal{D}W e^{-\frac{H[\Phi,W]}{k_{\rm B}T}}\ , \tag{3.16}$$

where the functional, now including explicit dependence on $\mathbf{u}$,

$$H[\Phi,W] = -\int d\mathbf{r}d\mathbf{u}W(\mathbf{r},\mathbf{u})\Phi(\mathbf{r},\mathbf{u}) + \frac{\rho_0}{2V}\int d\mathbf{r}d\mathbf{r}'d\mathbf{u}d\mathbf{u}'\Phi(\mathbf{r},\mathbf{u})f(\mathbf{r},\mathbf{r}',\mathbf{u},\mathbf{u}')\Phi(\mathbf{r}',\mathbf{u}') - n_{\rm p}\ln Q[W]\ , \tag{3.17}$$

is referred to as the effective Hamiltonian, and $Q[W]$ is the single chain partition function, resulting from the integration over the coordinates $\{\mathbf{r}_\alpha\}$ which factor into the product of n_p single chains with partition function

$$Q[W] = \int d\mathbf{r} d\mathbf{u} \exp\left[-\frac{\kappa}{2N}\int_0^1 ds \left|\frac{d\mathbf{u}(s)}{ds}\right|^2 - \int_0^1 ds W(\mathbf{r}(s),\mathbf{u}(s))\right] \ . \tag{3.18}$$

This is the partition function of a single worm-like chain in a field $W(\mathbf{r},\mathbf{u})$.

From this partition function we can calculate several observable quantities. A central quantity is the concentration given by the ensemble average (denoted by $\langle\cdots\rangle$) of the microscopic density operator

$$\langle\Phi(\mathbf{r},\mathbf{u})\rangle = -n_\mathrm{p}\frac{\mathcal{D}\ln Q[W]}{\mathcal{D}W(\mathbf{r},\mathbf{u})} \ . \tag{3.19}$$

which is conjugate to the field, W.

We have now transformed the system into an integral over two fluctuating fields Φ and W. All the transformations thus far have been exact and could, at least in principle, be calculated through functional integral techniques or simulated through (field theoretic) Monte-Carlo or Langevin simulation; however, analytic techniques are virtually non-existent for this model and the current simulation methods are computationally intensive. Even the much simpler Gaussian chain model runs into difficulties. Therefore, our approach will be to invoke the saddle point approximation, which will allow us to replace the fluctuating fields W and Φ with their average in the usual mean field sense.

3.2 Mean Field Approximation

Explicitly, the mean field approximation, referred to as SCFT, amounts to evaluating the partition function, Eq. (3.16), in the saddle point approximation. We assume the integral is dominated by field configurations $w(\mathbf{r},\mathbf{u})$ and $\phi(\mathbf{r},\mathbf{u})$ obtained from the saddle points of the effective Hamiltonian, Eq. (3.17),

$$\left.\frac{\mathcal{D}H[\Phi,W]}{\mathcal{D}W(\mathbf{r},\mathbf{u})}\right|_{\phi,w} = \left.\frac{\mathcal{D}H[\Phi,W]}{\mathcal{D}\Phi(\mathbf{r},\mathbf{u})}\right|_{\phi,w} = 0 \ . \tag{3.20}$$

The derivative with respect to the W field yields

$$\phi(\mathbf{r},\mathbf{u}) = -n_\mathrm{p}\left.\frac{\mathcal{D}\ln Q[W]}{\mathcal{D}W(\mathbf{r},\mathbf{u})}\right|_{\phi,w} = \langle\Phi(\mathbf{r},\mathbf{u})\rangle_w \ , \tag{3.21}$$

which implies that in the saddle point approximation the ϕ field corresponds to the average segment density, i.e. the concentration, of a single chain in the field $w(\mathbf{r},\mathbf{u})$. The derivative with respect to the Φ field results in the self-consistent field equation

$$w(\mathbf{r},\mathbf{u}) = N\int d\mathbf{r}'d\mathbf{u}' f(\mathbf{r},\mathbf{r}',\mathbf{u},\mathbf{u}')\phi(\mathbf{r}',\mathbf{u}') \ . \tag{3.22}$$

The field $w(\mathbf{r},\mathbf{u})$ depends exclusively on the concentration, $\phi(\mathbf{r}',\mathbf{u}')$, of a single chain in the field, $w(\mathbf{r},\mathbf{u})$. Therefore all that remains is to evaluate this single chain partition function for a worm-like chain in an external (but self-consistent) field.

3.3 Worm-like Chain in an External Field

In order to evaluate the single chain partition function, Eq. (3.18), we will use methods in analogy to stochastic processes. The goal is to get the Fokker-Planck equation. This is analogous to the Feynman-Kac transformation in quantum mechanics. Consider the partial partition function of a constrained chain $q(\mathbf{r},\mathbf{u},s)$, which represent the probability density that the end of a worm-like chain with contour length s is at position $\mathbf{r}$ and the tangent vector of the end segment is $\mathbf{u}$. We can express the partial partition function in the form of a Chapman-Kolmogorov equation as

$$q(\mathbf{r},\mathbf{u},s+\Delta s) = \int d(\Delta\mathbf{r})\int d(\Delta\mathbf{u})T_{\mathrm{r}}(\Delta\mathbf{r},\Delta\mathbf{u};\mathbf{r}-\Delta\mathbf{r},\mathbf{u}-\Delta\mathbf{u})q(\mathbf{r}-\Delta\mathbf{r},\mathbf{u}-\Delta\mathbf{u},s) \ . \tag{3.23}$$

with T_{r} the transition probability. We can write the relation between $\mathbf{r}$ and $\mathbf{u}$ as (recall $\mathbf{u}(s) = \ell_c^{-1}\frac{d}{ds}\mathbf{r}(s)$)

$$\Delta\mathbf{r} = \ell_c\int_s^{s+\Delta s} ds\mathbf{u}(s) = \ell_c\mathbf{u}\Delta s + \mathcal{O}(\Delta s^2) \ . \tag{3.24}$$

Thus, to first order in Δs we can treat $\mathbf{r}$ as deterministic since all the stochastic nature is contained in $\mathbf{u}$. The transition probability then has the form

$$T_{\mathrm{r}}(\Delta\mathbf{r},\Delta\mathbf{u};\mathbf{r},\mathbf{u}) = t_{\mathrm{r}}(\Delta\mathbf{u};\mathbf{r},\mathbf{u})\delta(\Delta\mathbf{r}-\mathbf{u}\Delta s) \tag{3.25}$$

with t_{r} the new transition probability. Substituting this leads to the simplified Chapman-Kolmogorov equation

$$q(\mathbf{r},\mathbf{u},s+\Delta s) = \int d(\Delta\mathbf{u})t_{\mathrm{r}}(\Delta\mathbf{u};\mathbf{r},\mathbf{u}-\Delta\mathbf{u})q(\mathbf{r},\mathbf{u}-\Delta\mathbf{u},s) \ . \tag{3.26}$$

Expanding to order Δs on the left hand side and to order $\Delta \mathbf{u}^2$ on the right-hand side leads to

$$\Delta s \left[\frac{\partial}{\partial s} + \ell_c \mathbf{u} \cdot \nabla_{\mathbf{r}} + w(\mathbf{r}, \mathbf{u}) \right] q(\mathbf{r}, \mathbf{u}, s) + \mathcal{O}(\Delta s^2) = - \nabla_{\mathbf{u}} \cdot [\langle \Delta \mathbf{u} \rangle_{t_r} q(\mathbf{r}, \mathbf{u}, s)] + \frac{1}{2} \nabla_{\mathbf{u}} \nabla_{\mathbf{u}} : [\langle \Delta \mathbf{u} \Delta \mathbf{u} \rangle_{t_r} q(\mathbf{r}, \mathbf{u}, s)] + \mathcal{O}(\langle \Delta \mathbf{u} \Delta \mathbf{u} \Delta \mathbf{u} \rangle_{t_r}) \ . \tag{3.27}$$

Here the angle brackets denote and average with respect to the transition probability $t_r \approx e^{\Delta U_B / k_B T}$, with $\Delta U_B \equiv \kappa |\Delta \mathbf{u}|^2 / (2N)$ (field term just adds constant in the integral over $\Delta \mathbf{u}$). The transition probability is Gaussian since we have $\Delta \mathbf{u}$ constrained to the unit sphere so we can write

$$\frac{\Delta U_B}{k_B T} = \frac{\kappa}{2N \Delta s} |\Delta \mathbf{u}|^2 = \frac{\kappa}{2N \Delta s} [(\Delta \theta)^2 + (\sin \theta \Delta \varphi)^2] \ . \tag{3.28}$$

Thus the transition probability has first and second moments

$$\langle \Delta \mathbf{u} \rangle_{t_r} = 0 \ , \ \langle \Delta \mathbf{u} \Delta \mathbf{u} \rangle_{t_r} = \frac{N \Delta s}{\kappa} (e_\theta e_\theta + e_\phi e_\phi) \tag{3.29}$$

Substituting this into Eq. (3.27) gives the desired Fokker-Planck, or diffusion, equation

$$\frac{\partial q(\mathbf{r}, \mathbf{u}, s)}{\partial s} + \ell_c \mathbf{u} \cdot \nabla_{\mathbf{r}} q(\mathbf{r}, \mathbf{u}, s) = \frac{\ell_c}{2 \ell_p} \nabla_{\mathbf{u}}^2 q(\mathbf{r}, \mathbf{u}, s) - w(\mathbf{r}, \mathbf{u}) q(\mathbf{r}, \mathbf{u}, s) \ , \tag{3.30}$$

where we have used $N / \kappa = \ell_c / \ell_p$.

From the partial partition function, we can calculate the unconstrained single chain partition function as

$$Q = \int d\mathbf{r} d\mathbf{u} \, q(\mathbf{r}, \mathbf{u}, s) q^\dagger(\mathbf{r}, \mathbf{u}, s) \ , \tag{3.31}$$

where $q^\dagger$ is the partial partition function starting at the other end of the chain, $s = 1$, and satisfies Eq. (3.30) with the left hand side multiplied by -1. Similarly, the concentration is

$$\phi(\mathbf{r}, \mathbf{u}) = \frac{1}{Q} \int ds q(\mathbf{r}, \mathbf{u}, s) q^\dagger(\mathbf{r}, \mathbf{u}, s) \ . \tag{3.32}$$

Finally, the free energy per polymer is

$$\frac{F}{n_p k_B T} = - \ln Q - \frac{\rho_0}{2V} \int d\mathbf{r} d\mathbf{u} w(\mathbf{r}, \mathbf{u}) \phi(\mathbf{r}, \mathbf{u}) \ . \tag{3.33}$$

where the second term subtracts off the double counting from the polymers interacting with a mean field.

Chapter 4

Extended State

We begin our study of LC polymer brushes in a simple solvent using self-consistent field theory and assuming azimuthal symmetry, symmetry in rotations about the axis perpendicular to the grafting plane. The polymers are modelled as worm-like chains with MS interactions. For good solvent conditions and comparatively weak LC interactions the brush is strongly stretched and aligns along the axis perpendicular to the grafting plane. In the flexible limit, with only isotropic interactions, the brush approaches the parabolic profile predicted by Milner, Witten and Cates[15] with the characteristic depletion layer and tail predicted by numerical SCFT.[17] For semi-flexible polymers, the profile deviates significantly due to the finite extensibility of worm-like chains and continuously transforms into an extended nematic state with increasing LC interaction strength.

4.1 Theory

Consider a brush of n_p polymers grafted to a flat substrate of area, $\mathcal{A}$, at $z = 0$, immersed in a solvent of n_s molecules. Each polymer consists of N segments of length b, giving a total contour length of $\ell_c = bN$. The configuration of the polymer chain is specified by the space curve $\mathbf{r}(s)$, where the backbone parameter runs from $s = 0$ at the grafted end to 1 at the free end. The orientation of the chain is then given by the unit vector $\mathbf{u}(s) = \ell_c^{-1} \frac{d}{ds}\mathbf{r}(s)$.

Treating the solvent implicitly also allows the grafting density, $\sigma = n_p/\mathcal{A}$, to be absorbed into the scaled concentration

$$\phi(z, \mathbf{u}) \equiv \frac{b\rho_0}{\sigma} \langle \phi(\mathbf{r}, \mathbf{u}) \rangle \ , \tag{4.1}$$

which is normalized such that

$$\frac{1}{\ell_c}\int dz\phi(z) = 1 \ , \tag{4.2}$$

where $\phi(z) = \int d\mathbf{u}\phi(z,\mathbf{u})$. Note that we assume the grafting density is sufficient that there is no need to constrain the lateral position of the grafting points, which implies that ensemble-average concentrations will have no x or y dependence. In terms of the scaled concentrations, the field equation, Eq. (3.2), becomes

$$w(z,\mathbf{u}) = \int d\mathbf{u}' G(\mathbf{u},\mathbf{u}')\phi(z,\mathbf{u}') \ , \tag{4.3}$$

where

$$G(\mathbf{u},\mathbf{u}') = \Lambda_0 - \Lambda_2 P_2(\mathbf{u}\cdot\mathbf{u}') \tag{4.4}$$

involves the reduced interaction parameters

$$\Lambda_0 \equiv \frac{\nu_0\sigma N}{b\rho_0} \ , \ \Lambda_2 \equiv \frac{\nu_2\sigma N}{b\rho_0} \ . \tag{4.5}$$

The SCFT requires us to solve the statistical mechanics for the partition function, Eq. (3.18), of a single polymer in the field with the s segment fixed at position $\mathbf{r}$ with orientation $\mathbf{u}$, which divides the molecule into two parts. The partition function of the constrained chain can be written as the product, $q(z,\mathbf{u},s)q^\dagger(z,\mathbf{u},s)$, of partial partition functions for the two parts of the molecule. The $q(z,\mathbf{u},s)$ for the part of the chain with the grafted end satisfies the differential equation, Eq. (3.1), in reduced coordinates,

$$\frac{\partial q}{\partial s} + \ell_c u_z \frac{\partial q}{\partial z} = \frac{\ell_c}{2\ell_p}\nabla^2_{\mathbf{u}} q - wq \ , \tag{4.6}$$

with $u_z = \cos(\theta)$ the component of the molecular axis along the z coordinate and an initial condition $q(z,\mathbf{u},0) = g(z)$. The grafting function, $g(z)$, typically taking a similar form as a delta function. The $q^\dagger$ for the part of the chain with the free end satisfies Eq. (4.6) with the left hand side multiplied by -1 subject to $q^\dagger(z,\mathbf{u},1) = 1$. The boundary conditions are a fixed at $q(0,\mathbf{u},s) = q^\dagger(0,\mathbf{u},s) = 0$ and $q(\infty,\mathbf{u},s) = q^\dagger(\infty,\mathbf{u},s) = 0$, the former corresponding to an impenetrable wall and the latter is due to finite extensibility of the worm-like chain.

Once the partial partition functions are known, the distribution of polymers is

$$\phi(z,\mathbf{u}) = \frac{\ell_c}{Q}\int_0^1 dsq(z,\mathbf{u},s)q^\dagger(z,\mathbf{u},s) \ , \tag{4.7}$$

where

$$Q = \int dz d\mathbf{u}\, q(z,\mathbf{u},s) q^{\dagger}(z,\mathbf{u},s) \ , \tag{4.8}$$

is a partition function of an unconstrained chain. Note that the integration in Eq. (4.8) is independent of s. The field must be adjusted such that $\phi(z,\mathbf{u})$ satisfies Eq. (4.3).

The orientational order of the polymer chains can be characterized by the tensor order parameter,[18,77,80]

$$\mathcal{Q}_{ij}(z) = \frac{3}{2\phi(z)} \int d\mathbf{u} \left(u_i u_j - \frac{\delta_{ij}}{3} \right) \phi(z,\mathbf{u}) \ , \tag{4.9}$$

where $i,j \in \{x,y,z\}$. The Kronecker delta is included to make the tensor traceless (i.e., $\mathrm{Tr}\mathcal{Q} = 0$). The symmetric tensor can be expressed in the diagonal form

$$\mathcal{Q}_{ij} = \frac{3\mathcal{S}}{2} \left(n_i n_j - \frac{\delta_{ij}}{3} \right) + \frac{\mathcal{P}}{2} \left(l_i l_j - m_i m_j \right) \ , \tag{4.10}$$

where $\mathbf{n}$, $\mathbf{l}$ and $\mathbf{m}$ are three orthogonal eigenvector, referred to as unit directors. The largest eigenvalue corresponding to the nematic director, $\mathbf{n}$, defines the uniaxial order parameter, $\mathcal{S}(z)$, which takes on values between zero for an isotropic phase and one for a fully-ordered nematic phase. The difference between the two smallest eigenvalues defines the biaxial order parameter, $\mathcal{P}(z)$.

The field equation often has multiple solutions corresponding to different metastable phases, and so we need to evaluate their free energy to determine which is the stable equilibrium phase. In mean-field theory, the free energy is given by Eq. (3.6) but here we replace the field with MS interactions using Eq. (4.3),

$$F = -n_p k_B T \ln Q - \frac{1}{\ell_c} \int dz U(z) \ . \tag{4.11}$$

The logarithmic term provides the free energy of n_p chains in the mean field, which double counts the interaction energy. To correct for this, the second term subtracts U_{total}, where the energy density can be expressed as

$$\begin{aligned} \frac{U(z)}{n_p k_B T} &= \frac{1}{2} \int d\mathbf{u} d\mathbf{u}' \phi(z,\mathbf{u}) G(\mathbf{u},\mathbf{u}') \phi(z,\mathbf{u}') \ , \\ &= \left(\frac{\Lambda_0}{2} - \frac{\Lambda_2}{3} \mathrm{Tr}\mathcal{Q}^2(z) \right) \phi^2(z) \ , \\ &= \frac{1}{2} \left[\Lambda_0 - \Lambda_2 \left(\mathcal{S}^2(z) + \frac{\mathcal{P}^2(z)}{3} \right) \right] \phi^2(z) \ . \end{aligned} \tag{4.12}$$

The partial partition functions, q and $q^\dagger$ are solved according to the numerical scheme described in A.2, q with a grafted initial condition $q(z, \mathbf{u}, 0) = g(z)$, where $g(z)$ is a grafting function, typically taking a similar form as a delta function. $q^\dagger$ is the partial partition function starting at the free end of the chain and has a free initial condition $q^\dagger(z, \mathbf{u}, 0) = 1$. The boundary conditions are a fixed 0 condition for both the partial partition functions at $z = 0$ and $z = \infty$, the former corresponding to an impenetrable wall and the latter is due to finite extensibility of the worm-like chain. The field must be adjusted such that the concentration satisfies the field equation, Eq. (4.3). To avoid potential divergences in the algorithm we graft the polymer a small distance dz from the interface and approximate the delta function with a strongly peaked Gaussian, $g(z) = \exp[-(z/\xi)^2]$, where $\xi = \ell_c/32$ controls the sharpness of the peak. For accurate comparisons with SST in Fig. 4.1 and 4.2 we use a grid spacing of $dz = \ell_c/3200$, $ds = 1/3200$ and $n_{LP} = 10$, with n_{LP} the number of Legendre polynomials. For the shorter chains, (more rigid) we find a grid spacing of $dz = \ell_c/800$, $ds = 1/800$ and $n_{LP} = 10$ to be sufficient.

4.2 Results

We begin by examining the flexible limit with no LC interactions. In this case, the parabolic profile predicted by SST for Gaussian chains is achieved in the flexible limit $\ell_c \gg \ell_p$ provided classical brush height,[17]

$$L = \left(\frac{8\Lambda_0 \ell_p}{\pi^2 \ell_c}\right)^{1/3} \ell_c \ , \tag{4.13}$$

is larger than the average end-end length, R_0, but significantly smaller than the contour length, ℓ_c, which implies $R_0 \ll L \ll \ell_c$. In the flexible limit, $R_0 \approx \sqrt{2\ell_p \ell_c}$ for a worm-like chain.[77] The concentration from SST is

$$\phi^{\mathrm{SST}}(z) = \frac{3R_0}{2L^3}(L^2 - z^2) \ , \tag{4.14}$$

with end-segment distribution

$$\phi_{\mathrm{e}}^{\mathrm{SST}}(z) = \frac{3zR_0}{L^3}\sqrt{L^2 - z^2} \ . \tag{4.15}$$

Within our model the distribution of end segments is found by calculating

$$\phi(z, s) = \frac{\ell_c}{Q} \int d\mathbf{u} q(z, \mathbf{u}, s) q^\dagger(z, \mathbf{u}, s) \ , \tag{4.16}$$

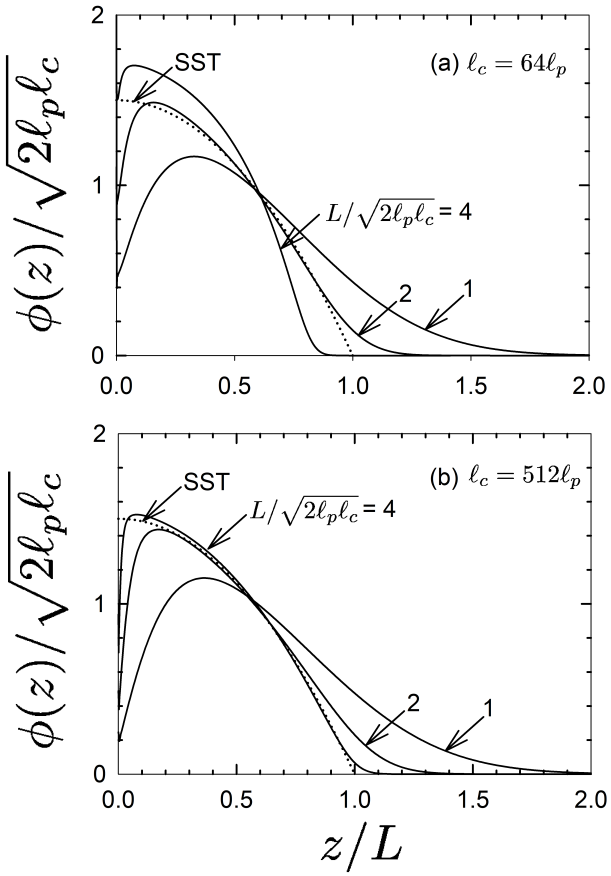

Fig 4.1. (a) Brush profiles, $\phi(z)$, for interactions corresponding to $L/\sqrt{2\ell_p\ell_c} = 1$, 2, 4 and $\Lambda_2 = 0$, calculated for flexible worm-like chains of (a) $\ell_c = 64\ell_p$ and (b) $\ell_c = 512\ell_p$. The dotted curve shows the classical profile predicted by SST for Gaussian chains with no LC interactions.

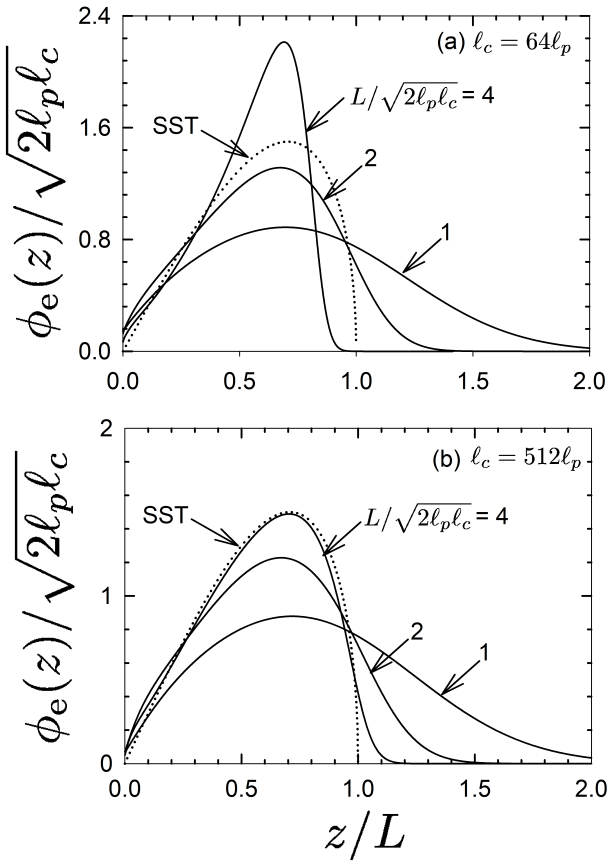

Fig 4.2. (a) Chain end distributions, $\phi_e(z)$, for interactions corresponding to $L/\sqrt{2\ell_p\ell_c} = 1$, 2, 4 and $\Lambda_2 = 0$, calculated for flexible worm-like chains of (a) $\ell_c = 64\ell_p$ and (b) $\ell_c = 512\ell_p$. The dotted curve shows the classical profile predicted by SST for Gaussian chains with no LC interactions.

and setting $s = 1$, that is $\phi_e(z) = \phi(z, 1)$.

Fig. 4.1 shows the concentration profiles as the isotropic interactions, $L/\sqrt{2\ell_p\ell_c} \sim \Lambda_0^{1/3}$, is increased for worm-like chains of different flexibility, ℓ_c/ℓ_p, in the absence of LC interactions (i.e., $\Lambda_2 = 0$). The polymers in Fig. 4.1(a) approach the prediction from SST as the classical height increases from $L/\sqrt{2\ell_p\ell_c} = 1$ to 2, corresponding to weak to intermediate stretching. However, when $L/\sqrt{2\ell_p\ell_c} = 4$ the classical height is roughly 70% of the total contour length, so the profile deviates significantly from the prediction from SST since it ignores the finite extensibility of the polymer. Similar behaviour is observed in 4.1(b) for the more flexible polymers. In this case, the profile for $L/\sqrt{2\ell_p\ell_c} = 4$ is very close to the SST prediction, but we can already begin to observe the effects of finite extensibility even for this very flexible polymer. For $L/\sqrt{2\ell_p\ell_c} = 4$, the concentration near the grafting plane has already increased past the SST prediction, despite the relatively small classical height of 25% of the total contour length. Although small, this deviation will become more significant for stronger stretching.

Analogous plots of the distribution of free ends, $\phi_e(z)$, shown in Fig. 4.1 display similar deviation from SST predictions. Most notably as the more rigid chains in (a) become strongly stretched $L/\sqrt{2\ell_p\ell_c} = 4$, the distribution is sharper than that predicted by SST. In fact, as $L \to \infty$ the end distribution will approach a delta function with all the ends concentrated at $z = \ell_c$. As was discussed previously by Deng *et al.*,[21] we can conclude that SST is valid in the intermediate stretching regime. As a general rule, in order for SST to be valid we require $\ell_c \gg \ell_p$ and $R_0 \ll L \ll \ell_c$, and as a rule of thumb we find $2R_0 \lesssim L \lesssim \frac{1}{4}\ell_c$ to be sufficient.

In order to explore the possible LC phases of the brush, we now turn our attention to more rigid polymers with increasing LC interaction strength. Fig. 4.3 shows the concentration profiles as the LC interactions, Λ_2, are increased for worm-like chains ranging from semi-flexible, $\ell_c = 16\ell_p$, to rigid, $\ell_c = \ell_p$. In the absence of LC interactions (i.e., $\Lambda_2 = 0$), the most flexible polymers in Fig. 4.3(a) have a parabolic-like profile, similar to that predicted by SST for flexible Gaussian chains. In this case, the classical brush height, Eq. (4.13), is nearly 80% of the polymer contour length, ℓ_c. Naturally, there is a significant deviation from the classical profile. In any case, increasing the LC interaction, Λ_2, and reducing the flexibility, ℓ_c/ℓ_p, both cause the profile to deviate from the parabolic-like profile toward a step-like profile of height ℓ_c. For the most rigid polymer with strong LC interactions, the concentration profile extends slightly beyond the contour length of the polymers; this is because we used a sharply peaked Gaussian for the grafting function, $g(z)$, rather than a Dirac delta function.

Fig. 4.4 shows the corresponding distribution of free ends as the LC interactions, Λ_2, are

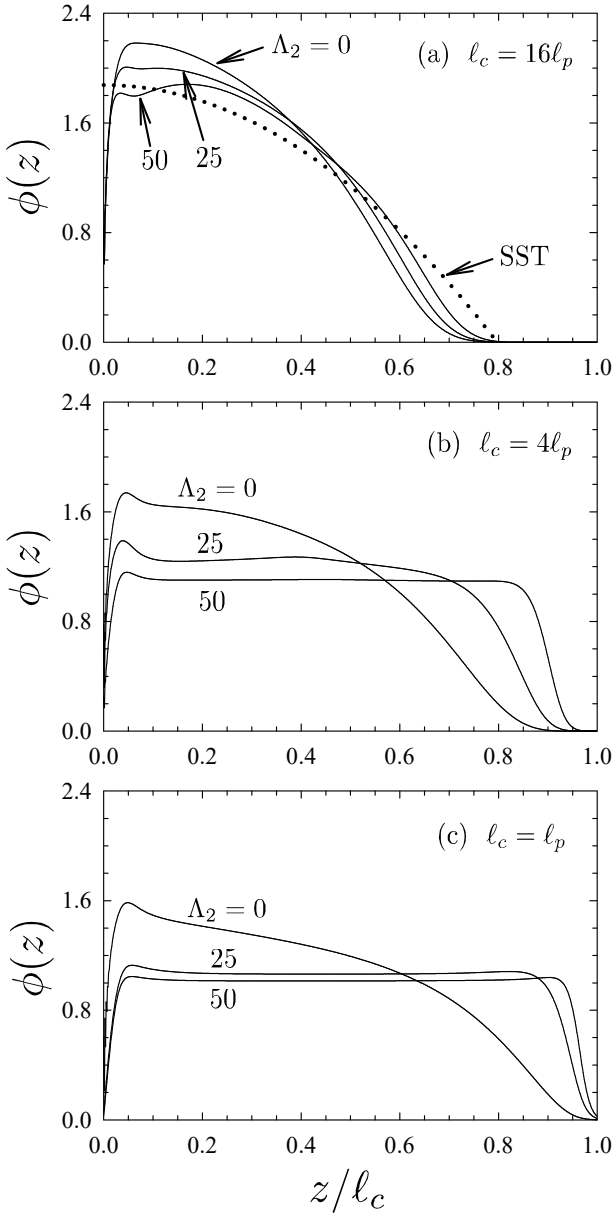

Fig 4.3. Concentration profiles, $\phi(z)$, corresponding to $\Lambda_0 = 10$ and $\Lambda_2 = 0$, 25, and 50, calculated for worm-like chains of (a) $\ell_c = 16\ell_p$, (b) $\ell_c = 4\ell_p$, and (c) $\ell_c = \ell_p$. The dotted curve in (a) denotes the parabolic profile predicted by SST for Gaussian chains with no LC interactions.

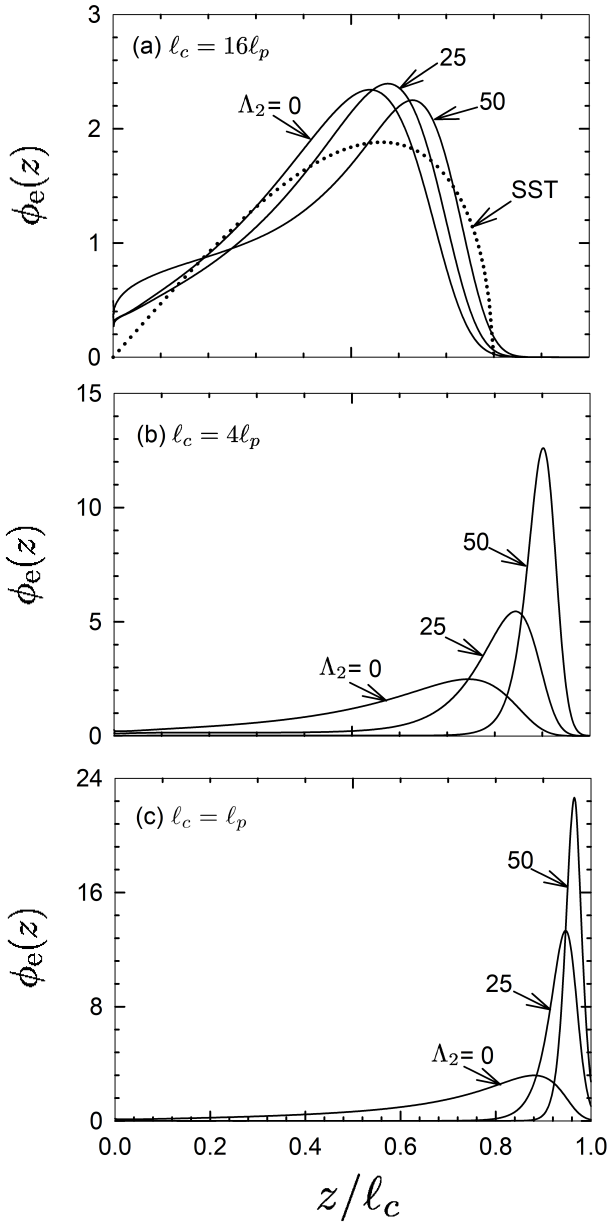

Fig 4.4. (a) Chain end distributions, $\phi_e(z)$, for interactions corresponding to $\Lambda_0 = 10$ and $\Lambda_2 = 0$, 25, and 50, calculated for worm-like chains of (a) $\ell_c = 16\ell_p$, (b) $\ell_c = 4\ell_p$, and (c) $\ell_c = \ell_p$. The dotted curve in (a) shows the classical profile predicted by SST for Gaussian chains with no LC interactions.

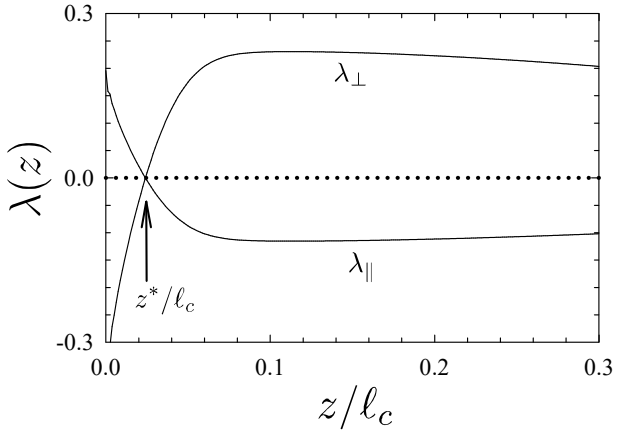

Fig 4.5. Eigenvalues of the tensor order parameter, $\mathcal{Q}_{ij}(z)$, for worm-like chains of $\ell_c = 16\ell_p$ with interaction parameters of $\Lambda_0 = 10$ and $\Lambda_2 = 25$. The eigenvalue $\lambda_\perp(z)$ corresponds to an eigenvector in the z direction and the two degenerate eigenvalues $\lambda_\parallel(z)$ correspond to eigenvectors in the x-y plane. Their crossing point defines z^*.

increased. In the absence of LC interactions (i.e., $\Lambda_2 = 0$), the most flexible polymers in Fig. 4.3(a) have ends distributed throughout the brush, similar to the prediction from SST for flexible Gaussian chains. Just as for the total concentration, the free end distribution still deviates significantly from the SST prediction since the classical brush height, Eq. (4.13), is nearly 80% of the polymer contour length, ℓ_c. For the more rigid cases in (b) and (c), for strong LC interactions, the end segment distribution is sharply peaked at the edge of the brush, similar to the Alexander-de Gennes approximation. This is due to the high degree of nematic order.

To assess the orientation of the polymer chains, we diagonalize the tensor order parameter, $\mathcal{Q}_{ij}(z)$, defined in Eq. (4.9). Under the azimuthal symmetry, the tensor has a single eigenvalue, $\lambda_\perp(z)$, corresponding to an eigenvector in the z direction, and two degenerate eigenvalues, $\lambda_\parallel(z)$, corresponding to eigenvectors in the x-y plane. Given that $\mathcal{Q}_{ij}(z)$ is traceless, it follows that $\lambda_\perp(z) + 2\lambda_\parallel(z) = 0$, and thus $\lambda_\perp(z)$ and $\lambda_\parallel(z)$ have opposite signs. As shown in Fig. 4.5, there is a point near the surface, $z = z^*$, where the eigenvalues simultaneously switch sign. This implies that the polymer chains are generally oriented perpendicular to the grafting surface, except in the vicinity of the surface (i.e., $z < z^*$) where they tend to orient parallel to the surface. This is consistent with a general trend for worm-like chains to align parallel to surfaces and interfaces;[81,82] however, we do find that the length of the parallel region depends relatively strongly on the width of our grafting function, $g(z)$, and therefore would require a more accurate grafting function to conclusively determine the behaviour near the grafting plane.

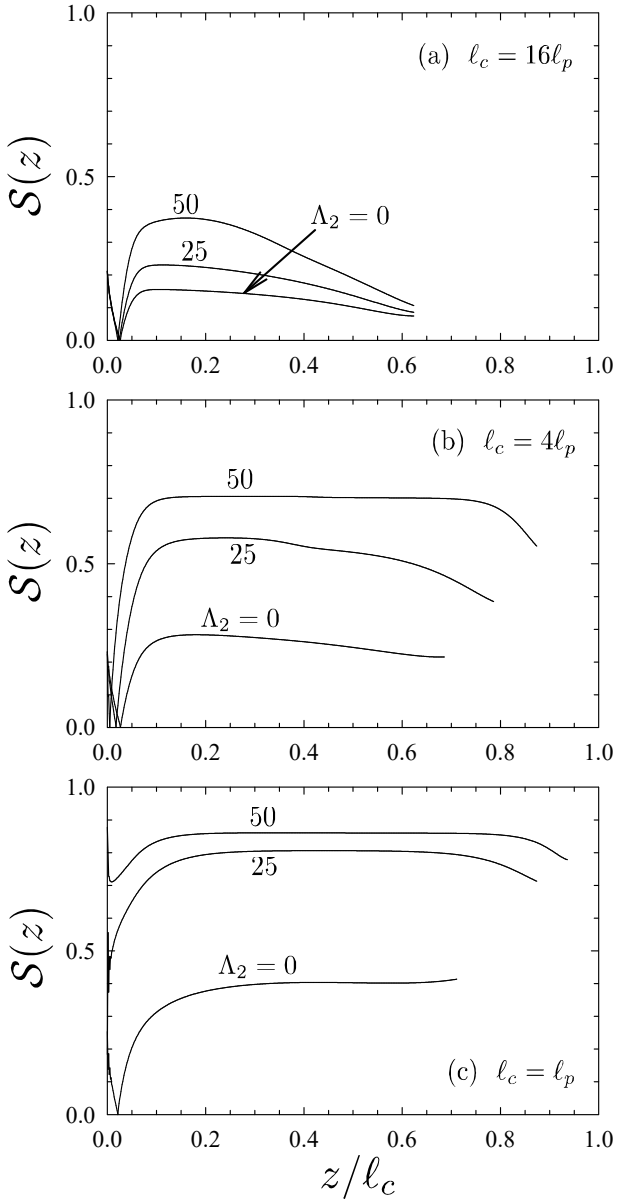

Fig 4.6. Uniaxial order parameter, $\mathcal{S}(z)$, corresponding to $\Lambda_0 = 10$ and $\Lambda_2 = 0$, 25, and 50, calculated for worm-like chains of (a) $\ell_c = 16\ell_p$, (b) $\ell_c = 4\ell_p$, and (c) $\ell_c = \ell_p$.

By convention, the uniaxial order parameter, $\mathcal{S}(z)$, is defined as the largest eigenvalue, and the corresponding eigenvector defines the nematic director $\mathbf{n}$. Thus, the director is oriented in the x-y plane near the surface and switches to the z direction away from the surface. From the decomposition of $\mathcal{Q}_{ij}(z)$ in Eq. (4.10), it follows that the biaxial order parameter takes on the value $\mathcal{P}(z) = \frac{3}{2}\lambda_{\perp}(z)$ in the surface region, $z < z^*$, and then $\mathcal{P}(z) = 0$ in the region beyond, $z > z^*$.

The dependence of the uniaxial order parameter, $\mathcal{S}(z)$, on the system parameters is illustrated in Fig. 4.6. Note that it becomes computationally difficult to determine $\mathcal{S}(z)$ as the polymer concentration approaches zero, and so the curves are only plotted for $\phi(z) \gtrsim 0.01$. As expected, $\mathcal{S}(z)$ is smallest for our most flexible chains, $\ell_c = 16\ell_p$, without LC interactions, $\Lambda_2 = 0$. Reducing the flexibility, ℓ_c/ℓ_p, and increasing the LC interaction, Λ_2, and both cause an increase in orientational order. Indeed, $\mathcal{S}(z)$ approaches the maximum allowed value of one for the most rigid polymer, $\ell_c = \ell_p$, with the strongest LC interaction, $\Lambda_2 = 50$. In all cases, the region of parallel alignment with the wall shrinks as the LC interactions increase in strength.

4.3 Discussion

The Gaussian chain model that is the basis for the parabolic profile is infinitely extensible; therefore, it results in unphysical behaviour as the brush height approaches the contour length of the polymer. The worm-like chain model is the natural extension to account for finite extensibility. Consistent with previous calculations,[21] we find that for flexible chains the brush profile agrees with the parabolic profile in an intermediate stretching regime. For intermediate stretching, the deviations from the parabolic profile such as the depletion layer near the grafting plane and exponentially-decaying tail at the outer edge of the brush are completely consistent with those predicted by numerical SCFT of Gaussian chains. As the brush becomes strongly stretched and the brush height approaches the contour length of the polymer, we observe significant deviations from the parabolic profile. In fact, in the strong stretching limit, the step profile predicted by Alexander and de Gennes would be a better approximation. As a general rule, in order for the parabolic profile to be valid, we require $\ell_c \gg \ell_p$ and $R_0 \ll L \ll \ell_c$, and as a rule of thumb, we find $2R_0 \lesssim L \lesssim \frac{1}{4}\ell_c$ to be sufficient. For semi-flexible, $\ell_c \sim 16\ell_p$, or rigid polymers, $\ell_c \sim 4\ell_p$, the parabolic profile is inappropriate and this effect is further exacerbated by LC interactions. Therefore, for many bio and LC polymers, which tend to range from semi-flexible to rigid, the worm-like chain model is necessary for an accurate description of the brush.

One of the main benefits of the worm-like chain model is that it accounts for the

orientation of individual polymer segments. This allows us to explore the possible LC phases of the brush. In the absence of LC interactions, since the brush is strongly stretched, it already possesses a relatively high degree of nematic order, aligning along the axis normal to the grafting plane. As LC interactions are increased, this order increases resulting in a continuous transformation, i.e. no transition, into an extended nematic phase. This is in contrast to the isotropic-nematic transition observed for a melt of polymers in Appendix B, where the transition is first order. The continuous transformation from strongly stretched to extended nematic is consistent with previous results for a brush of worm-like chains with Onsager interactions.[21] An interesting behaviour is observed near the grafting plane. The alignment of the polymer brush rapidly switches from perpendicular to parallel alignment. This is caused by the loss of translational entropy as the density goes to zero at the grafting plane due its impenetrability. This behaviour is generally seen for LC polymers near interfaces with and without LC interactions.[82,81]

4.4 Summary

We have investigated semi-dilute main-chain LC polymer brushes in good solvent, using SCFT for worm-like chains with MS interactions. The calculation assumes sufficient overlap among the polymers such that the brush has no lateral structure (i.e., no dependence on x and y), but a small enough polymer concentration such that the solvent can be treated implicitly. Under these assumptions, the grafting density and solvent size can be scaled out of the problem, reducing the number of system parameters to three: the scaled isotropic interaction strength Λ_0, the scaled anisotropic LC interaction strength Λ_2, and the number of persistence lengths per chain ℓ_c/ℓ_p. Our study focuses on good solvent conditions that favour an extended brush (i.e., $\Lambda_0 > 0$) for polymers ranging from flexible (i.e., $\ell_c = 512\ell_p$) to relatively rigid (i.e., $\ell_c = \ell_p$).

Our study begins by considering the effects of finite extensibility on strongly stretched flexible polymers. For intermediate amounts of stretching $2R_0 \lesssim L \lesssim \frac{1}{4}\ell_c$ the concentration and end distribution are in good agreement with the SST of Milner, Witten and Cates[15] with the usual deviation from SST from the depletion layer near the grafting plane and exponentially decaying tail at the free end predicted by numerical SCFT of Gaussian chains.[17] Once the brush height approaches the contour length of the polymers, we observe significant deviations.

In addition to isotropic interactions, our model allows us to consider LC interactions and to observe the orientational ordering of the brush for polymers ranging from semi-flexible (i.e., $\ell_c = 16\ell_p$) to relatively rigid (i.e., $\ell_c = \ell_p$). As the LC interactions are increased, the

brush continuously transforms into a nematic state aligned along the axis normal to the grafting plane. For strong LC interactions the brush approaches a step profile with the ends of the chains concentrated at the outer edge of the brush.

All of our results thus far are consistent with previous calculations carried out by Deng *et al.*[21] using Onsager interactions, provided the isotropic interactions are sufficiently strong for the brush to remain strongly stretched. Within the MS model, the LC interactions can overcome the isotropic interactions and a number of studies have predicted that the brush will collapse into a high density nematic state.[9,26,10] As we will show in the following chapters, this is where we will begin to see qualitatively distinct behaviour from the Onsager form of LC interactions.

Chapter 5

Backfolding Transitions

We continue our study of LC polymer brushes maintaining azimuthal symmetry with strong LC interactions. For good solvent conditions, the isotropic interactions favour a stretched brush while the anisotropic LC interactions favour folding into a high-density nematically collapsed brush. The brush undergoes first-order transitions as the number of folds increases depicted in Fig. 5.1. The folding transitions can be qualitatively understood through a simple analytic model balancing the energetic benefit from increased LC alignment and the cost associated with the bending energy of hairpin folds. These results hold under azimuthal symmetry but, as we will show in the following chapter, will become unstable in favour of a tilted state.

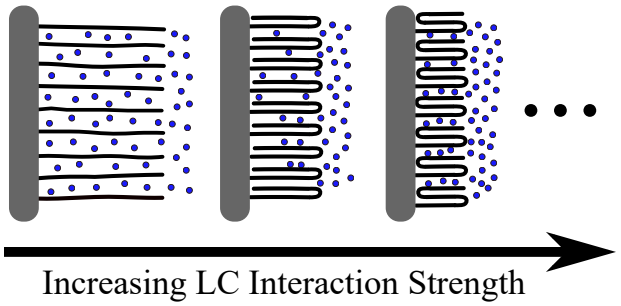

Fig 5.1. Diagram depicting the folded states. As LC interaction strength increases the brush collapses, first with a single fold, then two and so on.

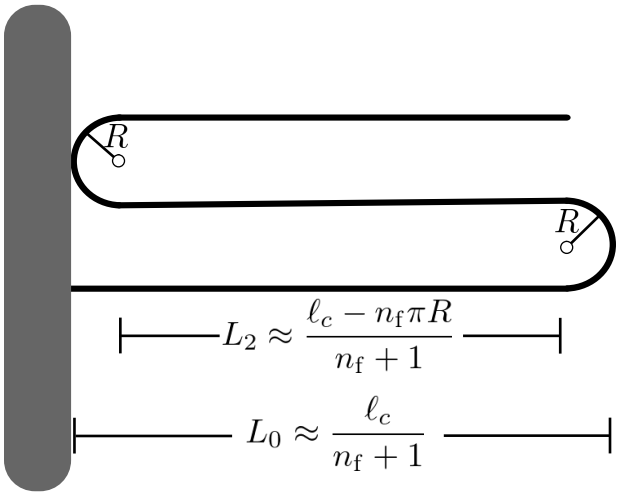

Fig 5.2. Diagram depicting the folded states, here we assume the polymer is perfectly straight except in the regions where it forms a hairpin fold. The folds are assumed to be a semi-circle with radius R and the straight portions have a length $L_2 = (\ell_c - n_\mathrm{f}\pi R)/(n_\mathrm{f}+1)$, which, when $n_\mathrm{f} \geq 2$ ignores the initial portion of length R at $s = 0$. L_0 is the distance from the grafting substrate to the end of the first fold, and for sharp fold is $L_0 \approx \ell_c/(n_\mathrm{f}+1)$.

5.1 Theory

5.1.1 SCFT

We begin by solving the SCFT of a worm-like polymer brush with implicit solvent and MS interactions assuming azimuthal symmetry identically to chapter 4. In terms of numerics, in order to resolve the sharp hairpin folds, we use a very fine grid spacing of $dz = \ell_c/3200$, $ds = 1/3200$ and $n_{LP} = 20$.

5.1.2 Uniform Distribution Approximation

Anticipating the collapse of the brush into a backfolded phase we now present a simple description of the transition assuming the polymers are sufficiently well aligned as to have a uniform distribution and follow a single trajectory $\mathbf{r}(s)$. Through simple energetic arguments we can qualitatively describe the transition and gain intuition for its behaviour.

Consider a strongly nematic polymer with n_f folds, depicted in Fig. 5.2, the free energy of this conformation can be approximated as the sum of the bending, excluded volume and

LC interaction energies

$$F = U_{\rm B} + U_0 + U_2 \ . \tag{5.1}$$

Assuming the fold is a semicircle of radius R, the bending energy, Eq. (2.1), is

$$U_{\rm B} = n_{\rm f}\frac{\kappa}{2N}\int_0^1 ds \left|\frac{d\mathbf{u}(s)}{ds}\right|^2 = n_{\rm f}\frac{\pi\ell_{\rm p}}{2R} \ . \tag{5.2}$$

If the LC interactions are sufficiently strong than we can approximate the concentration with a step profile $\phi(z) = (n_{\rm f}+1)$ if $z \le L_0 \approx \ell_{\rm c}/(n_{\rm f}+1)$ and 0 otherwise. Within this approximation the excluded volume energy is given by the first component of Eq. (4.12),

$$\frac{U_0}{n_{\rm p}k_{\rm B}T} = \frac{\Lambda_0}{2\ell_c}\int dz\phi^2(z) = \frac{\Lambda_0}{2}(n_{\rm f}+1) \ . \tag{5.3}$$

Finally, if we assume the straight portions are fully uniaxial nematic ($Tr\mathcal{Q}^2 = \frac{3}{2}\mathcal{S}^2$, $\mathcal{S}=1$) and the bent portions have $\mathcal{S}=0$ then the LC interaction energy is, from the second component of Eq. (4.12),

$$\begin{aligned}\frac{U_2}{n_{\rm p}k_{\rm B}T} &= -\frac{\Lambda_2}{2\ell_c}\int dz\phi^2(z)\mathcal{S}^2(z) \\ &= -\frac{\Lambda_2}{2}(n_{\rm f}+1)\left(1-\frac{n_{\rm f}\pi R}{\ell_{\rm c}}\right) \ .\end{aligned} \tag{5.4}$$

The total free energy of a strongly nematic state with $n_{\rm f}$ folds is then

$$\frac{F}{n_{\rm p}k_{\rm B}T} = n_{\rm f}\frac{\pi\ell_{\rm p}}{2R} - \frac{\Lambda_2}{2}(n_{\rm f}+1)\left(1-\frac{\Lambda_0}{\Lambda_2}-\frac{n_{\rm f}\pi R}{\ell_{\rm c}}\right) \ . \tag{5.5}$$

Here we have two unknowns, the radius of the fold, R, and the number of folds, $n_{\rm f}$. Minimizing with respect to the radius of the fold yields

$$R = \sqrt{\frac{\ell_{\rm p}\ell_{\rm c}}{\Lambda_2(n_{\rm f}+1)}} \ . \tag{5.6}$$

Substituting this into Eq. (5.5) we have

$$\frac{F}{n_{\rm p}k_{\rm B}T} = \frac{\Lambda_0-\Lambda_2}{2}(n_{\rm f}+1) + n_{\rm f}\pi\sqrt{\frac{\Lambda_2(n_{\rm f}+1)\ell_{\rm p}}{\ell_{\rm c}}} \ . \tag{5.7}$$

If we equate the energy of the n_f and $n_\mathrm{f}+1$ states we can find the phase transitions,

$$\Lambda_0 = \Lambda_2 - \pi\sqrt{\Lambda_2}\sqrt{\frac{(n_\mathrm{f}+1)\ell_p}{\ell_c}}\left[\sqrt{(n_\mathrm{f}+2)(n_\mathrm{f}+1)} - n_\mathrm{f}\right] \ . \tag{5.8}$$

Note that this equation is still valid when $n_\mathrm{f} = 0$. Since the transition involves a discrete jump in the number of folds it will be discontinuous.

5.2 Results

Armed with a simple model, we now investigate the full SCFT solutions. The configurations of strongly stretched polymers in the collapsed nematic states are depicted in Fig. 5.3. The segmental distribution is plotted as a function of both the contour position, s, and spatial location, z, of the polymer at fixed ℓ_c/ℓ_p, Λ_0 and Λ_2 for one, two and three fold states. The profile predicted by the uniform distribution approximation is overlaid as a dashed line. At $z = 0$ one end ($s = 0$) of the polymers are grafted to a flat substrate while the other ends ($s = 1$) are free. In the one fold state, Fig. 5.3(a), the polymers fold halfway along their contour ($s = 0.5$) to form two aligned segments of equal length. Similarly the two, Fig. 5.3(b), and three, Fig. 5.3(c), fold states fold at $s = 1/3$ and $s = 1/4$ to form 3 and 4 segments of equal length respectively. The high degree of nematic order is demonstrated by the sharp localization of polymer concentration around straight paths. The profile closely follows the black dashed line, representing a fully ordered state with semi-circular folds with radius R given by Eq. (5.6) as depicted in Fig. 5.2.

The folds are highly localized in order to maximize the amount of nematic order. Since the folds involve a reversal in direction, they break nematic order by turning parallel to the grafting plane. Aligning the folds reduces the amount of broken nematic order and aligns the parallel portions of the polymer which results in integer numbers of folds. The size of the fold is determined by a balance between the LC interactions, isotropic interactions and bending energies. The result of which, for our simplified model, gives a radius in Eq. (5.6) drawn as the dashed black line. The radius of the folds appears to be consistent with those predicted, including the decrease in radius as the number of folds increases. These hairpin folds are relatively sharp, with the radius of the largest one shown only roughly 4.4% of the length of the polymer. In terms of the persistence length the widest hairpin shown is still less than 1/3 the persistence length of the polymer, with the sharpest being less than 1/7 the persistence length of the polymer. Since the folds are sub-persistence length they have a relatively large energetic cost.

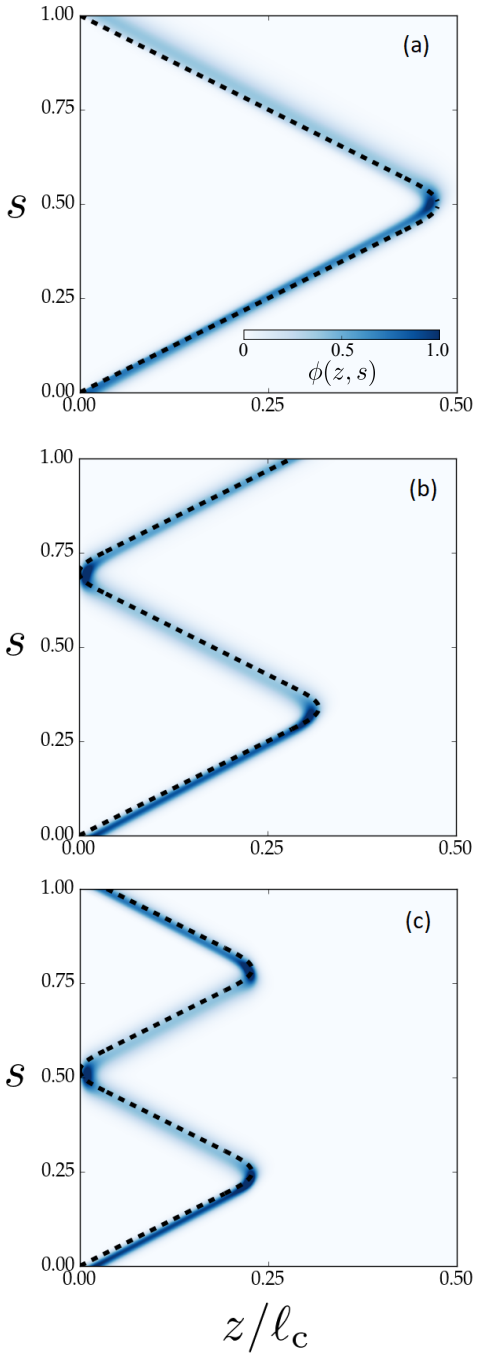

Fig 5.3. Density plot of $\phi(z, s)$, with $\Lambda_0 = 10$, $\Lambda_2 = 65$ and $\ell_c = 4\ell_p$ for (a) 1 fold, (b) 2 fold and (c) 3 fold states. Dashed line corresponds to the profile depicted in Fig. 5.2 with radius given by Eq. (5.6) to be $R/\ell_c \approx 0.044$, 0.036 and 0.031 for 1, 2 and 3 folded states respectively.

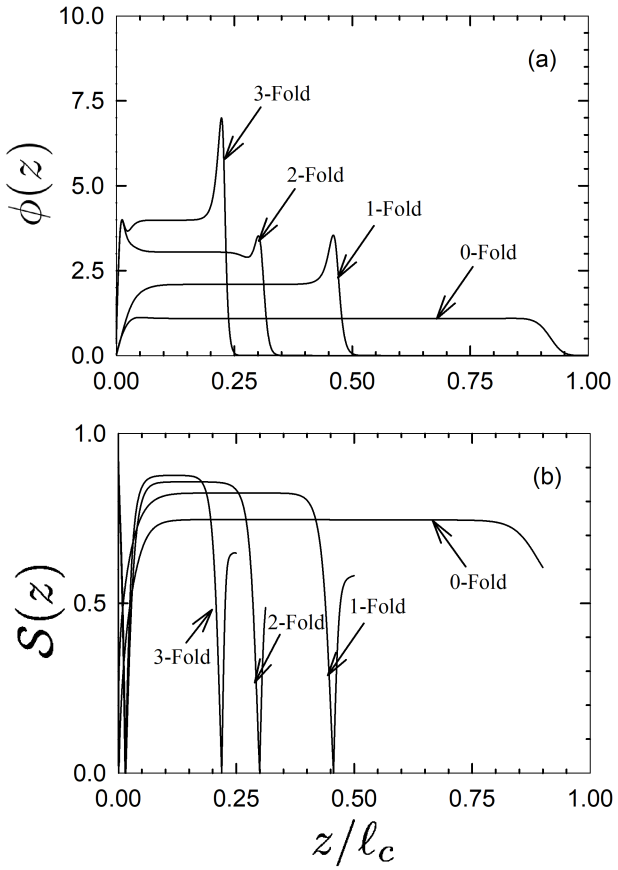

Fig 5.4. (a) Concentration, $\phi(z)$, with $\ell_c = 4\ell_p$ and $\Lambda_2 = 65$, for 0,1,2,3 fold states and (b) corresponding scalar nematic order parameter $\mathcal{S}(z)$. Discontinuities in $\mathcal{S}(z)$ represent a switch between perpendicular and parallel alignment.

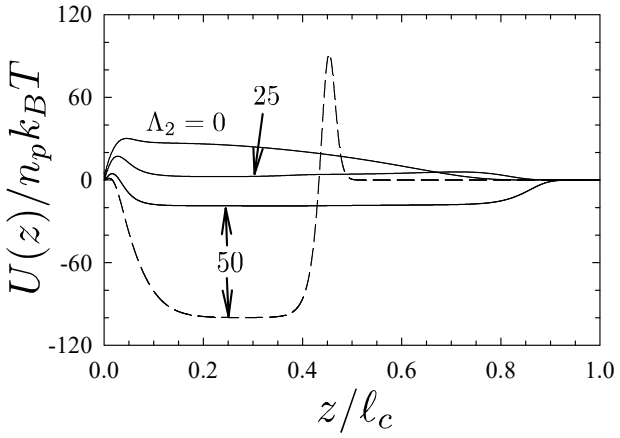

Fig 5.5. Energy density, $U(z)$, for an extended brush of worm-like chains with $\ell_c = 4\ell_p$ and interaction strengths of $\Lambda_0 = 10$ and $\Lambda_2 = 0$, 25 and 50 (solid curves). For the latter parameter combination, $U(z)$ is plotted for a brush of folded chains (dashed curve).

The corresponding polymer concentration and scalar nematic order parameter as a function of distance from the grafting plane, z, are plotted in Fig. 5.4 (a) and (b) respectively for the zero, one, two and three fold nematic states. Each concentration profile is step-like with a sharp peak where the folds take place and an increasing density with each fold. As the polymers collapse, the higher density results in stronger LC interactions which increases the amount of order, as demonstrated by an increasing order parameter $\mathcal{S}$ with increasing number of folds. Where the polymer folds, $\mathcal{S}$ switches from parallel to perpendicular alignment analogously to Fig. 4.5, where $\lambda_{\parallel} > \lambda_{\perp}$. Parallel alignment is necessary for a reversal in direction.

Fig. 5.5 illustrates the energetic advantage of the backfolded state by comparing its interaction density, $U(z)$, with that of the extended state. In the absence of LC interactions, $U(z)$ is positive for all z, and thus the extended state is favoured. However, as Λ_2 becomes sufficiently large, $U(z)$ eventually becomes negative. Given that the energy density is proportional to $\phi^2(z)$, folding approximately doubles this energetic advantage. However, the transition will not happen until $U(z)$ is sufficiently large to compensate the energy cost of folding. This has two contributions; one is the energy penalty of folding worm-like chains and the other is the loss of nematic order in the folding region. The sharpness of the fold is dictated by a competition between these two energy penalties; the interaction energy favours a sharp fold while the bending energy favours a gradual fold. The transition occurs at $\Lambda_2 = 43.3$ well beyond the $\Lambda_2 \approx 30$ where $U(z)$ first becomes negative, reflecting the high cost of hairpin folds. Naturally, as Λ_2 increases further, $U(z)$ is able to compensate for additional folds per chain, and thus producing a series of discontinuous folding transitions.

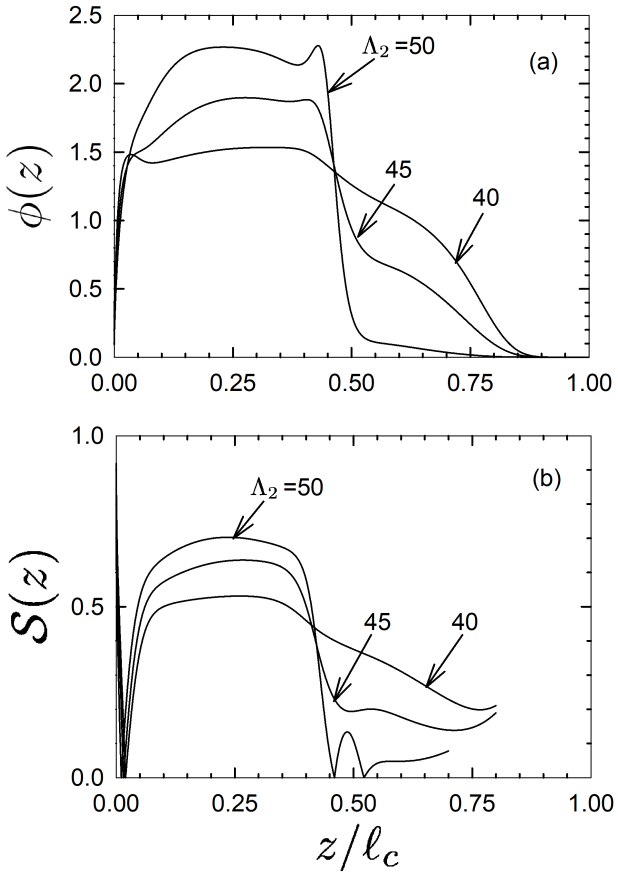

Fig 5.6. (a) Concentration, $\phi(z)$, with $\ell_c = 8\ell_p$ for $\Lambda_2 = 40, 45, 50$ depicting the continuous transition from disordered to one fold nematic states and (b) corresponding scalar nematic order parameter $\mathcal{S}(z)$. The discontinuity of $\mathcal{S}(z)$ for $\Lambda_2 = 50$ results from the polymers switching from perpendicular to parallel alignment in the region of the fold.

Maintaining a constant isotropic interaction strength, Λ_0, we now investigate a more flexible polymer $\ell_c = 8\ell_p$. Due to the increased flexibility, the brush is less ordered, folds more readily and is not as strongly stretched. As Λ_2 is increased from the disordered (moderately stretched) state for this more flexible polymer, as demonstrated in Fig. 5.6, it continuously deforms into the one fold state, with an increasing fraction of the polymers folding. Beyond this we observe discontinuous transitions. The concentration profiles in (a) depict the continuous transition from a disordered moderately stretched brush ($\Lambda_2 = 40$) to a nematically collapsed brush in the one fold state ($\Lambda_2 = 50$). The disordered profile has a relatively small fraction of polymers in the one fold state, does not exhibit the step profile of the zero fold nematic state and has a scalar nematic order parameter significantly lower than seen for the more rigid polymer in Fig. 5.4. This state still has an order parameter of roughly 0.3 to 0.5 since it is moderately stretched. The intermediate state, $\Lambda_2 = 45$, has a significant fraction of the polymers in both the extended disordered state and the one fold collapsed nematic state. The polymers in the high density nematic state have a high degree of order, while the polymers extending past this portion are weakly ordered, as seen by the order parameter in Fig. 5.6(b). The strength of the LC interactions is proportional to the density of polymer; therefore, the low density regions have relatively weak LC interactions and a lower degree of order.

This behaviour is further demonstrated by considering the polymer configurations corresponding to these three states plotted in Fig. 5.7. Since these polymers are more flexible and are therefore not as strongly ordered, the segmental concentration profiles are more diffuse than those in Fig. 5.3. For the disordered state in (a), the polymers are primarily grouped around an extended distribution with decreasing order as they extend outwards. For $\Lambda_2 = 45$ in (b), two divergent paths occur halfway along the length of the polymers $s = 0.5$. A fraction of the polymers continue to follow the extended path of the disordered brush in (a) while the remainder fold into a nematically collapsed state. In (c), the majority of the polymers have collapsed into the one fold state.

So far, we have demonstrated the existence of the zero, one, two and three fold nematic states; however, we have yet to discuss which of these states is stable. In Fig. 5.8 we, plot the free energies corresponding to the states in the previous figures as a function of the LC interaction strength, Λ_2, for fixed isotropic interaction strength $\Lambda_0 = 10$. We plot the free energy for (a) the more rigid polymer $\ell_c = 4\ell_p$ and (b) the more flexible $\ell_c = 8\ell_p$. In both, as Λ_2 increases the free energy decreases and the states with higher number of folds have steeper slopes since in our model there is an energetic benefit from increased nematic alignment. Additionally, the folded states appear to have relatively linear free energy curves. In (a), we observe clear transitions taking place sequentially with increasing numbers of folds, and the states persist past the transition, a characteristic

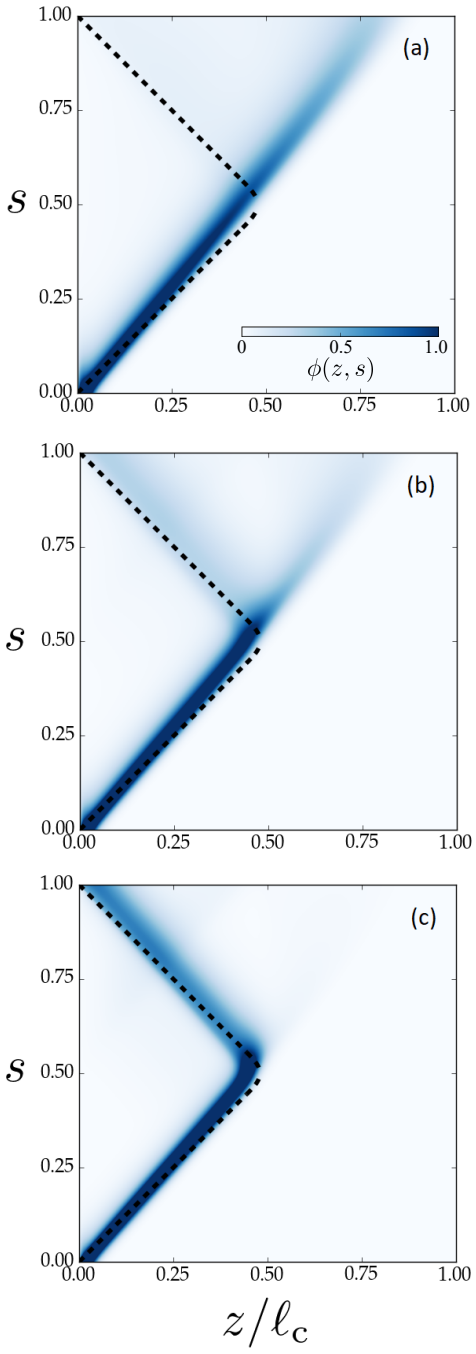

Fig 5.7. Density plot of $\phi(z, s)$, with $\Lambda_0 = 10$ and $\ell_c = 8\ell_p$ for (a) $\Lambda_2 = 40$, (b) $\Lambda_2 = 45$ and (c) $\Lambda_2 = 50$. Dashed line corresponds to the profile depicted in Fig. 5.2 with radius given by Eq. (5.6) to be $R/\ell_c \approx 0.040$, 0.037 and 0.035 for $\Lambda_2 = 40$, 45 and 50 respectively.

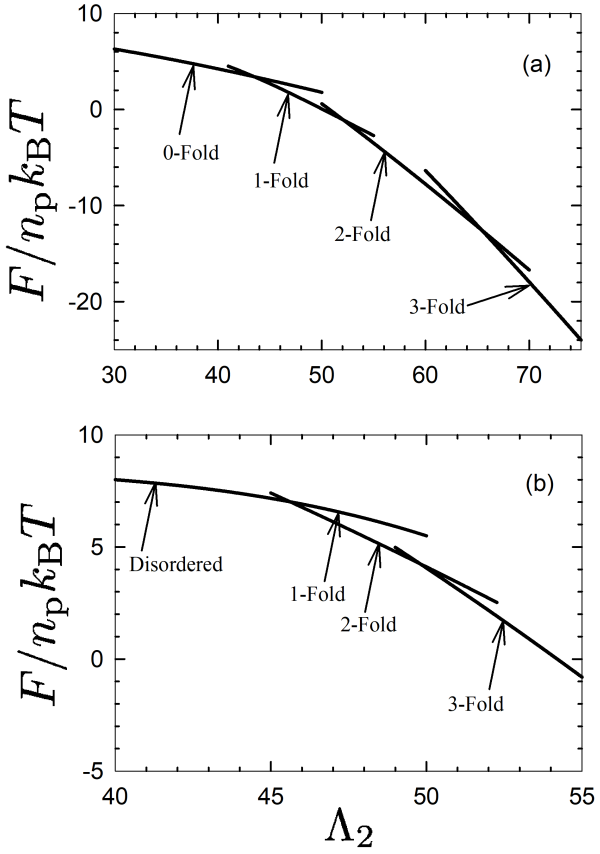

Fig 5.8. Free energy as a function of Λ_2 with fixed $\Lambda_0 = 10$ for (a) $\ell_c = 4\ell_p$, and (b) $\ell_c = 8\ell_p$. Crossing points denote first-order transitions.

behaviour of a first-order transition. In (b), we observe similar behaviour; however, since the brush does not exhibit a zero fold nematic state and transitions continuously from disordered to one fold, we do not observe the zero to one fold transition. The continuous transformation from disordered to one fold can be seen by the continuously decreasing slope. All of the transitions in (b) occur at lower Λ_2, because the increased flexibility reduces the cost associated with backfolding into the collapsed states.

By following the phase boundaries between the folded states as a function of Λ_0 and Λ_2 for $\ell_c = 4\ell_p$ and $8\ell_p$, we construct phase diagrams in Fig. 5.9. An increase in Λ_0 can be thought of as an increase in the quality of solvent; therefore, as Λ_0 increases an increasing number of solvent molecules penetrate into the brush and force it to stretch out which decreases the number of folds. As Λ_2 is increased, the polymers gain an increased benefit

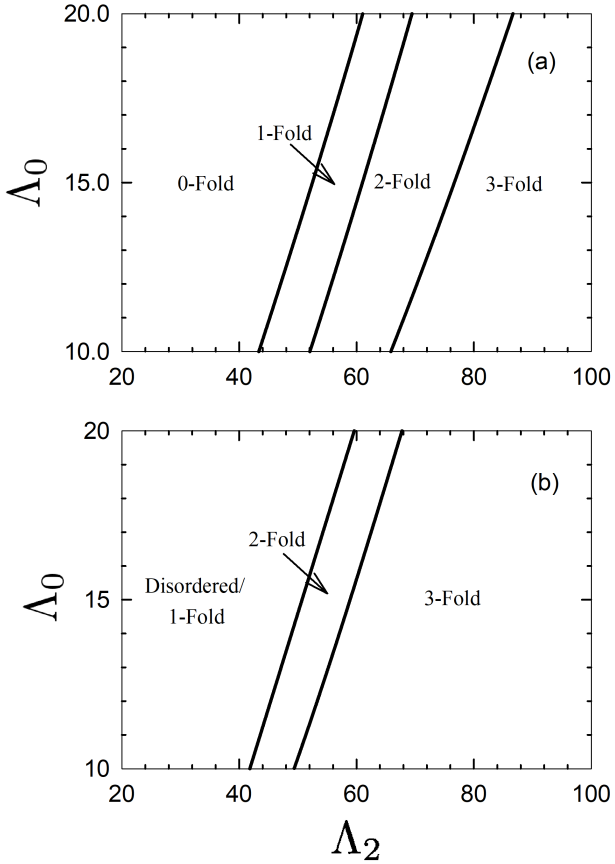

Fig 5.9. Phase diagram in the $\Lambda_0 - \Lambda_2$ plane for (a) $\ell_c = 4\ell_p$, and (b) $\ell_c = 8\ell_p$.

from alignment which draws the polymers together, collapsing the brush and increasing the number of folds. All the phase boundaries observed have similar slopes and are relatively linear. Presumably, there are increasing integer numbers of folds not shown here due to numerical difficulties resolving large numbers of folds with sharp hairpins. The phase boundary between the zero and one fold states is not present in (b) since it continuously transitions from disordered to one fold. All the transitions for the more flexible polymers in (b) take place at lower values of Λ_2 due to the reduced energetic penalty for folding.

The simplified model described in 5.1.2 yields simple analytic results for free energies and phase transitions between the folded states. The free energy, Eq. 5.7, is plotted in Fig. 5.10 as a function of Λ_2 for fixed $\Lambda_0 = 10$ at $\ell_c = 4\ell_p$ and $8\ell_p$ in (a) and (b) respectively, to be compared with the numerical SCFT counterparts in Fig. 5.8. In both we

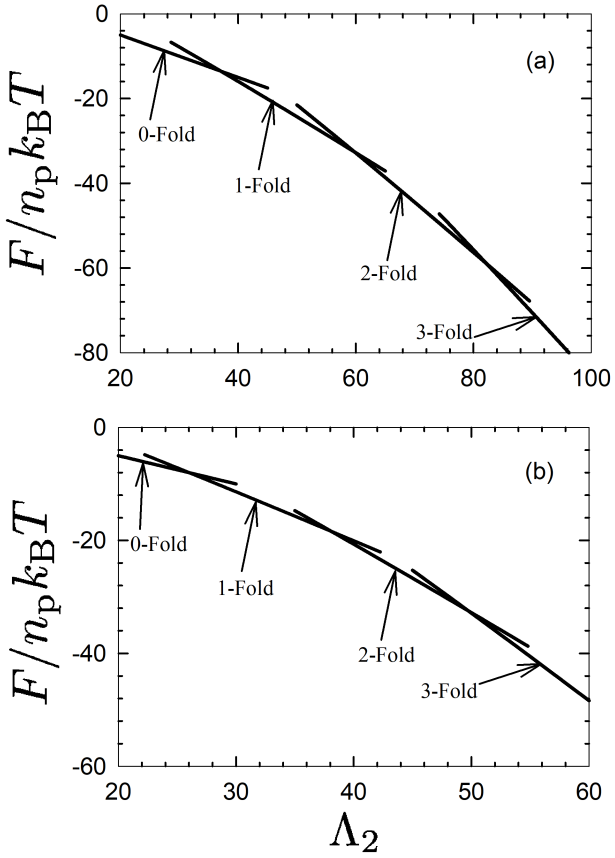

Fig 5.10. Free energy of the simplified model, Eq. (5.7), as a function Λ_2 fixed $\Lambda_0 = 10$ for (a) $\ell_c = 4\ell_p$, and (b) $\ell_c = 8\ell_p$.

see very similar qualitative behaviour, the free energies are decreasing in Λ_2 with steeper slopes for states with higher numbers of folds and transition sequentially through first order transitions. The free energies from the simple model and numerical SCFT both follow relatively linear curves. In (b) the simple model incorrectly predicts the existence of a transition from zero to one fold, this is because the model assumes the polymers are strongly nematic, which is not the case for the more flexible polymer for the values of Λ_2 where this transition takes place. In both cases the simple model predicts transitions in a similar parameter range to those observed from SCFT, which can be more readily observed through the phase diagrams.

Fig. 5.11 is the phase diagram constructed from Eq. 5.8 for the zero, one, two and three fold states with identical parameter to Fig. 5.9. As with the free energy we see

similar qualitative behaviour: the phase boundaries are relatively linear with similar slopes between the folded states. The main differences are the predicted values for the phase transitions. In (a) we see that the simple model underestimates the values of Λ_2 required for the brush to fold. This could be due to the assumption that the straight portions of the polymer are perfectly ordered (i.e., $\mathcal{S} = 1$), in reality we know that it will always be less than this, as is clearly demonstrated in Fig. 5.4(b) with values of $\mathcal{S} \approx 0.7$ for the least ordered state. However, the underestimation does not continue for the two and three fold states. As the number of folds increases, the assumption that the profile is flat and the bends do not contribute to the nematic order become increasingly invalid. The profiles in Fig. 5.4(a) have sharp peaks where the polymers fold and in (b) the order parameter is non-zero. Despite these shortcomings, the simple model predicts transition for parameter values that are surprisingly close to those from SCFT with very similar qualitative behaviour.

5.3 Discussion

Strong LC interactions can cause a polymer brush to collapse; however, in order to collapse while maintaining nematic order and azimuthal symmetry the polymers must undergo rapid reversal in direction, forming hairpin folds. Previously, the energy penalty associated with these folds was not accounted for. In accounting for this penalty, we find that the brush is still able to collapse; however, the transition occurs through multiple distinct folded states with specific conformations. In order to maximize the LC alignment, the polymers fold into segments of equal length such that the folds all take place at the boundaries of the polymer profile demonstrated in Fig. 5.3. This maintains the largest fraction of polymer nematically aligned between the folds while aligning the folded portions oriented parallel to the grafting plane. The polymers closely follow the simple conformation depicted in Fig. 5.2 represented by the dashed black line in Fig. 5.3. The radius of the fold in the simple model, Eq. (5.6), appears to reasonably well approximate the radius of the hairpins from numerical SCFT calculations. The simple model predicts that the radius of the fold decreases with the number of folds. Comparing Fig. 5.3 (a), (b) and (c) the change in radius of the dashed line is consistent with the numerical density; however, since the dependence is relatively weak, $(n_\mathrm{f} + 1)^{-1/2}$, the radius from (a) to (c) is only $\sqrt{2} \approx 1.4$ times smaller so it is difficult to conclusively determine the validity of this dependence.

Rather than assuming a semi-circle, a more precise way to estimate the shape and bending energy of a hairpin fold would be to minimize the bending, isotropic and LC interaction energies with respect to the shape of the fold, similar to recent work by Chen [66] where they minimize the energy of a hairpin, accounting just for the bending energy of a

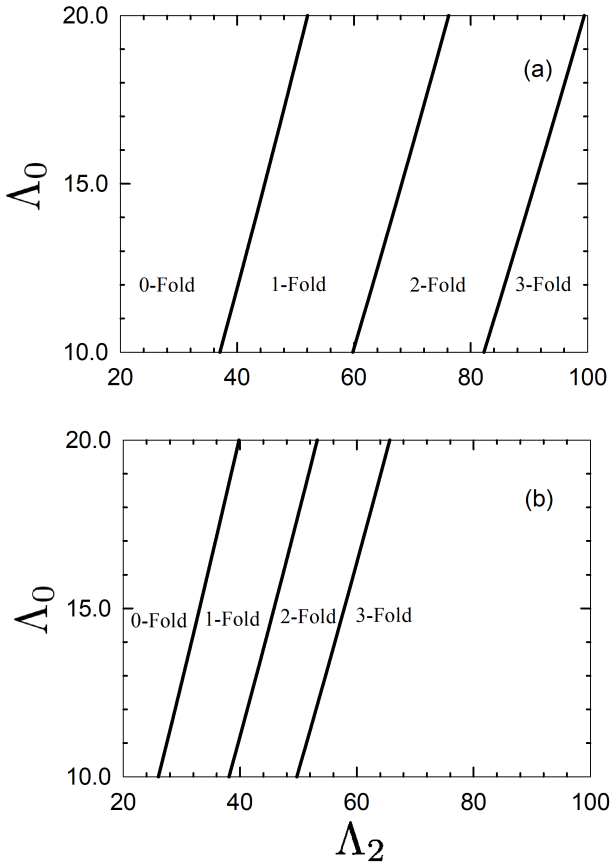

Fig 5.11. Phase diagram in $\Lambda_0 - \Lambda_2$ plane of the simplified model, Eq. 5.8, for (a) $\ell_c = 4\ell_p$, and (b) $\ell_c = 8\ell_p$.

worm-like chain, to obtain the shape and energetic cost of a hairpin. For comparison, their bending energy is $1.43557/R$ (here R is half the distance between parallel segments, which for a semi-circle is simply the radius) while that of our assumed semi-circle is $\pi/2R \approx 1.57/R$. We see identical dependence on R with similar energy costs. We can't simply readjust the energy and expect to be more accurate since our model has strong isotropic and LC interactions, increased accuracy would require a full treatment of these energies as well. Since the precise shape should not effect the qualitative behaviour, in the interest of simplicity we maintain the assumption that the fold is a semi-circle.

Despite the approximations, the simple model appears to qualitatively describe the nematic collapse of an LC polymer brush. The model allows for simple, intuitive explanations for the collapse of the brush. The LC interactions act as an attractive potential drawing parallel segments of the brush together. Once this attraction is strong enough to overcome both the excluded volume from increased density and bending energy from hairpin folds, the brush collapses. As it overcomes the energy cost from integer increases in the number of hairpins, the brush collapses through multiple distinct folded states. The analytic free energies in Fig. 5.10 closely resemble the corresponding numerical SCFT free energies in Fig. 5.8. Eq. (5.7) predicts that the steepness of the free energy curves should increase linearly with n_f; rough estimates of slopes in Fig. 5.8 point towards this being true but more folding states would be required to accurately validate this claim. Eq. (5.8) predicts that the phase boundaries separating the folded states (Λ_0 against Λ_2) will be relatively linear for large Λ_2, small ℓ_p/ℓ_c or small n_f. Additionally, the analytic theory predicts the change in Λ_2 between transitions will increase with the number of folds and decrease with ℓ_p/ℓ_c. This is demonstrated in Fig. 5.11 and is in agreement with the behaviour of the numerical SCFT calculations in Fig. 5.9. The main shortcoming of the simple model is that it can only describe polymers in a strongly nematic state.

Due to numerical difficulties, we were unable to explore a wide variety of flexibility, represented by the ratio of the contour to persistence length, ℓ_c/ℓ_p, which is large for a flexible polymer. In the weakly nematic states, we expect that the trend of the more flexible polymer being less strongly stretched and continuously transitioning from disordered to a folded state (Fig. 5.6, 5.7 and 5.8 (b)) to continue. For the strongly nematic state, we turn to the analytic model to gain additional insight into the dependence on flexibility. Eq. (5.7) predicts that the free energy is independent of the persistence length in the zero fold state and increases as the polymer becomes more rigid as $(\ell_p/\ell_c)^{1/2}$ when $n_\mathrm{f} > 0$, with an increased slope with increasing number of folds. Physically, a more rigid polymer has a larger penalty from forming hairpin folds. If there are no folds there is no penalty and the larger the number of folds the larger the cost. Eq. (5.8) predicts that the phase boundaries of Λ_0 against ℓ_c/ℓ_p decrease as $-(\ell_c/\ell_p)^{-1/2}$, once again with a steeper slope for states with

more folds. When $\ell_c/\ell_p \to \infty$, the transitions become independent of the number of folds and takes place at $\Lambda_0 = \Lambda_2$. The first transition, from zero to one fold, requires a negative Λ_0 when $\Lambda_2 < 2\pi^2\ell_p/\ell_c$, representing the limit for a backfolding state to exist in a good solvent.

5.4 Summary

We have continued our investigation of semi-dilute main-chain LC polymer brushes in good solvent, using SCFT for worm-like chains with MS interactions. Our study focuses on good solvent conditions that favour an extended brush (i.e., $\Lambda_0 > 0$) and LC interactions becoming strong enough to collapse the brush (i.e., $\Lambda_2 \gtrsim \Lambda_0$) for polymers ranging from semi-flexible (i.e., $\ell_c = 8\ell_p$) to relatively rigid (i.e., $\ell_c = 4\ell_p$). In this study we consider only azimuthally-symmetric solutions of the field Eq. (4.3).

Consistent with previous predictions,[9,10] we find that once the LC interactions are sufficiently strong, the brush will collapse into a high density nematic state; however, the phase that we observe is distinct from the micro-phase segregated brush predicted by Ref. [26] for freely jointed chains on a lattice. We do observe a collapse to a backfolded state, but through a series of transitions corresponding to integer numbers of folds. Due to the bending penalty in the worm-like chain model, the LC interactions need to be sufficiently strong to overcome the cost of forming hairpin defects, which results in a series of discontinuous transitions with increasing LC interaction strength.

We provide a simple model assuming a uniform distribution with polymers following a single trajectory that permits analytic calculations and qualitatively describes the transitions. The trajectories of the polymers predicted by this model are in good agreement with the most probable trajectories predicted from numerical SCFT provided the polymers are sufficiently well ordered and show good qualitative agreement between the free energy and phase diagrams.

The present calculations were restricted to azimuthally symmetric solutions; however, this assumption relies on the polymer being strongly stretched and breaks down upon the collapse of the brush. Indeed, if we break the azimuthal symmetry then backfolding is not the only way for the brush to increase its density; it can instead tilt to gain an identical increase in density without the cost of hairpin folds. In the following chapter we will investigate this possibility.

Chapter 6

Tilting Transition

Now that we have established that the brush will indeed collapse under strong LC interactions, we continue studying SCFT of worm-like polymer brushes but allow for the possibility of tilting through broken azimuthal symmetry. We continue to focus on the phase behaviour in the strongly stretched regime. So long as the brush is strongly stretched, the assumption that the polymers align perpendicular to the grafting plane made in all the previous studies is true; however, in the collapsed state this is no longer the case. Upon breaking azimuthal symmetry, we find that the backfolded configurations are unstable and pre-empted by a tilted nematic phase. Schematic diagram of the phases is shown in Fig. 6.1.

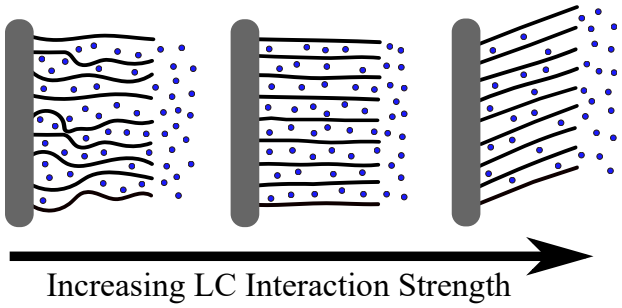

Fig 6.1. Diagram depicting the transition to a tilted brush. As LC interaction strength increases the brush extends into a nematic phase before collapsing into a tilted nematic brush.

6.1 Theory

6.1.1 SCFT

Once again the theory is identical to Chapter 4; however, we now allow for azimuthally asymmetric solutions. This requires the full numerical treatment in terms of spherical harmonics described in Appendix A. We continue to graft the polymer with a strongly peaked Gaussian, $g(z) = \exp[-(z/\xi)^2]$, where $\xi = \ell_c/32$. For all calculations, we use a grid spacing of $\Delta z = \ell_c/800$, $\Delta s = 1/800$ and spherical harmonics of up to degree 10.

6.1.2 Uniform Distribution Approximation

In the same spirit as Chapter 5, we begin by developing a simplified model that will give a qualitative description of the transition. If the polymers are strongly nematic, then we can assume the the distribution will be uniform. We expect this approximation to be valid for rigid polymers. Within the semi-dilute approximation (implicit-solvent model), the free energy is identical to the model for backfolding, Eq. (5.1), with no bending energy and a concentration $\phi \sim 1/\cos(\theta_{\mathbf{n}})$; however, it becomes immediately evident that without a cost associated with increasing the density (previously from folding) the transition will be an instability. In reality, once the brush collapses by tilting the semi-dilute approximation breaks down and it becomes necessary to explicitly account for the solvent molecules, as discussed in Chapter 2. Due to the added parameters and computational difficulty full SCFT calculations with explicit solvent are beyond the scope of this thesis. Although the numerical calculations are restricted to an implicit solvent model, in the uniform distribution approximation we can treat the solvent interactions explicitly and then take the limit of low grafting density for comparison.

The free energy of LC polymer brush can be approximated as the sum of polymer-solvent interactions, LC interactions and solvent entropy

$$F = U_{\mathrm{ps}} + U_2 - TS_{\mathrm{s}} \ , \tag{6.1}$$

respectively. Assuming an incompressible mixture, the solvent concentration, ϕ_{s}, can be expressed in terms of the polymer concentration as

$$\phi_{\mathrm{s}}(z) = 1 - \Sigma\phi(z) \ , \tag{6.2}$$

where we have defined the scaled grafting density

$$\Sigma \equiv \frac{\sigma}{b\rho_0} \ . \tag{6.3}$$

This allows us express all quantities in terms of the polymer concentration. The polymer-solvent interactions are represented by the standard pairwise potential, Eq. (2.12),

$$\begin{aligned}\frac{U_{\rm ps}}{n_{\rm p}k_{\rm B}T} &= \frac{\chi}{\alpha\ell_c}\int_0^\infty dz\phi(z)\phi_{\rm s}(z)\\ &= -\frac{\chi\Sigma}{\alpha\ell_c}\int_0^\infty dz\phi^2(z) + \frac{\chi}{\alpha}\ ,\end{aligned} \tag{6.4}$$

with $\alpha \equiv v_{\rm s}\rho_0/N$ the ratio of solvent to polymer size. The constant χ/α will not have any effect and will be dropped in all future expressions. The LC interaction energy is identical to the implicit solvent model

$$\frac{U_2}{n_{\rm p}k_{\rm B}T} = -\frac{\Lambda_2}{3\ell_c}\int_0^\infty dz\phi^2(z){\rm Tr}\mathcal{Q}^2(z)\ . \tag{6.5}$$

Finally, the solvent entropy is

$$\begin{aligned}\frac{S_{\rm s}}{n_{\rm p}k_{\rm B}} &= -\frac{1}{v_s n_{\rm p}}\int d\mathbf{r}\phi_{\rm s}(z)\ln\phi_{\rm s}(z)\\ &= -\frac{1}{\alpha\Sigma\ell_{\rm c}}\int_0^\infty dz(1-\Sigma\phi(z))\ln(1-\Sigma\phi(z))\ ,\end{aligned} \tag{6.6}$$

where we recall $n_{\rm p} = \sigma\mathcal{A}$. The free energy per polymer is then

$$\frac{F}{n_{\rm p}k_{\rm B}T} = \frac{1}{\ell_c}\int_0^\infty dz\left[-\frac{\chi\Sigma}{\alpha}\phi^2(z) - \frac{\Lambda_2}{3}\phi^2(z){\rm Tr}\mathcal{Q}^2(z) + \frac{1}{\alpha\Sigma}(1-\Sigma\phi(z))\ln(1-\Sigma\phi(z))\right]\ . \tag{6.7}$$

In the limit of low polymer concentration $\Sigma\phi(z) \ll 1$, the free energy is (Taylor expanding the logarithmic term to third order)

$$\frac{F}{n_{\rm p}k_{\rm B}T} \approx \frac{1}{\ell_c}\int_0^\infty dz\left[-\frac{\phi(z)}{\alpha} + \left(\Lambda_0 - \frac{\Lambda_2}{3}{\rm Tr}\mathcal{Q}^2(z)\right)\phi^2(z) + \frac{\Sigma^2}{6\alpha}\phi^3(z)\right] \tag{6.8}$$

where we recall $\Lambda_0 = \frac{\Sigma}{\alpha}(1-2\chi)$.

Assuming a fully uniaxial nematic (${\rm Tr}\mathcal{Q}^2 = \frac{3}{2}\mathcal{S}^2$ and $\mathcal{S}=1$) step profile $\phi(z) = \phi$, if $z \le \ell_{\rm c}/\phi$ and $\phi(z) = 0$ otherwise with ϕ the (constant) polymer concentration at position z, the free energy becomes

$$\begin{aligned}\frac{F}{n_{\rm p}k_{\rm B}T} &= -\frac{\alpha(\Lambda_2-\Lambda_0)+\Sigma}{2\alpha}\phi + \frac{(1-\Sigma\phi)}{\alpha\Sigma\phi}\ln(1-\Sigma\phi)\\ &\approx -\frac{1}{\alpha} - \frac{\Lambda_2-\Lambda_0}{2}\phi + \frac{\Sigma^2}{6\alpha}\phi^2\ ,\end{aligned} \tag{6.9}$$

where we have replaced χ with Λ_0 using $\Lambda_0 = \frac{\Sigma}{\alpha}(1-2\chi)$ and the second line is in the low Σ limit. This function is minimized at $\phi = -\infty$ provided the first term is positive; however, since we have a fixed total concentration of polymer the free energy is minimized at the minimum concentration $\phi = 1$, i.e. the extended state. When the first term becomes negative a new minima appears, which becomes the global minimum when

$$\begin{aligned} \Lambda_2^c &= \Lambda_0 - \frac{\Sigma}{\alpha} - \frac{2}{\alpha}\left[\frac{\ln(1-\Sigma)}{\Sigma} + 1\right] \\ &\approx \Lambda_0 + \frac{2\Sigma^2}{3\alpha} \ . \end{aligned} \tag{6.10}$$

In the implicit solvent model the term involving Σ^2 is assumed to be negligible which leads to a transition at $\Lambda_2^c = \Lambda_0$, and in this case the transition is an instability that causes the concentration to diverge.

Eq. (6.10) is the critical LC interaction strength that causes the brush to collapse into a high density nematic state. Previously, it was believed this collapse would form through backfolding which increases the density of the nematic state; however, in order to maintain nematic order backfolding results in hairpin folds which take place over short length scales (sub-persistence length) resulting in a non negligible energetic costs for even the most flexible polymers. In order for the brush to collapse it is not necessary for it to backfold, the nematic director can instead tilt at an angle $\theta_{\mathbf{n}}$ relative to the z axis which results in the same increase in density without the cost of hairpin defects. The transition from moderately stretched, to strongly stretched nematic and finally to a tilted state is depicted in Fig. 6.1.

The tilted configuration corresponds to a concentration $\phi = 1/\cos(\theta_{\mathbf{n}})$. Minimizing with respect to $\theta_{\mathbf{n}}$ yields two solutions: $\theta_{\mathbf{n}} = 0$ and

$$\Lambda_2 = \Lambda_0 - \frac{\Sigma}{\alpha} - \frac{2}{\alpha}\left[\frac{\cos^2(\theta_{\mathbf{n}})}{\Sigma}\ln\left(1 - \frac{\Sigma}{\cos(\theta_{\mathbf{n}})}\right) + \cos(\theta_{\mathbf{n}})\right] \ , \tag{6.11}$$

which becomes a global minimum when Eq. (6.10) is satisfied. In the limit of low grafting density we can explicitly solve for the tilt angle

$$\cos(\theta_{\mathbf{n}}) = \frac{2\Sigma^2}{3\alpha(\Lambda_2 - \Lambda_0)} \ . \tag{6.12}$$

Eq. (6.12) has two solutions, symmetric positive and negative tilt angles. After reaching the spinodal a transitions corresponding to a spontaneously broken symmetry occurs and the tilt angle of the brush continuously increases with Λ_2 until it reaches melt density $\cos(\theta_{\mathbf{n}}) = \Sigma$.

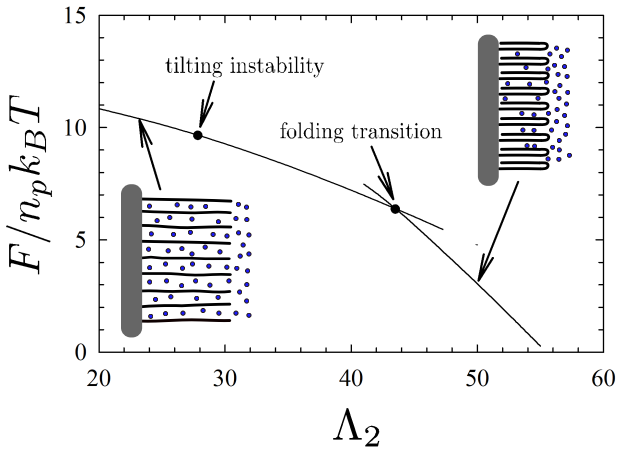

Fig 6.2. Free energy, F, as a function of Λ_2 for the extended and folded phases, corresponding to $\Lambda_0 = 10$ and $\ell_c = 4\ell_c$. Dots denote the locations of a first-order folding transition and the spinodal, where the extended phase becomes unstable with respect to tilting.

6.2 Results

To validate that the tilted phase is indeed preferred over the backfolded state in the full SCFT calculation, we begin by considering the extended to single fold transition presented in Chapter 5. Therefore we begin by maintaining the assumption of azimuthal symmetry. Since the isotropic and LC interactions enter Eq. (4.12) with opposite signs, they compete against each other. Positive Λ_0 favours low $\phi(z)$ (i.e., extended brushes) while positive Λ_2 favours high $\phi(z)$ (i.e., collapsed brushes). In order to determine which state is the stable phase, we compare their free energies in Fig. 6.2. As the LC interaction strength is increased, the free energy of the backfolded state crosses the extended state. It is thus a discontinuous or first-order transition. However, folding is not the most efficient way to increase the polymer density. The most effective way of increasing $\phi(z)$ is for the polymers to tilt, since this avoids the energy penalty associated with folds. However, like most calculations, this is prevented by our assumption of azimuthal symmetry. Our symmetric self-consistent fields, $w_0(z, u_z)$, only depend on $u_z = \cos\theta$ because we restrict our expansion in spherical harmonics, $Y_{lm}(\theta, \varphi)$, to $m = 0$.

To determine the spinodal of the extended state, where it becomes unstable with respect to tilting, we evaluate the Jacobian,

$$J_{II'} = \delta_{II'} - \int d\mathbf{u}'' G(\mathbf{u}, \mathbf{u}'') \frac{\mathcal{D}\phi(z, \mathbf{u}'')}{\mathcal{D}w(z', \mathbf{u}')} \tag{6.13}$$

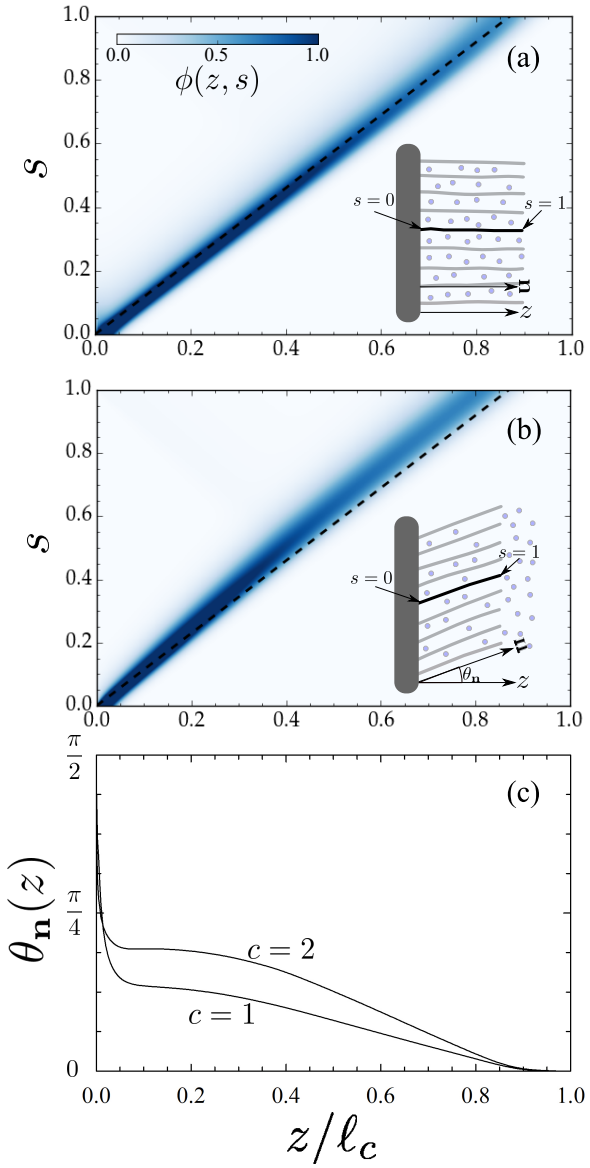

Fig 6.3. Density plots of the concentration, $\phi(z,s)$, for (a) the azimuthal symmetric field, $w_0(z,u_z)$, and (b) the symmetrically broken field, $w_0(z,u_z)+2\delta w(z,\mathbf{u})$, calculated for $\ell_c = 4\ell_p$, $\Lambda_0 = 10$ and $\Lambda_2 = 28$. In both the dashed line follows the most probable unperturbed ($c=0$) path for comparison. (c) Tilt angle of the director as a function of distance from the grafting surface for different levels of broken symmetry.

of the field, Eq. (4.3). Here, the index $I \equiv \{z, \mathbf{u}\}$ is shorthand notation for the arguments of $w(z, \mathbf{u})$ and $\phi(z, \mathbf{u})$. The functional derivative inside the integral is the change in the polymer distribution at z and $\mathbf{u}''$ due to a small change in the field at z' and $\mathbf{u}'$, which we evaluate numerically. In practice, we expand all functions in spherical harmonics and so the indices of the Jacobian actually represent $I \equiv \{z, l, m\}$. Since we are interested in knowing the azimuthal symmetry is broken, we evaluate the Jacobian for the symmetric field solution, $w_0(z, u_z)$. The solution is stable if all the eigenvalues of $J_{II'}$ are positive, and it becomes unstable at the point where an eigenvalue of zero occurs. The dot in Fig. 6.2 denotes the point, $\Lambda_2 \approx 28$, where the extended state become unstable with respect to tilting. As expected, this instability pre-empts the folding transition.

To confirm that the instability does indeed correspond to tilting, we can examine an eigenvector, $\delta w(z, \mathbf{u})$, corresponding to the zero eigenvalue. Note that the zero eigenvector is degenerate because the chains can tilt in any azimuthal direction; we select the eigenvector corresponding to a tilt in the $\varphi = 0$ direction. The fact that its corresponding eigenvalue is zero implies that

$$w(z, \mathbf{u}) = w_0(z, u_z) + c\delta w(z, \mathbf{u}) \tag{6.14}$$

remains an approximate solution to the field equation for small c.

The tilt can be inferred by examining the distribution $\phi(z, s)$ for the s'th segment of the polymer. Fig. 6.3 plots $\phi(z, s)$ for the symmetric and asymmetric fields corresponding to $c = 0$ and $c = 2$, respectively. For the symmetric field in plot (a), the most probable location of the s'th segment reaches a height of $z \approx 0.8\ell_c$. However, for the asymmetric field, the polymers do not reach the same height since they are tilted. For a uniform tilt, the height would be reduced by a factor $\cos(\theta_{\mathbf{n}})$. Another way of inferring the tilt is to diagonalize the $\mathcal{Q}_{ij}(z)$ tensor to obtain the nematic director, $\mathbf{n}(z)$. Fig. 6.3(c) shows the tilt of the director, $\theta_{\mathbf{n}}(z)$. Once the symmetry is broken (i.e., $c > 0$), the angle decreases continuously as the polymers move away from the grafting plane. Furthermore, adding a larger amount of the eigenvector, $\delta w(z, \mathbf{u})$, to the symmetric solution, $w_0(z, u_z)$, increases the amount of tilt.

The diagonalizing $\mathcal{Q}_{ij}(z)$ also provides the uniaxial, $\mathcal{S}(z)$, and biaxial, $\mathcal{P}(z)$, order parameters plotted in Fig. 6.4. The polymer concentration, $\phi(z)$, increases as the chains tilt, which in turn enhances the level of LC order as evident by the increase in $\mathcal{S}(z)$. The tilt of the director relative to the grafting surface breaks the rotational symmetry about $\mathbf{n}$, which induces a small degree of biaxiality into the brush. The increase of both $\mathcal{S}(z)$ and $\mathcal{P}(z)$ reduces the interaction energy as illustrated in Fig. 6.4(c). The reduction in energy continues monotonically as c increases, and thus the tilt angle will jump all the way to 90°

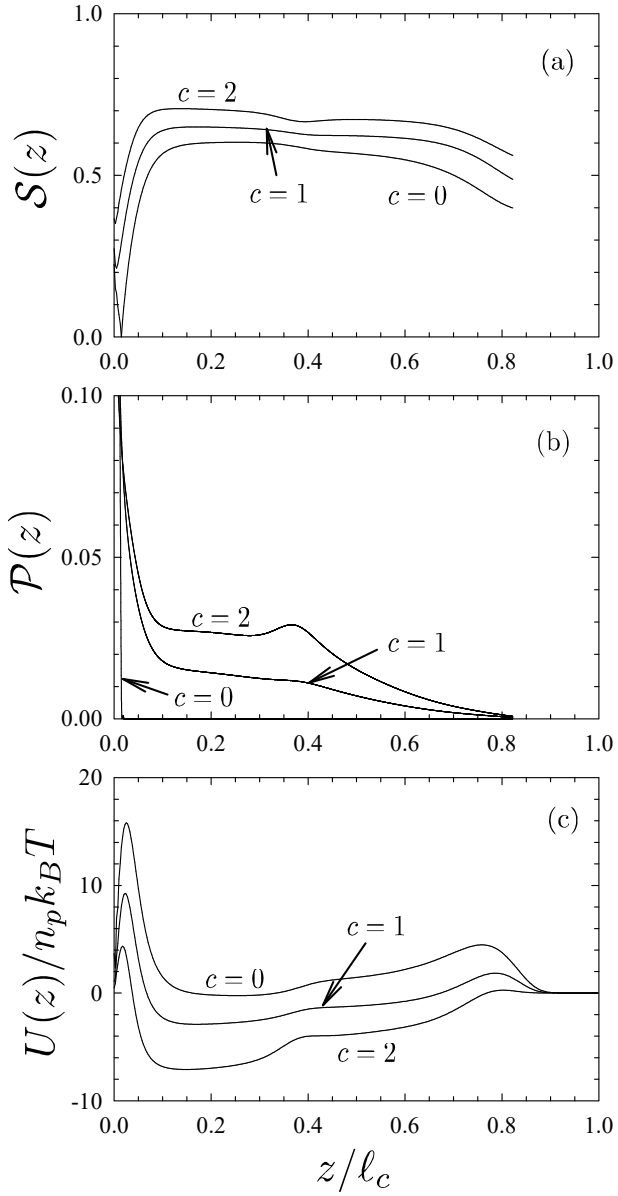

Fig 6.4. (a) Uniaxial order parameter, (b) biaxial order parameter, and (c) energy density corresponding to self-consistent fields, Eq. (6.14), with different levels of broken symmetry, calculated for $\ell_c = 4\ell_p$, $\Lambda_0 = 10$ and $\Lambda_2 = 27.8$.

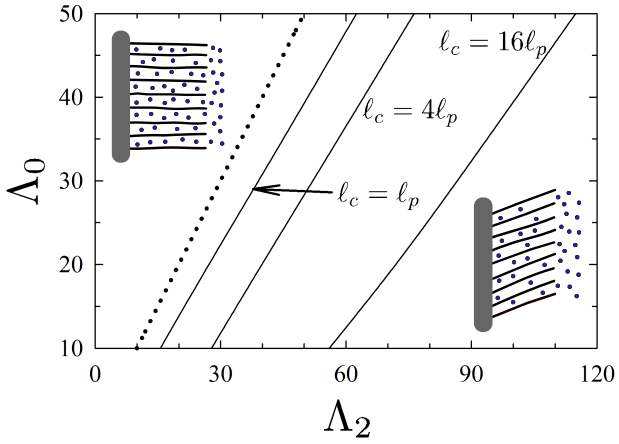

Fig 6.5. Phase diagram showing the boundary between extended and tilted brushes, calculated for polymers of different flexibility. The dotted line, $\Lambda_2 = \Lambda_0$, denotes the minimum LC interactions required before tilting can possibly occur.

as soon as the spinodal is crossed. As we discussed previously, this unphysical behaviour is a limitation of the semi-dilute approximation for the solvent entropy. If we include the cubic term in S_s, the spinodal will coincide with a second-order transition, beyond which the equilibrium tilt angle evolve continuously away from 0° as Λ_2 is increases.

Although the current model is insufficient to determine the equilibrium properties of the tilted phase, all we need is its boundary in order to calculate a phase diagram as depicted in Fig. 6.5. As mentioned previously, the more flexible polymer, $\ell_c = 16\ell_p$, is not as well ordered and therefore requires stronger LC interaction strength, Λ_2, to overcome the excluded volume interactions, Λ_0. As we will show in Section 6.3, once the polymers become perfectly ordered we expect them approach the limit $\Lambda_0 = \Lambda_2$ (Eq. (6.10) assuming the Σ^2 term is negligible), plotted as a dotted line in Fig. 6.5. In reality there will always be a deviation due to the depletion layer in the proximity of the grafting plane.

The phase transition for the two more rigid polymers, $\ell_c = \ell_p$ and $4\ell_p$, increases relatively linearly while the most flexible $\ell_c = 16\ell_p$ has an increasing slope for small values of Λ_0. The transition occurs when the LC interactions overcome the isotropic, ie. when $\Lambda_0 \sim \mathcal{S}^2\Lambda_2$ ($\mathcal{P} \approx 0$). Once the polymers are strongly ordered, the order parameter, $\mathcal{S}$, increases relatively slowly with Λ_0 and Λ_2, so $\mathcal{S}$ is roughly constant and the phase transition increases linearly with Λ_2. The most flexible polymer is not well ordered when Λ_0 is small and $\mathcal{S}$ increases rapidly resulting in an increasing slope $\Lambda_0/\Lambda_2 \sim \mathcal{S}^2$. When Λ_2 is large $\mathcal{S}$ becomes roughly constant and the phase transition increases linearly.

Although the tilting instability pre-empts the folding transition, Fig. 6.6(a) shows a

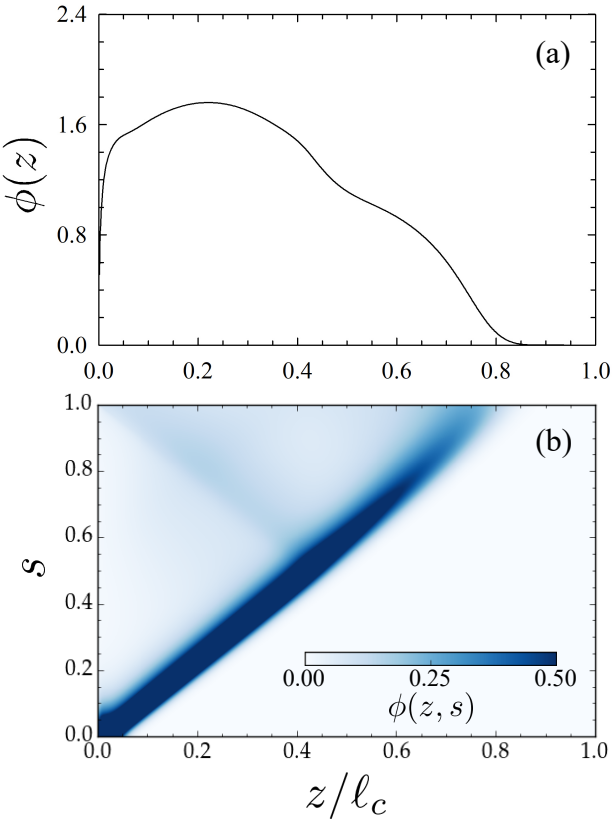

Fig 6.6. (a) Concentration profile, $\phi(z)$, and (b) s-segment distribution, $\phi(z,s)$, for an extended brush of relatively flexible polymers just prior to the tilting transition; $\Lambda_0 = 20$, $\Lambda_2 = 71$ and $\ell_c = 16\ell_p$.

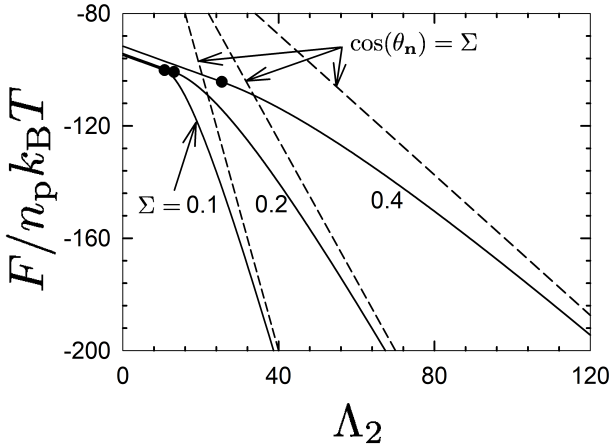

Fig 6.7. Free energy assuming a uniform distribution, Eq. (6.9), as a function of Λ_2 for multiple $\Sigma = 0.1$, 0.2, 0.4, fixed $\Lambda_0 = 10$ and $\alpha = 0.01$.

concentration profile for our most flexible polymer, $\ell_c = 16\ell_p$, just prior to the tilting transition that is reminiscent of the microphase segregated brushes predicted by Birshtein and co-workers. Although the effect is not nearly as pronounced, the inner half of the brush, $0 \lesssim z \lesssim 0.4\ell_c$, exhibits a polymer concentration that is distinctly higher than that of the outer region, $0.4\ell_c \lesssim z \lesssim 0.8\ell_c$. The concentration distributions, $\phi(z, s)$, plotted in Fig. 6.6(b) illustrates that this results due to a small equilibrium population of backfolded chains among the extended chains. Evidently, the entropy gain by having two distinct populations is enough to compensate for the bending penalty of a few chains, provided the chains are not too stiff.

To explore the effects of grafting density we turn to the simplified model presented in 6.1.2. In Fig. 6.7 we plot the free energy as a function of Λ_2 for increasing grafting density. In all cases, after the spinodal (denoted by a dot), the concentration continuously increases until it reaches the melt density at an angle $\cos(\theta_{\mathbf{n}}) = \Sigma$, which can be observed by the free energy asymptoting to the free energy of a tilted melt brush represented by a dashed line. For low grafting density the tilt angle increases rapidly in Λ_2 as described approximately by Eq. 6.12 while for larger values of grafting density the increase is more gradual. Additionally, an increase in grafting density shifts the spinodal to higher values of Λ_2. This effect is further demonstrated in the phase diagram in Fig. 6.8, where the phase boundaries follow Eq. (6.10). For small values of $\Sigma = 0.1$ or 0.2 the shift is relatively small; however, this shift increases rapidly as Σ is further increased to 0.4 and as $\Sigma \to 1$ the transition shifts to $\Lambda_2 \to \infty$. As the density increases the entropy of mixing the few

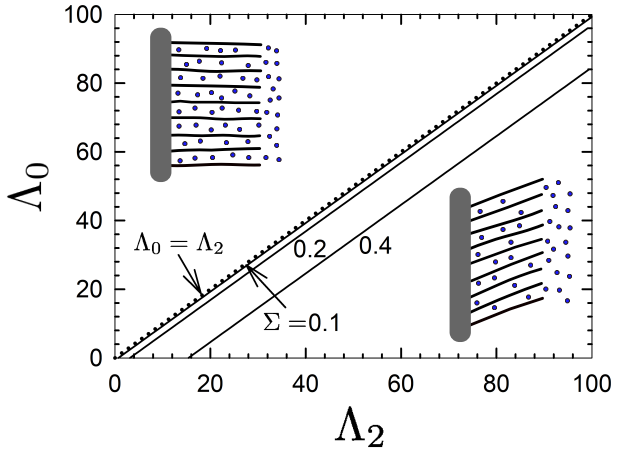

Fig 6.8. Phase diagram in Λ_0-Λ_2 plane for multiple $\Sigma = 0.1$, 0.2, 0.4 and fixed $\alpha = 0.01$. The solution in the limit of low grafting density, $\Lambda_0 = \Lambda_2$, is plotted as a dotted line.

remaining solvent molecules dominates and the concentration only ever asymptotically approaches melt density.

6.3 Discussion

Within the implicit solvent model the transition is an instability; however, it is well known that the semi-dilute approximation breaks down in the poor solvent regime.[77] Beyond the semi-dilute approximation higher order corrections to the solvent entropy will limit the degree of tilting. Prior to tilting the configuration is symmetric about positive or negative tilt angles $\theta_{\mathbf{n}}$ as well as rotations about the azimuthal angle $\varphi_{\mathbf{n}}$, so the transition results in spontaneously broken symmetry in the angles relative to the z axis.

Eq. (6.10) implies that inclusion of Σ^2 and higher terms push the tilting instability in Fig. 6.5 towards slightly larger Λ_2 as shown in Fig. 6.8. We can also qualitatively account for the effect of a reduced average order parameter (i.e., $\mathcal{S} < 1$) by making the substitution $\Lambda_2 \to \Lambda_2 \mathcal{S}^2$. This simply pushes the spinodal to larger Λ_2 by a factor of $\mathcal{S}^{-2}$, which is indeed qualitatively consistent with our phase diagram in Fig. 6.5. Furthermore, we can account for the fact that tilting increases the nematic order, as illustrated in Fig. 6.4(a). In this case, it is better to follow the more conventional Landau expansion of F in even powers of $\theta_{\mathbf{n}}$. (Note that odd powers are excluded due to the symmetry between positive and negative tilts.) In this spirit, the angular dependence of the nematic order parameter

takes the form $\mathcal{S}^2 \approx \mathcal{S}_0^2 + \frac{C}{2}\theta_{\mathbf{n}}^2$, where $C > 0$. Expanding the free energy in the uniform distribution approximation, Eq. (6.9), about $\theta_{\mathbf{n}} = 0$,

$$\frac{\Delta F}{nk_{\mathrm{B}}T} \approx \frac{A}{2}\left(1 - \frac{\Lambda_2}{\Lambda_2^{\mathrm{c}}}\right)\theta_{\mathbf{n}}^2 + \frac{B}{4}\theta_{\mathbf{n}}^4 \ , \tag{6.15}$$

where $\Delta F \equiv F - F_0$ is the free energy relative to the $\theta_{\mathbf{n}} = 0$ configurations. In general the specific form of A and B is unimportant beyond their sign, but in the limit of low grafting density they are:

$$A = \frac{\mathcal{S}_0^2 + C}{2\Lambda_2^{\mathrm{c}}} \text{ and } B = \frac{5\Lambda_2^{\mathrm{c}}}{12}\left(1 - \frac{\Lambda_2}{\Lambda_2^{\mathrm{c}}} + \frac{2\Sigma^2 - \alpha C\Lambda_2}{5\alpha\left(\Lambda_0 + \frac{2\Sigma^2}{3\alpha}\right)}\right) \ , \tag{6.16}$$

with a shifted critical point $\Lambda_2^{\mathrm{c}} = (\Lambda_0 + \frac{2\Sigma^2}{3\alpha})/(\mathcal{S}_0^2 + C)$. For small C, the only significant change is a shift in the spinodal to smaller Λ_2, which is obtained by equating the $\theta_{\mathbf{n}}^2$ coefficient to zero. However, if C becomes sufficiently large, $C > 2\Sigma^2/(\alpha\Lambda_2^{\mathrm{c}})$, the $\theta_{\mathbf{n}}^4$ coefficient becomes negative, which implies a first-order transition. Note that the coefficient of the $\theta_{\mathbf{n}}^6$ term (not shown) is still positive when this occurs. Thus, for small Λ_0 or large ℓ_c/ℓ_p, we expect the spinodal to be pre-empted by a discontinuous tilting transition.

In light of our findings, there are a considerable number of previous studies that need to be reconsidered, specifically those where strong LC interactions cause the brush to collapse by the way of chain folding. In such cases, it is essential to account for the penalty of hairpin folds and to allow the nematic director, $\mathbf{n}$, the freedom to tilt. It is likely the phase behavior predicted in studies that fail to do so will be replaced by more stable tilted phases. This includes, for example, the much discussed microphase-segregated brushes (MSB).[26,62,63,35,36] Fig. 6.6 does provide some indication that the MSB might emerge prior to the tilting instability for sufficiently flexible polymers. However, this is the situation where the tilting transition may become first order, in which case it will also pre-empt the spinodal and thus possibly also the MSB.

Investigating the switch of the tilting transition from continuous to discontinuous with SCFT will be challenging. As we pointed out, one would have to forego the semi-dilute approximation, which would increase the parameter space of the model. If one just included the cubic term for S_s, then there would only be the one additional system parameter, $N\Sigma^2/v_{\mathrm{s}}\rho_0$, from Eq. (6.9). However, this approximation would also breakdown at high concentrations, and so it would probably be necessary to include the full expression for S_s. In this case the number of system parameters would increase to five: the scaled isotropic interaction parameter, $\nu_0 N$, the scaled LC interaction parameter, $\nu_2 N$, the polymer flexibility, ℓ_c/ℓ_p, the dimensionless grafting density, $\sigma/b\rho_0$, and the size of the polymer relative

to the solvent, $N/v_s\rho_0$. In addition to the extraordinarily large parameter space, the numerics of solving the self-consistent field, $w(z,\mathbf{u})$, for a tilted phase would be demanding. When Tang *et al.*,[76] were confronted with this problem, they resorted to solving the statistical mechanics of the single worm-like chain in $w(z,\mathbf{u})$ using Monte Carlo simulations. However, this can likely be overcome with improved numerical methods for solving the diffusion Eq. (4.6).[83]

The previous study of worm-like polymer brushes by Deng *et al.*[21] did constrain the orientation of $\mathbf{n}$, but Onsager interactions, $f(\mathbf{u},\mathbf{u}') = \epsilon|\mathbf{u}\times\mathbf{u}'|$,[6,77] are not strong enough to cause the brush to collapse. It can be shown that Onsager interactions are, to leading order in anisotropic interactions, equivalent to setting a fixed ratio $\nu_2 = \frac{5}{8}\nu_0$,[84] which according Fig. 6.5 puts the system well in the extended brush regime. This can be physically understood by noting that the interactions are original entirely from the repulsive excluded-volume interactions between cylindrically shaped polymers, and thus the system always favours low density. One shortcoming of the Onsager interaction, however, is that it overlooks the attractive interactions (e.g., van der Waals forces). The MS approach, on the other hand, represents a general expansion of all the interactions truncated at leading order in anisotropic interactions, and therefore applies to a wider class of polymers. More importantly though, the Onsager approach overlook interactions involving the solvent molecules as well as the solvent entropy, S_s, both of which contribute to the excluded-volume parameter, ν_0. This is of no consequence in bulk phases, because $\phi(z)$ is uniform and thus the value of ν_0 has no impact. However, this is not the case for polymer brushes, and thus it is inappropriate to just use Onsager interactions.

The advantage of the present SCFT approach with the worm-like chain model is its considerable versatility. For instance, the interaction can be extended to include any type of orientational interaction as well as allowing for a finite range to the interactions by using a more general $G(|\mathbf{r}-\mathbf{r}'|,\mathbf{u},\mathbf{u}')$ in Eq. (4.4). The grafting function, $g(z,\mathbf{u})$, can also be readily selected to include any desired dependence on the orientation of the grafted segment ($s = 0$).[8] In reality, main-chain LCs often involve rigid mesogenic segments joined together by relatively flexible linkers. This can be modeled by simply allowing the bending modulus, κ, to alternate as a function of s between a finite value for the linkers and infinity for the mesogens.[8] It is also straightforward to allow distinct interactions for the linkers and the mesogens. The SCFT can readily handle branched architectures, and therefore the calculation can also be extended to side-chain LCs.[51,52,53,54] In this case, it would be important to include a bending energy between the mesogen side-chains and the relatively flexible backbone, in order to couple the orientation of the backbone with that of the mesogens. Furthermore, the simple solvent molecules could readily be replaced by LC molecules. Provided that the grafting density is sufficient that the fields only depends

on z (i.e, the system is in the brush vs mushroom regime), the computational cost of these extensions is not that much. Nevertheless, these extensions will greatly increase the number of system parameters.

6.4 Summary

We have investigated semi-dilute main-chain LC polymer brushes in good solvent, using SCFT for worm-like chains with MS interactions. The calculation assumes sufficient overlap among the polymers such that the brush has no lateral structure (i.e., no dependence on x and y), but a small enough polymer concentration such that the solvent can be treated implicitly. Under these assumptions, the grafting density and solvent size can be scaled out of the problem, reducing the number of system parameters to three: the scaled isotropic interaction strength Λ_0, the scaled anisotropic LC interaction strength Λ_2, and the number of persistence lengths per chain ℓ_c/ℓ_p. Our study focuses on good solvent conditions that favour an extended brush (i.e., $\Lambda_0 > 0$) and LC interactions becoming strong enough to collapse the brush (i.e., $\Lambda_2 \gtrsim \Lambda_0$) for polymers ranging from semi-flexible (i.e., $\ell_c = 16\ell_p$) to relatively rigid (i.e., $\ell_c = \ell_p$).

The study begins by considering azimuthally-symmetric solutions, $w_0(z, u_z)$, of the field Eq. (4.3). Under this constraint, the extended brush collapses by a series of first-order folding transitions, as the LC interaction become strong enough to compensate for an increasing number of folds per chains. However, these transitions overlook the fact that the brush can increase its concentration without the cost of hairpin folds, by instead tilting. Indeed, when the constraint is relaxed, the extended brush becomes unstable with respect to tilting prior to the folding transitions. Within the semi-dilute approximation, the brush concentration increases indefinitely, and thus it becomes necessary treat the solvent entropy, Eq. (6.6), more accurately. Doing so will result in a second-order tilting transition coinciding with the spinodal that likely switches to a first-order tilting transition pre-empting the spinodal, as the polymers become increasingly flexible.

In light of our new findings, it would be prudent to reconsider previous studies that omitted the penalty for hairpin folds and/or assumed a nematic director normal to the grafting surface. Although the SCFT for worm-like chains will become considerably computational for tilted phases, it should be manageable provided the lateral symmetry is retained. The reward of using this approach is its remarkable versatility. Generalization, for example, to multicomponent brushes, orientationally-dependent grafting conditions, and LC solvents are trivial. The approach can even be extended, with relatively little additional cost, to more elaborate architectures such as main-chain LC polymers consisting of

rigid mesogens connected by semi-flexible segments or side-chain LC polymers consisting of a semiflexible backbone with mesogen side-groups. Thus, the SCFT for worm-like chains should be able to handle most of the systems that experimentalists are likely to study.

Chapter 7

Conclusion and Outlook

Using SCFT of the worm-like chain model, with implicit solvent and MS type LC interactions, we have investigated the equilibrium phase behaviour of an LC polymer brush, taking into account polymer rigidity and breaking azimuthal symmetry. We first focus on the extended state in Chapter 4. Comparing the solution for flexible worm-like chains to the classical SST of Milner, Witten and Cates[15] we show that for strong stretching there is good agreement provided the classical brush height, L, satisfies $2R_0 \lesssim L \lesssim \frac{1}{4}\ell_c$ and is flexible $\ell_c \gg \ell_p$. The deviations for flexible chains such as the depletion layer near the grafting plane and exponentially decaying tail are consistent with numerical SCFT of Gaussian chains.[17] Once the brush height approaches the contour length of the polymer, the Gaussian chain model is no longer valid and significantly over estimates the brush height. For worm-like chains, we find that in this limit the brush approaches a step profile with all the ends concentrated at the outer edge of the brush, analogous to the Alexander-de Gennes approximation consistent with previous SCFT calculations for worm-like chains.[21] For brushes ranging from semi-flexible to rigid, SST is never valid and it will always be necessary to use a semi-flexible model. This is further exacerbated once we incorporate LC interactions. As LC interactions are increased, the brush continuously transforms into a nematic state with the polymers aligned along the axis normal to the grafting plane, consistent with previous calculations involving Onsager interactions.[21]

In the extended state, the brush aligns normal to the grafting plane, implying azimuthal symmetry. In Chapter 5, we study the nematic collapse of an LC polymer brush maintaining azimuthal symmetry. Under these conditions, we find that for strong LC interactions the brush collapses through a number of distinct, first order, backfolding transitions. In order to increase the density of the nematic state, the brush folds first in half, then thirds, fourths, and so on. We provide a simple analytic model, assuming a uniform distribution,

which predicts these transitions and yields excellent qualitative agreement with numerical SCFT, even accurately reproducing the most probable configurations of the folded states. In reality, however, the polymer brush is not necessarily azimuthally symmetric. The assumption is based on the brush being strongly stretched, which is not always the case in the collapsed state, which leads us to the main result of this thesis.

In Chapter 6, we break the azimuthal symmetry and show that the backfolded states are no longer stable, and are pre-empted by a tilting transition. In order to increase the density of the nematic state, it is not necessary for the brush to backfold, but it can instead tilt. This achieves an identical increase in concentration without the energy cost of forming hairpin defects and will therefore always be the preferred configuration of a semi-flexible polymer brush in the nematically collapsed state. Within the implicit solvent model, the transition to a tilted brush is an instability, which will become continuous once the semi-dilute approximation is relaxed. We predict this transition to be a continuous symmetry breaking transition provided the polymers are sufficiently rigid.

There are three mains lessons gained from the current study. First, we stress the importance of careful treatment of the molecular interactions, specifically the proper treatment of solvent molecules and LC interactions. For an extended configuration, the implicit solvent model offers a convenient simplification; however, it breaks down in the collapsed state. Whether the solvent is treated implicitly or explicitly the polymer solvent interactions should be carefully accounted for. For LC interactions the MS form is more general than Onsager interactions. The Onsager form is most valid in the melt phase, where no solvent molecules are present, and we have shown that even in this case the MS theory gives not only identical qualitative behaviour but similar quantitative description. For the specific case of a polymer brush, Onsager interactions do not properly treat the solvent molecules and miss qualitatively distinct behaviour, the collapse of the brush under strong LC interactions.

Secondly, accounting for the bending energy penalty through the worm-like chain model has dramatically changed the qualitative behaviour of the LC collapse of a polymer brush as compared to the freely jointed chain model. To the best of our knowledge, all previous calculations and simulations investigating the nematic collapse of a polymer brush used some variant of the freely jointed chain model, which gave rise to backfolded conformations. These previous studies need to be re-evaluated in this new light.

Finally, the previous studies assumed the polymers align perpendicular to the grafting plane, which is generally true for a strongly stretched brush, but breaks down once the brush collapses. We stress the importance of critically examining this assumption when investigating the LC properties of a polymer brush. It is likely that once this assumption

is relaxed previously discussed collapsed phases, such as the MSB, may become unstable in favour of tilted configurations.

Keeping these lessons in mind, this model can easily be extended to describe many different models of LC polymer brushes. For example, many main chain LC polymers consists of flexible and rigid segments grafted together. By varying the rigidity of the polymer along the backbone $\kappa \rightarrow \kappa(s)$ this model can easily be adapted to flexible-rigid multi blocks. Additionally, by grafting polymers to the backbone this model can be adapted to describe side-chain LC polymers.

One motivation for this work was to investigate the ability of polymer brushes to induce local orientational alignment to LC solvent molecules. Now that we have a good description of the equilibrium phase behaviour of an LC polymer brush immersed in a simple solvent our model can readily be extended to replace the solvent molecules with LC or LC polymers. The LC molecules could be treated as rigid rods, while polymers would be treated as worm-like chains, identical to the brush molecules. In either case at least one additional parameter would be required.

References

[1] S. T. Milner. Polymer brushes. *Science*, 251(4996):905–914, 1991.

[2] B. Zhao and W. J. Brittain. Polymer brushes: surface-immobilized macromolecules. *Prog. Polym. Sci.*, 25(5):677–710, 2000.

[3] W. L. Chen, R. Cordero, H. Tran, and C. K. Ober. 50th anniversary perspective: polymer brushes: novel surfaces for future materials. *Macromolecules*, 50(11):4089–4113, 2017.

[4] M. Amiji and K. Park. Surface modification of polymeric biomaterials with poly (ethylene oxide), albumin, and heparin for reduced thrombogenicity. *J. Biomater. Sci.*, 4(3):217–234, 1993.

[5] N. Houbenov, S. Minko, and M. Stamm. Mixed polyelectrolyte brush from oppositely charged polymers for switching of surface charge and composition in aqueous environment. *Macromolecules*, 36(16):5897–5901, 2003.

[6] L. Onsager. The effects of shape on the interaction of colloidal particles. *Ann. NY Acad. Sci.*, 51(4):627–659, 1949.

[7] W. Maier and A. Saupe. Eine einfache molekulare theorie des nematischen kristallinflüssigen zustandes. *Z. Naturforsch.*, 13(7):564–566, 1958.

[8] A. Halperin and D. R. M Williams. Liquid crystalline brushes: An anchoring transition. *EPL*, 21(5):575–580, 1993.

[9] T. M. Birshtein, A. A. Mercurieva, V. A. Pryamitsyn, and A. Polotzkiy. Liquid-crystalline ordering in polymer brushes. *Macromol. Theory Simul.*, 5(2):215–223, 1996.

[10] D. V. Kuznetsov and J. Z. Y. Chen. Semiflexible polymer brushes: A scaling theory. *J. Chem. Phys.*, 109(16):7017–7027, 1998.

[11] A. Halperin and D. R. M. Williams. Liquid crystalline polymers in nematic solvents: interfacial behaviour and active anchoring. *J. Phys. Condens. Matter*, 6(23A):A297, 1994.

[12] J. Hoogboom, T. Rasing, A. E. Rowan, and R. J. M. Nolte. LCD alignment layers. Controlling nematic domain properties. *J. Mater. Chem.*, 16:1305–1314, 2006.

[13] M. W. Matsen. Self-consistent field theory and its applications. In *Soft Matter: Polymer Melts and Mixtures*, volume 1. Wiley-VCH, Weinheim, 2006.

[14] T. M. Beardsley and M. W. Matsen. Universality between experiment and simulation of a diblock copolymer melt. *Phys. Rev. Lett.*, 117:217801, 2016.

[15] S. T. Milner, T. A. Witten, and M. E. Cates. Theory of the grafted polymer brush. *Macromolecules*, 21(8):2610–2619, 1985.

[16] S. T. Milner. Strong-stretching and Scheutjens-Fleer descriptions of grafted polymer brushes. *J. Chem. Soc., Faraday Trans.*, 86:1349–1353, 1990.

[17] J. U. Kim and M. W. Matsen. Finite-stretching corrections to the Milner-Witten-Cates theory for polymer brushes. *Eur. Phys. J. E*, 23(2):135–144, 2007.

[18] Y. Jiang, S. Li, and J. Z. Y. Chen. Perspective: parameters in a self-consistent field theory of multicomponent wormlike-copolymer melts. *Eur. Phys. J. E*, 39(10):91, 2016.

[19] P. Stasiak and M. W. Matsen. Efficiency of pseudo-spectral algorithms with Anderson mixing for the SCFT of periodic block-copolymer phases. *Eur. Phys. J. E*, 34(10):110, 2011.

[20] M. W. Matsen. Fast and accurate SCFT calculations for periodic block-copolymer morphologies using the spectral method with Anderson mixing. *Eur. Phys. J. E*, 30(4):361, 2009.

[21] M. Deng, Y. Jiang, H. Liang, and J. Z. Y. Chen. Wormlike polymer brush: A self-consistent field treatment. *Macromolecules*, 43(7):3455–3464, 2010.

[22] J. Z. Y. Chen. Theory of wormlike polymer chains in confinement. *Prog. Polym. Sci.*, 54-55:3 – 46, 2016.

[23] C. Greco, Y. Jiang, J. Z. Y. Chen, K. Kremer, and K. C. Daoulas. Maier-Saupe model of polymer nematics: Comparing free energies calculated with self consistent field theory and monte carlo simulations. *J. Chem. Phys.*, 145(18):184901, 2016.

[24] Y. Jiang, C. Greco, K. C. Daoulas, and J. Z. Y. Chen. Thermodynamics of a compressible Maier-Saupe model based on the self-consistent field theory of wormlike polymer. *Polymers*, 9(2), 2017.

[25] S. Alexander. Adsorption of chain molecules with a polar head a scaling description. *J. Phys. France*, 38(8):983–987, 1977.

[26] V. M. Amoskov, T. M. Birshtein, and V. A. Pryamitsyn. Theory of polymer brushes of liquid-crystalline polymers. *Macromolecules*, 29(22):7240–7250, 1996.

[27] P. Auroy, L. Auvray, and L. Léger. Characterization of the brush regime for grafted polymer layers at the solid-liquid interface. *Phys. Rev. Lett.*, 66:719–722, 1991.

[28] P. Auroy, L. Auvray, and L. Léger. Structures of end-grafted polymer layers: a small-angle neutron scattering study. *Macromolecules*, 24(9):2523–2528, 1991.

[29] K. Amini. Liquid crystalline polymer brushes. Master's thesis, University of Waterloo, 2016.

[30] M. Kleman and O. D. Lavrentovich. *Soft Matter Physics: An Introduction*. Springer Science & Business Media, 2004.

[31] S. Minko. *Grafting on Solid Surfaces: "Grafting to" and "Grafting from" Methods*. Springer Berlin Heidelberg, Berlin, Heidelberg, 2008.

[32] C. J. Hawker, A. W. Bosman, and E. Harth. New polymer synthesis by nitroxide mediated living radical polymerizations. *Chem. Rev.*, 101(12):3661–3688, 2001.

[33] K. Matyjaszewski, P. J. Miller, N. Shukla, B. Immaraporn, A. Gelman, B. B. Luokala, T. M. Siclovan, G. Kickelbick, T. Vallant, H. Hoffmann, and T. Pakula. Polymers at interfaces: using atom transfer radical polymerization in the controlled growth of homopolymers and block copolymers from silicon surfaces in the absence of untethered sacrificial initiator. *Macromolecules*, 32(26):8716–8724, 1999.

[34] M. Baum and W. J. Brittain. Synthesis of polymer brushes on silicate substrates via reversible addition fragmentation chain transfer technique. *Macromolecules*, 35(3):610–615, 2002.

[35] A. A. Mercurieva, T. M. Birshtein, and V. M. Amoskov. Theory of liquid-crystalline ordering in polymer brushes. *Macromol. Symp.*, 252(1):90–100, 2007.

[36] A. I. Tupitsyna, A. A. Darinskii, I. Emri, and M. P. Allen. Computer simulation of anisotropic polymer brushes. *Soft matter*, 4(1):108–121, 2008.

[37] P. G. de Gennes. Conformations of polymers attached to an interface. *Macromolecules*, 13(5):1069–1075, 1980.

[38] A. N. Semenov. Contribution to the theory of microphase layering in block-copolymer melts. *JETP*, 61(4):733, 1985.

[39] T. Cosgrove, T. G. Heath, J. S. Phipps, and R. M. Richardson. Neutron reflectivity studies of polymers adsorbed on mica from solution. *Macromolecules*, 24(1):94–98, 1991.

[40] J. B. Field, C. Toprakcioglu, R. C. Ball, H. B. Stanley, L. Dai, W. Barford, J. Penfold, G. Smith, and W. Hamilton. Determination of end-adsorbed polymer density profiles by neutron reflectometry. *Macromolecules*, 25(1):434–439, 1992.

[41] M. S. Kent, L. T. Lee, B. Farnoux, and F. Rondelez. Characterization of diblock copolymer monolayers at the liquid-air interface by neutron reflectivity and surface tension measurements. *Macromolecules*, 25(23):6240–6247, 1992.

[42] M. S. Kent, L. T. Lee, B. J. Factor, F. Rondelez, and G. S. Smith. Tethered chains in good solvent conditions: An experimental study involving Langmuir diblock copolymer monolayers. *J. Chem. Phys.*, 103(6):2320–2342, 1995.

[43] R. Baranowski and M. D. Whitmore. Theory of the structure of adsorbed block copolymers: Detailed comparison with experiment. *J. Chem. Phys.*, 103(6):2343–2353, 1995.

[44] M. P. Pépin and M. D. Whitmore. Monte carlo and numerical self-consistent field study of end-tethered polymers in good solvent. *J. Chem. Phys.*, 111(22):10381–10388, 1999.

[45] C. Seidel and R. R. Netz. Individual polymer paths and end-point stretching in polymer brushes. *Macromolecules*, 33(2):634–640, 2000.

[46] T. Kreer, S. Metzger, M. Müller, K. Binder, and J. Baschnagel. Static properties of end-tethered polymers in good solution: A comparison between different models. *J. Chem. Phys.*, 120(8):4012–4023, 2004.

[47] Roland R. Netz and M. Schick. Polymer brushes: from self-consistent field theory to classical theory. *Macromolecules*, 31(15):5105–5122, 1998.

[48] Shim, D.F.K. and Cates, M. E. Finite extensibility and density saturation effects in the polymer brush. *J. Phys. France*, 50(24):3535–3551, 1989.

[49] P. Y. Lai and A. Halperin. Polymer brush at high coverage. *Macromolecules*, 24(17):4981–4982, 1991.

[50] G. T. Pickett and T. A. Witten. End-grafted polymer melt with nematic interaction. *Macromolecules*, 25(18):4569–4574, 1992.

[51] B. Peng, D. Johannsmann, and J. Rühe. Polymer brushes with liquid crystalline side chains. *Macromolecules*, 32(20):6759–6766, 1999.

[52] B. Peng, J. Rühe, and D. Johannsmann. Homogeneously aligned liquid-crystal polymer brushes. *Adv. Mater.*, 12(11):821–824, 2000.

[53] F. Benmouna, B. Peng, J. Gapinski, A. Patkowski, J. Rühe, and D. Johannsmann. Dynamic light scattering from liquid crystal polymer brushes swollen in a nematic solvent. *Liq. Cryst.*, 28(9):1353–1360, 2001.

[54] P. J. Hamelinck and W. T. S. Huck. Homeotropic alignment on surface-initiated liquid crystalline polymer brushes. *J. Mater. Chem.*, 15(3):381–385, 2005.

[55] T. Uekusa, S. Nagano, and T. Seki. Unique molecular orientation in a smectic liquid crystalline polymer film attained by surface-initiated graft polymerization. *Langmuir*, 23(8):4642–4645, 2007.

[56] E. Vlasova, B. Volchek, I. Tarasenko, and G. Vlasov. Spectroscopic investigation of polypeptide plane brushes. In *Macromol. Symp.*, volume 305, pages 116–121. Wiley Online Library, 2011.

[57] H. A. Haque, M. Hara, S. Nagano, and T. Seki. Photoinduced in-plane motions of azobenzene mesogens affected by the flexibility of underlying amorphous chains. *Macromolecules*, 46(20):8275–8283, 2013.

[58] O. Sato, N. Iwata, T. Kasai, Y. Tsujii, S. Kang, J. Watanabe, and M. Tokita. Nematic liquid crystal anchoring strengths of high density polymer brush surfaces. *Liq. Cryst.*, 42(2):181–188, 2015.

[59] Y. Stetsyshyn, J. Raczkowska, A. Budkowski, K. Awsiuk, A. Kostruba, S. Nastyshyn, K. Harhay, E. Lychkovskyy, H. Ohar, and Y. Nastishin. Cholesterol-based grafted polymer brushes as alignment coating with temperature-tuned anchoring for nematic liquid crystals. *Langmuir*, 32(42):11029–11038, 2016.

[60] H. Tran, Y. Zhang, and C. K. Ober. Synthesis, processing, and characterization of helical polypeptide rod–coil mixed brushes. *ACS Macro Lett.*, 7(10):1186–1191, 2018.

[61] X. Li, T. Yanagimachi, C. Bishop, C. Smith, M. Dolejsi, H. Xie, K. Kurihara, and P. F. Nealey. Engineering the anchoring behavior of nematic liquid crystals on a solid surface by varying the density of liquid crystalline polymer brushes. *Soft matter*, 14(37):7569–7577, 2018.

[62] T. M. Birshtein, V. M. Amoskov, A. A. Mercurieva, and V. A. Pryamitsyn. Phase transitions in polymer brushes. *Macromol. Symp.*, 113(1):151–161, 1997.

[63] A. A. Darinskii, T. M. Birshtein, M. G. Saf'yannikova, V. M. Amoskov, A. I. Tupitsyna, and I. Emri. Microphase separation in brushes capable of liquid crystal ordering. *J. Polym. Sci. A*, 45(7):665–675, 2003.

[64] D. R. M. Williams and M. Warner. Statics and dynamics of hairpins in worm-like main chain nematic polymer liquid crystals. *Journal de Physique*, 51(4):317–339, 1990.

[65] T. Odijk. DNA confined in nanochannels: Hairpin tightening by entropic depletion. *J. Chem. Phys.*, 125(20):204904, 2006.

[66] J. Z. Y. Chen. Conformational properties of a back-folding wormlike chain confined in a cylindrical tube. *Phys. Rev. Lett.*, 118:247802, 2017.

[67] H. Lange and F. Schmid. Surface anchoring on liquid crystalline polymer brushes. *Computer physics communications*, 147(1-2):276–281, 2002.

[68] H. Lange and F. Schmid. Surface anchoring on layers of grafted liquid-crystalline chain molecules: A computer simulation. *J. Chem. Phys.*, 117(1):362–368, 2002.

[69] H. Lange and F. Schmid. An anchoring transition at surfaces with grafted liquid-crystalline chain molecules. *Eur. Phys. J. E*, 7(2):175–182, 2002.

[70] M. T. Downton and M. P. Allen. Computer simulation of liquid-crystal surface modification. *EPL*, 65(1):48, 2004.

[71] O. Kratky and G. Porod. Rntgenuntersuchung gelster fadenmolekle. *Recl. Trav. Chim. Pays-Bas*, 68(12):1106–1122, 1949.

[72] N. Saitô, K. Takahashi, and Y. Yunoki. The statistical mechanical theory of stiff chains. *J. Phys. Soc. Jpn.*, 22(1):219–226, 1967.

[73] A. A. Polotsky and T. M. Birshtein. Normal and lateral deformation of lyotropically ordered polymer brush. *Macromol. Theory Simul.*, 15(9):654–667, 2006.

[74] A. Milchev and K. Binder. Bending or buckling: Compression-induced phase transition in a semi-flexible polymer brush. *EPL*, 102(5):58003, 2013.

[75] A. Milchev and K. Binder. Unconventional ordering behavior of semi-flexible polymers in dense brushes under compression. *Soft Matter*, 10(21):3783–3797, 2014.

[76] J. Tang, X. Zhang, and D. Yan. Compression induced phase transition of nematic brush: A mean-field theory study. *The Journal of chemical physics*, 143(20):204903, 2015.

[77] G. Fredrickson. *The Equilibrium Theory of Inhomogeneous Polymers*. Oxford University Press, 2006.

[78] K. C. Daoulas, D. N. Theodorou, V. A. Harmandaris, N. C. Karayiannis, and V. G. Mavrantzas. Self-consistent-field study of compressible semiflexible melts adsorbed on a solid substrate and comparison with atomistic simulations. *Macromolecules*, 38(16):7134–7149, 2005.

[79] M. W. Matsen. Melts of semiflexible diblock copolymer. *J. Chem. Phys.*, 104(19):7758–7764, 1996.

[80] P. G. De Gennes and J Prost. *The physics of liquid crystals, 2nd edn. Clarendon*, volume 93. Oxford University Press, 1993.

[81] D. C. Morse and G. H. Fredrickson. Semiflexible polymers near interfaces. *Phys. Rev. Lett.*, 73:3235–3238, 1994.

[82] Y. Jiang and J. Z. Y. Chen. Isotropic-nematic interface in a lyotropic system of wormlike chains with the Onsager interaction. *Macromolecules*, 43(24):10668–10678, 2010.

[83] A. F. Hannon, R J. Kline, and D. DeLongchamp. Advancing the computational methodology of rigid rod and semiflexible polymer systems: A new solution to the wormlike chain model with rod-coil copolymer calculations. *J. Polym. Sci. B*, 57(1):29–39, 2019.

[84] S. M. Cui, O. Akcakir, and J. Z. Y. Chen. Isotropic-nematic interface of liquid-crystalline polymers. *Phys. Rev. E*, 51:4548–4557, 1995.

[85] T. M. Birshtein, A. A. Mercurieva, L. I. Klushin, and A. A. Polotsky. Liquid-crystalline polymer brushes: deformation and microphase segregation. *Comput. Theor. Polym. Sci.*, 8(1):179 – 189, 1998.

[86] L. I. Klushin, T. M. Birshtein, and A. A. Mercurieva. Microphase segregation in bridging polymeric brushes: Regular and singular phase diagrams. *Macromol. Theory Simul.*, 7(5):483–495, 1998.

[87] T. M. Birshtein and V. M. Amoskov. Homeotropic and planar structures in liquid-crystalline polymer brushes. *Comput. Theor. Polym. Sci.*, 10(1):159 – 163, 2000.

[88] V. M. Amoskov and T. M. Birshtein. Polydisperse anisotropic brushes. *Macromolecules*, 34(15):5331–5341, 2001.

[89] L. I. Klushin, T. M. Birshtein, and V. M. Amoskov. Microphase coexistence in brushes. *Macromolecules*, 34(26):9156–9167, 2001.

[90] T. M. Birshtein, V. M. Amoskov, L. I. Klushin, A. A. Mercurieva, A. A. Polotsky, and P. A. Iakovlev. Microphase coexistence in polymeric brushes. *Macromol. Symp.*, 191(1):51–58, 2003.

[91] T. Odijk. Theory of lyotropic polymer liquid crystals. *Macromolecules*, 19(9):2313–2329, 1986.

[92] A. R. Khokhlov and A. N. Semenov. Liquid-crystalline ordering in the solution of long persistent chains. *Physica A*, 108(2):546 – 556, 1981.

[93] J. Z. Y. Chen. Nematic ordering in semiflexible polymer chains. *Macromolecules*, 26(13):3419–3423, 1993.

[94] S. Blaber, P. Mahmoudi, R. K. W. Spencer, and M. W. Matsen. Effect of chain stiffness on the entropic segregation of chain ends to the surface of a polymer melt. *J. Chem. Phys.*, 150(1):014904, 2019.

[95] D. G. Anderson. Iterative procedures for nonlinear integral equations. *J. ACM*, 12(4):547–560, 1965.

[96] Y. Jiang, X. Zhang, B. Miao, and D. Yan. The study of the structure factor of a wormlike chain in an orientational external field. *J. Chem. Phys.*, 142(15):154901, 2015.

[97] B. Zdyrko and I. Luzinov. Polymer brushes by the "grafting to" method. *Macromol. Rapid Commun.*, 32(12):859–869, 2011.

[98] H. H. H. Homeier and E.O. Steinborn. Some properties of the coupling coefficients of real spherical harmonics and their relation to gaunt coefficients. *J. Mol. Struct.: THEOCHEM*, 368:31 – 37, 1996.

[99] A. J Liu and G. H Fredrickson. Free energy functionals for semiflexible polymer solutions and blends. *Macromolecules*, 26(11):2817–2824, 1993.

[100] S. Cheng, M. J. Stevens, and G. S. Grest. Ordering nanoparticles with polymer brushes. *J. Chem. Phys.*, 147(22):224901, 2017.

[101] D. Zhang, Y. Jiang, X. Wen, and L. Zhang. Phase separation and crystallization of binary nanoparticles induced by polymer brushes. *Soft Matter*, 9(6):1789–1797, 2013.

[102] D. Zhang, Y. Jin, J. Cheng, Y. Jiang, L. He, and L. Zhang. Self-assembly of nanorod/nanoparticle mixtures in polymer brushes. *J. Polym. Sci. B*, 52(4):299–309, 2014.

[103] Y. Hua, D. Zhang, and L. Zhang. Compression-driven migration of nanoparticles in semiflexible polymer brushes. *Polymer*, 83:67–76, 2016.

[104] R. B. Thompson, K. Ø. Rasmussen, and T. Lookman. Improved convergence in block copolymer self-consistent field theory by Anderson mixing. *J. Chem. Phys.*, 120(1):31–34, 2004.

APPENDICES

Appendix A

Numerical Method

In this chapter we present the numerical scheme used for solving the SCFT of a worm-like polymer brush interacting with an implicit solvent and MS type LC interactions. To solve the worm-like chain equation we will be using a method used previously,[94,78] but extended to include the azimuthal angle φ. We begin with the full treatment, including the spatial coordinate z, polar angle θ and azimuthal angle φ, then present the reduction from assuming azimuthal symmetry for a strongly stretched brush and finally a further reduction by assuming spatial homogeneity for a pure melt. We then conclude this chapter by describing the Anderson mixing scheme used for solving the field equations.

A.1 3D: Spherical Harmonics

If the grafting density is homogeneously distributed on the substrate then the concentration will be uniform along the axes parallel to the grafting plane (x, y) so these coordinates can be integrated out. Therefore, we will need 3 spatial coordinates: the distance from the grafting plane, z, the angle relative to the z axis, θ, and the azimuthal angle, φ as well as the backbone parameter s. The azimuthal angle φ allows for the polymers to align in any direction. The diffusion equation for the worm-like chain, Eq. (3.1), in the reduced coordinates is

$$\partial_s q(z, \mathbf{u}, s) + \ell_c u_z \partial_z q(z, \mathbf{u}, s) = \frac{\ell_c}{2\ell_p} \nabla^2_{\mathbf{u}} q(z, \mathbf{u}, s) - w(z, \mathbf{u}) q(z, \mathbf{u}, s) \ , \tag{A.1}$$

where $u_z = \cos(\theta)$ is the projection of $\mathbf{u}$ onto the z axis. Within this chapter ∂_z denotes the partial derivative with respect to z. In order to simplify the spherical Laplacian, $\nabla^2_{\mathbf{u}}$, we

will be evaluating the angular coordinates through spherical harmonic basis functions and using direct discretisation for z and s. The first step is therefore to expand all quantities in spherical harmonics. We will be using the real spherical harmonics with the Condon-Shortley phase defined as

$$Y_{lm}(\mathbf{u}) \equiv \begin{cases} (-1)^m\sqrt{2}\sqrt{\frac{(2l+1)}{4\pi}\frac{(l-|m|)!}{(l+|m|)!}}P_l^{|m|}(\cos(\theta))\sin(|m|\varphi) & \text{if } m<0 \\ \sqrt{\frac{(2l+1)}{4\pi}}P_l^m(\cos(\theta)) & \text{if } m=0 \\ (-1)^m\sqrt{2}\sqrt{\frac{(2l+1)}{4\pi}\frac{(l-|m|)!}{(l+|m|)!}}P_l^m(\cos(\theta))\cos(m\varphi) & \text{if } m>0 \end{cases} \tag{A.2}$$

where $P_l^m(\cos(\theta))$ are the associated Legendre polynomials,

$$P_l^m(x) \equiv (-1)^m(1-x^2)^{m/2}\frac{d^m}{dx^m}(P_l(x)) \ , \tag{A.3}$$

for non negative integer l and m. The associated Legendre polynomials are expressed in terms of the usual Legendre polynomials $P_l(x)$,

$$P_l(x) \equiv \frac{1}{2^l l!}\frac{d^l}{dx^l}(x^2-1)^l \ . \tag{A.4}$$

The spherical harmonics satisfy the normalization (recall $d\mathbf{u} = \sin(\theta)d\theta d\varphi$)

$$\int d\mathbf{u} Y_{lm}(\mathbf{u})Y_{l'm'}(\mathbf{u}) = \delta_{ll'}\delta_{mm'} \ , \tag{A.5}$$

with $\delta_{ll'}$ the Kronecker delta.

Expanding the relevant quantities in spherical harmonics we have the field,

$$w(z,\mathbf{u}) = \sum_{lm} w_{lm}(z)Y_{lm}(\mathbf{u}) \ , \tag{A.6}$$

concentration,

$$\phi(z,\mathbf{u}) = \sum_{lm} \phi_{lm}(z)Y_{lm}(\mathbf{u}) \ , \tag{A.7}$$

and partial partition functions

$$\begin{aligned} q(z,\mathbf{u},s) &= \sum_{lm} q_{lm}(z,s)Y_{lm}(\mathbf{u}) \\ q^\dagger(z,\mathbf{u},s) &= \sum_{lm} q^\dagger_{lm}(z,s)Y_{lm}(\mathbf{u}) \ . \end{aligned} \tag{A.8}$$

We begin by writing the field, Eq. (4.3), in terms of Legendre polynomials

$$w(z,\mathbf{u}) = \int d\mathbf{u}' \left(\Lambda_0 P_0(\mathbf{u}\cdot\mathbf{u}') - \Lambda_2 P_2(\mathbf{u}\cdot\mathbf{u}')\right)\phi(z,\mathbf{u}') \ . \tag{A.9}$$

Using Eq. (2.9) the first term gives the $l = 0$ and $m = 0$ component

$$w_{00}(z) = 4\pi\Lambda_0\phi_{00}(z) \ , \tag{A.10}$$

and the second yields

$$w_{2m}(z) = -\frac{4\pi\Lambda_2}{5}\sum_m \phi_{2m}(z) \ . \tag{A.11}$$

In general, for interactions of the form in Eq. (2.4) the coefficients are

$$w_{lm}(z) = -\sum_{lm}\Lambda_l\frac{4\pi}{2l+1}\phi_{lm}(z) \ . \tag{A.12}$$

The concentration is determined from the partial partition functions, using Eq. (A.8), (3.4) and (A.7), the concentration is

$$\sum_{l''m''}\phi_{l''m''}(z)Y_{l''m''}(\mathbf{u}) = \frac{1}{Q}\sum_{lm}\sum_{l'm'}\int ds q_{lm}(z,s)q^\dagger_{l'm'}(z,s)Y_{lm}(\mathbf{u})Y_{l'm'}(\mathbf{u}) \ . \tag{A.13}$$

Multiplying both sides by $Y_{l'''m'''}(\mathbf{u})$ and integrating over $\mathbf{u}$, by the orthogonality condition of the spherical harmonics, Eq. (A.5), we have

$$\phi_{l''m''}(z) = \frac{1}{Q}\sum_{l,l'}\sum_{m,m'}\psi^{mm'm''}_{ll'l''}\int_0^1 \mathrm{d}s q_{lm}(z,s)q^\dagger_{l'm'}(z,s) \tag{A.14}$$

where

$$\psi^{mm'm''}_{ll'l''} \equiv \int d\mathbf{u}Y_{lm}(\mathbf{u})Y_{l'm'}(\mathbf{u})Y_{l'''m'''}(\mathbf{u}) \tag{A.15}$$

are the Gaunt coefficients for the real spherical harmonics, which are calculated as described in Ref. [98].

Finally, the partition function, Eq. (3.5), is

$$Q = \sum_{lm}\int dz q_{lm}(z,s)q^\dagger_{lm}(z,s) \ , \tag{A.16}$$

by Eq. (A.5). Now all that remains is the evaluation of the partial partition functions, which is the most computationally intensive step.

A.1.1 Solution to the Worm-like Chain Equation

Our numerical methods have been discussed previously. We solve Eq. 4.6 using the numerical algorithm described in Refs. [78,94] but with the expansion in terms of spherical harmonics, $Y_{lm}(\theta,\varphi)$, rather than Legendre polynomials. We will be using a second order Lax-Wendroff approach to numerically solve Eq. (A.19). Taylor expanding $q(z,\mathbf{u},s)$

$$q(z,\mathbf{u},s+\Delta s) \approx q(z,\mathbf{u},s) + \Delta s\partial_s q(z,\mathbf{u},s) + \frac{(\Delta s)^2}{2}\partial_{ss} q(z,\mathbf{u},s) \tag{A.17}$$

leads to

$$\frac{q(z,\mathbf{u},s+\Delta s) - q(z,\mathbf{u},s)}{\Delta s} \approx \partial_s q(z,\mathbf{u},s) + \frac{\Delta s}{2}\partial_{ss} q(z,\mathbf{u},s) \ . \tag{A.18}$$

We will be using only difference equations for ∂_s, ∂_z and ∂_{zz} so we must write ∂_{ss} in terms of ∂_s, ∂_z and ∂_{zz}.

In the spherical harmonic basis, Eq. (A.1) can be written as

$$\begin{aligned} &Y_{lm}(\mathbf{u})\partial_s q_{lm}(z,s) + \ell_c\sqrt{\frac{4\pi}{3}}Y_{10}(\mathbf{u})Y_{lm}(\mathbf{u})\partial_z q_{lm}(z,s) \\ &= \frac{\ell_c}{2\ell_p}l(l+1)Y_{lm}(\mathbf{u})q_{lm}(z,s) - Y_{l'm'}(\mathbf{u})Y_{lm}(\mathbf{u})w_{l'm'}(z)q_{lm}(z,s) \ , \end{aligned} \tag{A.19}$$

where in this section we adopt the Einstein summation convention of implied summation over all repeated indices and we used that fact that $Y_{10}(\mathbf{u}) = \sqrt{3/(4\pi)}u_z$. Multiplying by $Y_{lm}(\mathbf{u})$ and integrating over $\mathbf{u}$ we have

$$\begin{aligned} &\delta_{l,l''}\delta_{mm''}\partial_s q_{lm}(z,s) + \ell_c\sqrt{\frac{4\pi}{3}}\psi^{0m''m}_{1l''l}\partial_z q_{lm}(z,s) \\ &= \frac{\ell_c}{2\ell_p}l(l+1)\delta_{l,l''}\delta_{mm''}q_{lm}(z,s) - w_{l'm'}(z)\psi^{m'm''m}_{l'l''l}q_{lm}(z,s) \ , \end{aligned} \tag{A.20}$$

By defining constants $c \equiv \frac{\ell_c}{2\ell_p}$ and $a \equiv \sqrt{\frac{4\pi}{3}}$, our equation becomes

$$\begin{aligned} &\delta_{l,l''}\delta_{mm''}\partial_s q_{lm}(z,s) + \ell_c a\psi^{0m''m}_{1l''l}\partial_z q_{lm}(z,s) \\ &= cl(l+1)\delta_{l,l''}\delta_{mm''}q_{lm}(z,s) - w_{l'm'}(z)\psi^{m'm''m}_{l'l''l}q_{lm}(z,s) \ , \end{aligned} \tag{A.21}$$

Or in matrix notation we have

$$I\partial_s \boldsymbol{q} + \ell_c a\Psi_1\partial_z\boldsymbol{q} = -cL\boldsymbol{q} - [\boldsymbol{w}\cdot\Psi]\boldsymbol{q} \ , \tag{A.22}$$

where I is the $lm \times l''m''$ identity matrix, $\boldsymbol{q}$ is a column vector with elements q_{lm}, Ψ_1 has elements $\psi_{1l''l}^{0m''m}$, L is an $lm \times l''m''$ diagonal matrix $L = diag(l(l+1)\delta_{m0}\delta_{m''0})$ and $[\boldsymbol{w}\cdot\Psi] = \sum_{l'm'} \psi_{l'l''l}^{m'm''m} w_{l',m'}$.

Deriving with respect to s leads to

$$I\partial_{ss}\boldsymbol{q} + \ell_c a \Psi_1 \partial_{sz}\boldsymbol{q} = -cL\partial_s\boldsymbol{q} - [\boldsymbol{w}\cdot\Psi]\partial_s\boldsymbol{q} \tag{A.23}$$

and with respect to z

$$I\partial_{sz}\boldsymbol{q} + \ell_c a \Psi_1 \partial_{zz}\boldsymbol{q} = -cL\partial_z\boldsymbol{q} - [\boldsymbol{w}\cdot\Psi]\partial_z\boldsymbol{q} - [\partial_z\boldsymbol{w}\cdot\Psi]\boldsymbol{q} \tag{A.24}$$

Combining these two equations ((A.23)-$\ell_c a\Psi_1$(A.24)) allows us to solve for $\partial_{ss}\boldsymbol{q}$ in terms of $\partial_s, \partial_z, \partial_{zz}$:

$$I\partial_{ss}\boldsymbol{q} = \ell_c^2 a\Psi_1 a\Psi_1 \partial_{zz}\boldsymbol{q} + \left[bca\Psi_1 L + \ell_c a\Psi_1[\boldsymbol{w}\cdot\Psi]\right]\partial_z\boldsymbol{q} - \left[cL + [\boldsymbol{w}\cdot\Psi]\right]\partial_s\boldsymbol{q} + \ell_c a\Psi_1[\partial_z\boldsymbol{w}\cdot\Psi]\boldsymbol{q} \ . \tag{A.25}$$

Which simplifies to

$$I\partial_{ss}\boldsymbol{q} = \ell_c^2 a^2 {\Psi_1}^2 \partial_{zz}\boldsymbol{q} + \ell_c a\Psi_1\left[cL + [\boldsymbol{w}\cdot\Psi]\right]\partial_z\boldsymbol{q} - \left[cL + [\boldsymbol{w}\cdot\Psi]\right]\partial_s\boldsymbol{q} + \ell_c a\Psi_1[\partial_z\boldsymbol{w}\cdot\Psi]\boldsymbol{q} \ , \tag{A.26}$$

where ${\Psi_1}^2 = \Psi_1\Psi_1$. Adding $\frac{\Delta s}{2}$(A.26) to the right hand side of Eq. (A.22) yields the form of Eq. (A.18)

$$\begin{aligned} I\partial_s\boldsymbol{q} =& \frac{\Delta s}{2}\ell_c^2 a^2 {\Psi_1}^2 \partial_{zz}\boldsymbol{q} + \ell_c a\Psi_1\left[\frac{\Delta s}{2}cL + \frac{\Delta s}{2}[\boldsymbol{w}\cdot\Psi] - I\right]\partial_z\boldsymbol{q} - \frac{\Delta s}{2}\left[cL + [\boldsymbol{w}\cdot\Psi]\right]\partial_s\boldsymbol{q} \\ &+ \left[\frac{\Delta s}{2}\ell_c a\Psi_1[\partial_z\boldsymbol{w}\cdot\Psi] - cL - [\boldsymbol{w}\cdot\Psi]\right]\boldsymbol{q} \end{aligned} \tag{A.27}$$

Solving for $\partial_s\boldsymbol{q}$

$$\begin{aligned} \left[\frac{\Delta s}{2}cL + \frac{\Delta s}{2}[\boldsymbol{w}\cdot\Psi] + I\right]\partial_s\boldsymbol{q} =& \frac{\Delta s}{2}\ell_c^2 a^2 {\Psi_1}^2 \partial_{zz}\boldsymbol{q} + \ell_c a\Psi_1\left[\frac{\Delta s}{2}cL + \frac{\Delta s}{2}[\boldsymbol{w}\cdot\Psi] - I\right]\partial_z\boldsymbol{q} \\ &+ \left[\frac{\Delta s}{2}\ell_c a\Psi_1[\partial_z\boldsymbol{w}\cdot\Psi] - cL - [\boldsymbol{w}\cdot\Psi]\right]\boldsymbol{q} \end{aligned} \tag{A.28}$$

Defining the matrices

$$A = \left[\frac{1}{2}cL + \frac{1}{2}[\boldsymbol{w}\cdot\Psi] + \frac{1}{\Delta s}I\right] \tag{A.29a}$$

$$B = \frac{\Delta s}{(\Delta z)^2}\frac{1}{2}\ell_c^2 a^2 {\Psi_1}^2 \tag{A.29b}$$

$$C = \frac{\Delta s}{2\Delta z}\ell_c a\Psi_1\left[\frac{1}{2}cL + \frac{1}{2}[\boldsymbol{w}\cdot\Psi] - \frac{1}{\Delta s}I\right] \tag{A.29c}$$

$$D = \left[\frac{\Delta s}{2}\ell_c a\Psi_1[\partial_z\boldsymbol{w}\cdot\Psi] - cL - [\boldsymbol{w}\cdot\Psi]\right] \tag{A.29d}$$

So our equation becomes

$$\Delta s A\partial_s\boldsymbol{q} = (\Delta z)^2 B\partial_{zz}\boldsymbol{q} + 2\Delta z C\partial_z\boldsymbol{q} + D\boldsymbol{q}\ . \tag{A.30}$$

Next we approximate the derivatives by letting, $i = s$, $i+1 = s+\Delta s$ and $j = z$, $j+1 = z+\Delta z$. Then we have our discretized derivatives:

$$\partial_s\boldsymbol{q} = \frac{1}{\Delta s}(\boldsymbol{q}^{i+1,j} - \boldsymbol{q}^{i,j}) \tag{A.31a}$$

$$\partial_z\boldsymbol{q} = \frac{1}{2\Delta z}(\boldsymbol{q}^{i,j+1} - \boldsymbol{q}^{i,j-1}) \tag{A.31b}$$

$$\partial_{zz}\boldsymbol{q} = \frac{1}{(\Delta z)^2}(\boldsymbol{q}^{i,j+1} - 2\boldsymbol{q}^{i,j} + \boldsymbol{q}^{i,j-1}) \tag{A.31c}$$

$$\tag{A.31d}$$

Substituting yields

$$A(\boldsymbol{q}^{i+1,j} - \boldsymbol{q}^{i,j}) = B(\boldsymbol{q}^{i,j+1} - 2\boldsymbol{q}^{i,j} + \boldsymbol{q}^{i,j-1}) + C(\boldsymbol{q}^{i,j+1} - \boldsymbol{q}^{i,j-1}) + D\boldsymbol{q}^{i,j}\ . \tag{A.32}$$

To get the desired forward marching solution we collect like terms and solve for $\boldsymbol{q}^{i+1,j}$

$$\boldsymbol{q}^{i+1,j} = A^{-1}[B-C]\boldsymbol{q}^{i,j-1} + A^{-1}[A+D-2B]\boldsymbol{q}^{i,j} + A^{-1}[B+C]\boldsymbol{q}^{i,j+1}\ . \tag{A.33}$$

A.2 Azimuthally Symmetric: Legendre Polynomials

If we assume the chain is strongly stretched the polymers will tend to align along the z axis, in which case the solution will be azimuthally symmetric (independent of φ). Integrating over φ yields the concentration

$$\phi(z,u_z) = \int_0^{2\pi} d\varphi\phi(z,\mathbf{u})\ , \tag{A.34}$$

normalized such that

$$\int dz du_z \phi(z, u_z) = \ell_c \ . \tag{A.35}$$

Similarly, integrating out φ from the field equation we have

$$w(z, u_z) = \int du'_z G(u_z, u'_z) \phi(z, u'_z) \ , \tag{A.36}$$

written in terms of the scaled interaction energy

$$G(u_z, u'_z) = \Lambda_0 - \Lambda_2 P_2(u_z) P_2(u'_z) \ . \tag{A.37}$$

Since the system is azimuthally symmetric, only the $m = 0$ spherical harmonics will be non-zero, which reduces to the Legendre polynomials in terms of u_z as

$$Y_{l0}(\mathbf{u}) = \sqrt{\frac{(2l+1)}{4\pi}} P_l(u_z) \ . \tag{A.38}$$

The Legendre polynomials satisfy the orthogonality relation

$$\int_{-1}^{1} du_z P_l(u_z) P_{l'}(u_z) = \frac{2}{2l+1} \delta_{l,l'} \tag{A.39}$$

Expanding the relevant quantities in Legendre polynomials we have the field,

$$w(z, u_z) = \sum_l w_l(z) P_l(u_z) \ , \tag{A.40}$$

concentration,

$$\phi(z, u_z) = \sum_l \phi_l(z) P_l(u_z) \ , \tag{A.41}$$

and partial partition functions

$$\begin{aligned} q(z, u_z, s) &= \sum_l q_l(z, s) P_l(u_z) \\ q^\dagger(z, u_z, s) &= \sum_l q_l^\dagger(z, s) P_l(u_z) \ . \end{aligned} \tag{A.42}$$

The coefficients are related to the previous spherical harmonic coefficients by

$$g_l(z) = \sqrt{\frac{(2l+1)}{4\pi}} g_{l0} \ , \tag{A.43}$$

in all cases.

In this case the field equation simplifies to

$$w(z, u_z) = \Lambda_0 \phi_0(z) - \Lambda_2 \phi_2(z) P_2(u_z) \ , \tag{A.44}$$

which, by the orthogonality of the Legendre polynomials, Eq. (A.39), implies coefficients

$$\begin{aligned} w_0(z) &= 2\Lambda_0 \phi_0(z) \ , \\ w_2(z) &= -\frac{2\Lambda_2}{5} \phi_2(z) \ . \end{aligned} \tag{A.45}$$

The concentration simplifies considerably

$$\phi_{l''}(z) = \frac{1}{Q} \sum_{l,l'} \Gamma_{ll'l''} \int_0^1 \mathrm{d}s q_l(z,s) q_{l'}^\dagger(z,s) \tag{A.46}$$

where

$$\Gamma_{l,l',l''} = \begin{pmatrix} l & l' & l'' \\ 0 & 0 & 0 \end{pmatrix} = (-1)^k \sqrt{\frac{(2k-2l)!(2k-2l')!(2k-2l'')!}{(2k+1)!}} \frac{k!}{(k-l)!(k-l')!(k-l'')!} \tag{A.47}$$

for $2k = l + l' + l''$ even and l, l', l'' satisfying $|l - l'| \leq l'' \leq l + l'$. It is zero otherwise. The factor $\Gamma_{l,l',l''}$ arises from the integral over three Legendre polynomials.

The partition function, Eq. (3.5), is

$$Q = \sum_l \frac{2}{2l+1} \int dz q_l(z,s) q_l^\dagger(z,s) \ , \tag{A.48}$$

by Eq. (A.39). The partial partition functions are solved according to the numerical scheme described in Section A.1.1 with only the $m = 0$ components.

A.3 Spatially Homogeneous Polymer Melt

In the melt state the distribution of polymer will be spatially homogeneous and we can therefore integrate out the remaining Cartesian coordinate, z, leaving only θ and φ; additionally, by orienting our coordinate system such that the z axis corresponds with the alignment direction of the nematic phase we are only left with the coordinate u_z. In these reduced coordinates we still maintain our expansions in terms of Legendre polynomials identical to Section A.2. Integrating the concentration over z we have

$$\phi(u_z) = \int dz \phi(z, u_z) \ , \tag{A.49}$$

normalized such that

$$\frac{1}{\ell_c} \int du_z \phi(u_z) = 1 \ . \tag{A.50}$$

Similarly, integrating out z from the field equation yields

$$w(u_z) = \int du'_z G(u_z, u'_z) \phi(u'_z) \ , \tag{A.51}$$

written in terms of the scaled interaction energy

$$G(u_z, u'_z) = \Lambda_2 P_2(u_z) P_2(u'_z) \ . \tag{A.52}$$

The greatest simplification is to the diffusion equation, Eq. (A.19), which becomes

$$\partial_s q(u_z, s) = \left[\frac{\ell_c}{2\ell_p} \nabla^2_{u_z} - w(u_z) \right] q(u_z, s) \ , \tag{A.53}$$

or in terms of Legendre polynomials, in matrix notation,

$$I \partial_s \boldsymbol{q} = -cL\boldsymbol{q} - [\boldsymbol{w} \cdot \Psi]\boldsymbol{q} \ . \tag{A.54}$$

This has the solution

$$\boldsymbol{q}(s) = e^{-[cL + [\boldsymbol{w} \cdot \Psi]]s} \boldsymbol{q}(0) \ . \tag{A.55}$$

In the melt phase both ends of the chain are free and therefore q and $q^\dagger$ satisfy the same initial condition, which we assume to be isotropic, $q(u_z, 0) = 1$, which implies

$$q_l(0) = \delta_{l0} \ , \tag{A.56}$$

and $q^\dagger(u_z, s) = q^\dagger(-u_z, 1-s)$. We therefore have the concentration

$$\phi(u_z) = \frac{1}{Q}\sum_{l,l'}\int_0^1 ds[e^{-[cL+[\boldsymbol{w}\cdot\Psi]]s}]_{l,0}P_l(u_z)[e^{[cL+[\boldsymbol{w}\cdot\Psi]]s}e^{-[cL+[\boldsymbol{w}\cdot\Psi]]}]_{l',0}P_{l'}(u_z)(-1)^{l'} \ , \quad \text{(A.57)}$$

or in Legendre coefficients

$$\phi_{l''} = \frac{1}{Q}\sum_{l,l'}(-1)^{l'}\psi_{l,l'',l'}\int_0^1 ds[e^{-[cL+[\boldsymbol{w}\cdot\Psi]]s}]_{l,0}[e^{[cL+[\boldsymbol{w}\cdot\Psi]]s}e^{-[cL+[\boldsymbol{w}\cdot\Psi]]}]_{l',0} \ , \quad \text{(A.58)}$$

with partition function

$$Q = \sum_l \frac{2}{2l+1}[e^{-[cL+[\boldsymbol{w}\cdot\Psi]]}]_{0,0} \ , \quad \text{(A.59)}$$

The free energy per chain is

$$F = -\ln(Q) - \frac{1}{2}\int \mathrm{d}u_z w(u_z)\phi(u_z) \ , \quad \text{(A.60)}$$

where in the isotropic phase $w = 0$ so $Q = 2$ and $F = -\ln 2$.

A.4 Anderson Mixing

The methods described above solve for a worm-like chain in a given external field; however, the field is not entirely external and must be calculated self-consistently. The field equations are solved using the Anderson mixing algorithm,[95] commonly used for block copolymers.[104,20,19] We begin by describing the simpler, but closely related, Picard iteration method, commonly referred to as "simple mixing". In simple mixing one starts with an initial guess for the field and iteratively updates it according to the scheme

$$w_{i+1}^{\text{in}}(\mathbf{r}, \mathbf{u}) = w_i^{\text{in}}(\mathbf{r}, \mathbf{u}) + \lambda d_i(\mathbf{r}, \mathbf{u}) \quad \text{(A.61)}$$

with λ the iteration step size, typically taking a small value $\lambda \sim 0.1$ and

$$d_i(\mathbf{r}, \mathbf{u}) \equiv w_i^{\text{out}}(\mathbf{r}, \mathbf{u}) - w_i^{\text{in}}(\mathbf{r}, \mathbf{u}) \ . \quad \text{(A.62)}$$

The input field $w_i^{\text{in}}(\mathbf{r},\mathbf{u})$ is used to calculate the concentration using the methods described in the previous section, the output field, $w_i^{\text{out}}(\mathbf{r},\mathbf{u})$, is then calculated from this concentration through the field equation and the input field is updated according to Eq. (A.61). From the deviation, Eq. (A.62), we define the total deviation

$$d_i^{\text{tot}} = \left| \frac{\int d\mathbf{r}d\mathbf{u} d_i^2(\mathbf{r},\mathbf{u})}{\int d\mathbf{r}d\mathbf{u}(w_i^{\text{out}}(\mathbf{r},\mathbf{u}))^2} \right| \tag{A.63}$$

simple mixing is performed until the total deviation is below a specified tolerance, typically $d_i^{\text{tot}} \sim 10^{-3}$.

The Anderson mixing scheme that we employ is similar to simple mixing, the key difference being that simple mixing updates the field based solely on the current iteration while Anderson mixing accounts for previous iteration steps and would give the best mixing parameters possible if the system of equations was linear. Although the system is non-linear, Anderson mixing can dramatically decrease the number of mixing steps required.

To incorporate the results of previous iterations, which we refer to as *histories*, we define the matrix

$$U_{nm} = \int d\mathbf{r}d\mathbf{u}(d_i(\mathbf{r},\mathbf{u}) - d_{i-n}(\mathbf{r},\mathbf{u}))(d_i(\mathbf{r},\mathbf{u}) - d_{i-m}(\mathbf{r},\mathbf{u})) \tag{A.64}$$

and the vector

$$V_m = \int d\mathbf{r}d\mathbf{u}(d_i(\mathbf{r},\mathbf{u}) - d_{i-m}(\mathbf{r},\mathbf{u}))d_i(\mathbf{r},\mathbf{u}) \ . \tag{A.65}$$

The indices n and m run over the number of histories chosen to keep. The product

$$A_n = \sum_m U_{nm}^{-1} V_m \tag{A.66}$$

gives the mixing coefficients and the field is then updated as

$$w_{i+1}^{\text{in}}(\mathbf{r},\mathbf{u}) = w_i^{\text{out}}(\mathbf{r},\mathbf{u}) + \sum_n A_n(w_{i-n}^{\text{out}}(\mathbf{r},\mathbf{u}) - w_i^{\text{out}}(\mathbf{r},\mathbf{u})) \ . \tag{A.67}$$

This procedure is repeated until the total deviation is below a specified tolerance.

Appendix B

Polymer Melt

In this appendix we study the bulk behaviour of LC polymers within the WLC model with MS interaction, focusing on the behaviour of the isotropic to nematic transition. Although this has already been studied in Ref. [96], it will serve as a test of numerics and will set bounds for when a brush will order. Additionally, this simplified system allows for direct comparisons between Onsager and MS interactions.

B.1 Theory

Consider an incompressible melt of n_p polymers in a volume V interacting through MS type LC interaction. Each polymer consists of N segments of length b, giving a total contour length of $\ell_c = Nb$. The configuration of the polymer chain is specified by the space curve $\mathbf{r}(s)$, where the backbone parameter runs from $s = 0$ at the grafted end to 1 at the free end. The orientation of the chain is then given by the unit vector $\mathbf{u}(s) = \ell_c^{-1}\frac{d}{ds}\mathbf{r}(s)$. In the mean field approximation the melt will be spatially homogeneous and therefore we need only consider the orientation of the polymers. By aligning our coordinate system with the alignment axis of the polymers the system is reduced to one coordinate, u_z, the angle that a polymer makes with the alignment, z, axis.

As discussed in A.3 the concentration is

$$\phi(u_z) = \int dz \phi(z, u_z) \ , \tag{B.1}$$

normalized such that

$$\int du_z \phi(u_z) = \ell_c \ . \tag{B.2}$$

The field equation

$$w(u_z) = \int du'_z G(u_z, u'_z)\phi(u'_z) \ , \tag{B.3}$$

is written in terms of the scaled interaction energy

$$G(u_z, u'_z) = -\Lambda_2 P_2(u_z)P_2(u'_z) \ . \tag{B.4}$$

with the reduced interaction parameters defined as previously

$$\Lambda_2 \equiv \frac{\nu_2 n_{\rm p} N}{V\rho_0} \ . \tag{B.5}$$

We have dropped the isotropic term Λ_0 since it will simply add a constant to field and will not change the concentration. The degree of polymerization, N, and contour length ℓ_c can be scaled out of the expressions by simply expressing all lengths in terms of $\ell_c = bN$. Thus the brush can be characterized by two parameters, $\ell_{\rm p}/\ell_{\rm c}$ and Λ_2.

To quantify the degree of orientational order we use the scalar nematic order parameter

$$\mathcal{S} = \int_{-1}^{1} du_z P_2(u_z)\phi(u_z) \ , \tag{B.6}$$

This allows us to express the field in term of the order parameter as

$$w(u_z) = -\mathcal{S}P_2(u_z) \ , \tag{B.7}$$

so the difference of free energy between the nematic and isotropic states, $\Delta F \equiv F_{\rm nem} - F_{\rm iso}$ is (A.60)

$$\frac{\Delta F}{n_{\rm p} k_{\rm B} T} = -\ln\left(\frac{Q}{2}\right) - \frac{\Lambda_2 \mathcal{S}^2}{2} \ , \tag{B.8}$$

where,

$$Q = \int_{-1}^{1} du_z \, q(u_z, s) q^{\dagger}(u_z, s) \tag{B.9}$$

is a single-chain partition function. The partial partition functions q and $q^{\dagger}$ are calculated as described in A.3.

We can directly compare the transition from using Onsager interactions through the relation described in Chapter 2

$$w(u_z) = -\sum_l \frac{\Lambda_{2l}}{2} \int_{-1}^{1} du'_z P_{2l}(u'_z)\phi(u'_z) \ , \tag{B.10}$$

where

$$\Lambda_{2l} = -\frac{\epsilon N}{V\rho_0}\frac{\pi(4l+1)(2l)!(2l-2)!}{2^{4l+1}(l-1)!l!(l+1)!} \ . \tag{B.11}$$

The relationship between the Onsager interaction strength ϵ and the MS interaction strength Λ_2 is found by equating the $l = 1$ components above.

B.2 Results

We begin by analysing the scalar nematic order parameter as a function of LC interaction strength Λ_2 in Fig. B.1. As Λ_2 is increased the order parameter discontinuously jumps from $\mathcal{S} = 0$ to $\mathcal{S} > 0$, the characteristic behaviour of a first order phase transition. From this plot we can see the nematic transition moves toward higher interaction strength as the persistence length decreases. Additionally, for higher persistence lengths we observe a steeper slope meaning the polymers transition to a high degree of order more rapidly. For very strong LC interactions $\mathcal{S}$ approaches its maximal possible value of 1.

In order to determine whether the isotropic or nematic phase is stable we compare their free energy in Fig. B.1. When the difference in free energy ΔF crosses 0 the system transitions from isotropic to nematic. The isotropic solution always exists but becomes unstable past the spinodal. Similarly the nematic phase persists below the transition before no longer being a solution. The distance over which it persists is very short, only perceptible on the scale shown for the most flexible polymer $\ell_c = 16\ell_p$ suggesting that the transition is only weakly first order.

By varying the persistence length we can construct a phase diagram separating the isotropic and nematic states in the ℓ_p/ℓ_c, Λ_2 plane depicted in Fig. B.2. Rigid polymer and high interaction strength result in nematic ordering. Previous calculations by Ref. [96] yield identical results for the transition. Additionally, we can directly compare the transition with that obtained through Onsager interaction. On the scale shown the difference in the transition from the two methods is negligible. To leading order in Legendre polynomials the transitions would be identical; however, in general the transition from Onsager interactions is always below the MS since it includes higher order Legendre polynomial interactions which all favour nematic ordering. We also compare the transition obtained from Landau series expansion in terms of the scalar order parameter $\mathcal{S}$ which will be given in detail within the discussion. In general it always over estimates the value of Λ_2 required or the transition.

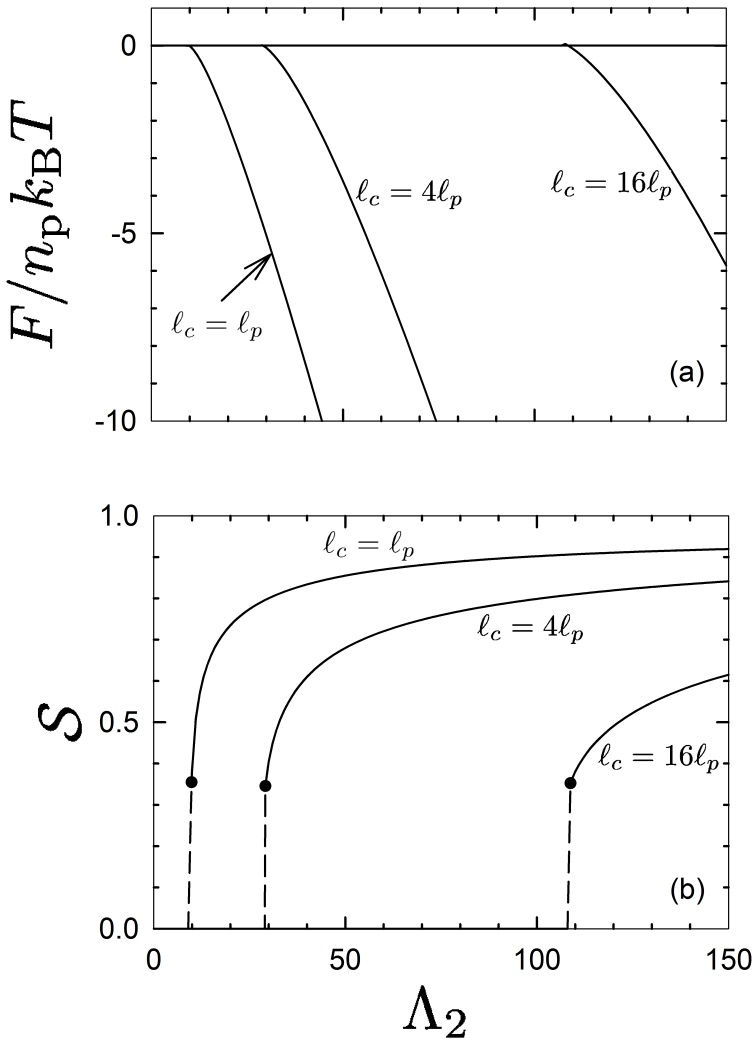

Fig B.1. (a) Free energy and (b) scalar nematic order parameter as a function of interaction strength for persistence lengths of $\ell_c = \ell_p$, $4\ell_p$ and $16\ell_p$.

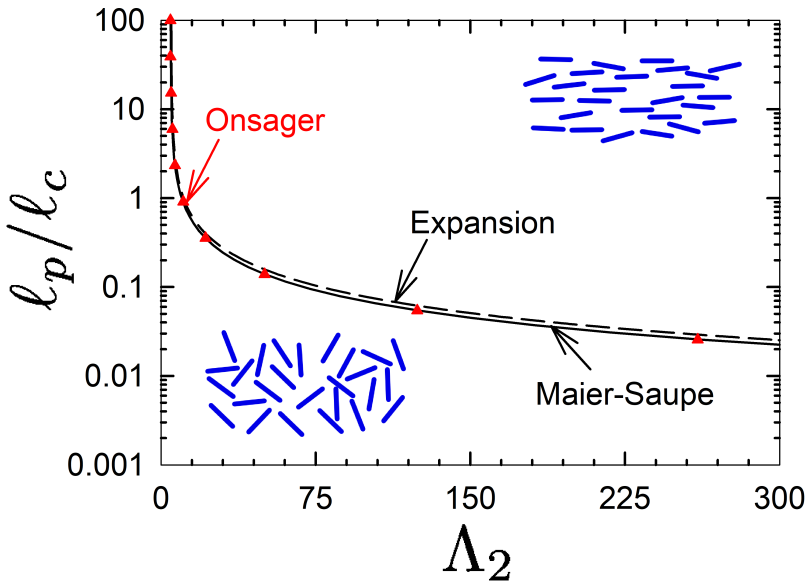

Fig B.2. Isotropic-nematic phase transition as a function of persistence length ℓ_p/ℓ_c and LC interaction strength Λ_2. Solid line and red triangles separate the isotropic and nematic phase for MS and Onsager interactions respectively, while the dashed line denotes the series expansion approximation.

B.3 Discussion

As discussed in Chapter 2 we can make a direct comparison between the Onsager and MS interactions by equating the $l = 0$ and $l = 2$ terms between the two via Eq. (B.11). In a melt the isotropic, $l = 0$, term does not effect the concentration and we can directly compare the phase diagrams from Onsager and MS interactions shown in Fig. B.2. Since near the phase transition their orientational order is small, the higher order terms in the Onsager interactions do not significantly contribute and the phase diagrams are identical on the scale shown. In general the the transition from Onsager interactions are slightly above the MS. Although the Onsager interactions include higher order terms this should not be misinterpreted as the Onsager model being more accurate, it will only be more accurate in the specific scenario where the dominant contributions are from excluded volume of rigid rods and it is questionable whether this is ever the case for semi-flexible polymers. In all other scenarios the MS interactions should be preferred and in any case can easily reproduce the Onsager results to a good approximation.

We find that the isotropic to nematic phase transition for a melt of worm-like polymers is a discontinuous phase transition, as is generally the case for LCs[30] and is well known behaviour of worm-like polymers.[96] Within our model this can be easily explained by expanding the free energy near the transition assuming the order parameter $\mathcal{S}$ is small.

The free energy, Eq. (B.8), is expressed exclusively in terms of the order parameter $\mathcal{S}$, LC interaction strength Λ_2 and the partition function Q. The first two terms will always appear in the combination $\Lambda_2\mathcal{S}$ which we will treat as an independent parameter to be minimized while the partition function will be evaluated assuming $\Lambda_2\mathcal{S}$ is small. As we approach the phase transition from the nematic state the order parameter $\mathcal{S}$ gets smaller and smaller until it vanishes at the phase transition. Therefore, close to the transition we can expand $\ln(Q)$ in small $\mathcal{S}$ by noting that from A.3 we have the partition function, Eq. (B.9),

$$Q = [e^{-[cL-\Lambda_2\mathcal{S}\Psi_2]}]_{0,0} \ . \tag{B.12}$$

In order to evaluate Q we must solve in infinite dimensional matrix exponential; however, since the higher order terms correspond to Legendre polynomials of increasing order which will be small near the phase transition we need only keep up to $l = 2$. Due to the symmetry of the interactions only even order terms survive so this will be accurate up to $l = 4$. Although this simplifies the system considerably, the functional form of the coefficients in the Taylor series are not simple. Nevertheless, near the phase transition the free energy

takes the form

$$\frac{\Delta F}{nk_{\mathrm{B}}T} = (\frac{1}{2} + A\Lambda_2)\Lambda_2\mathcal{S}^2 + B\Lambda_2^3\mathcal{S}^3 + C\Lambda_2^4\mathcal{S}^4 \tag{B.13}$$

The exact numerical values of the coefficients are unimportant for our purposes beyond their signs: $A < 0$, $B < 0$ and $C > 0$. If we didn't have B the phase transition would be continuous and occur at $\Lambda_2 = A/2$ and both $+\mathcal{S}$ and $-\mathcal{S}$ solutions would be global minima of the free energy. Since $B < 0$ the $-S$ is only ever a local minima and is therefore metastable, the $+\mathcal{S}$ solution transitions from a global minima, to a local minima before disappearing completely. As the polymers transition from nematic to isotropic, or isotropic to nematic it must discontinuously jump between the $\mathcal{S} = 0$ and $+\mathcal{S}$ solutions since they are metastable and the transition is first order. This is consistent with the original results of Maier and Saupe.[7] Including the third order term, the phase transition occurs at

$$\Lambda_2 = \frac{1}{2B + \frac{C^2}{2D}} \ . \tag{B.14}$$

The phase diagram described by this transition is plotted and compared with the exact numerical solution in Fig. B.2. If the transition were continuous the expansion would give the exact location of the phase transition; however, since it is discontinuous the order parameter does not become infinitesimally small near the transition and the approximation is not exact. Larger deviation are seen for larger values of Λ_2 since it is expanded in $\Lambda_2\mathcal{S}$. It should be noted that a more accurate calculation of this expansion has been previously carried out in Ref. [99]; however, it does not result in qualitatively distinct behaviour so the simpler calculation is sufficient for our purposes.

B.4 Summary

In the melt phase, within the mean field approximation, the distribution of LC polymers is spatially homogeneous. This greatly simplifies numerical SCFT calculation and allows for a precise description of the isotropic to nematic phase transition. We constructed a phase diagram completely consistent with previous calculations,[96] and we similarly find that the isotropic to nematic phase transition is first order. In addition, we find that the nematic phase becomes unstable relatively rapidly (small distance in Λ_2) below the transition, indicating that the transition is only weakly first order. To further illustrate that the transition is first order we expanded the free energy in terms of the order parameter $\mathcal{S}$ and compared this result with the exact numerical calculations. For a continuous transition $\mathcal{S}$

gets infinitesimally small near the transition and the Taylor series becomes exact; however, this is not the case for a discontinuous transition. Near the transition $\mathcal{S}$ discontinuously jumps resulting in a systematic deviation between the two results, this arises from the non zero cubic, $\mathcal{S}^3$, term in the Taylor series expansion.

We have provided a direct comparison for the phase transition calculated from both MS and Onsager interactions. We find that the Onsager interactions do not give qualitatively distinct behaviour. In general Onsager interaction result in a lower LC interaction strength required for the melt to order; however, the difference relatively small. Since MS interactions can represent a wider class of polymers and accurately reproduce the results from Onsager interactions and, as we discussed in Chapter 2, the issues with Onsager interactions are even more severe in the presence of solvent molecules, MS interactions should be preferred.